



Università degli Studi di Padova
Facoltà di Ingegneria
Dipartimento di Ingegneria Industriale

Corso di Laurea Magistrale in
Ingegneria Aerospaziale

**CUSTOMIZED VAWT BLADE MANUFACTURING
THROUGH FILAMENT WINDING AND ADDITIVE
MANUFACTURING**

Relatore

Ch.mo Prof. Giovanni Lucchetta

Laureando: Lorenzo Berto

Matricola: 1106538

Anno Accademico 2017 - 2018

Dedicated to my parents

Contents

Abstract	iii
Abstract Italiano	v
List of Symbols	vii
List of Acronyms	ix
1 Introduction	1
1.1 Vertical Axis Wind Turbines Description	1
1.2 Straight VAWT Blade Manufacturing Overview	2
1.3 Blade Customization through Additive Manufacturing	3
1.4 Additive Manufacturing - Filament Winding Process Chain	4
2 Mandrel Design and Printing	7
2.1 Netfabb - Model Design	7
2.2 Netfabb Within - Model Optimization	8
2.3 Printing technology - FDM versus Polyjet	12
2.4 CatalystEX - 3D Model Printing	14
2.5 Preliminary Printing Test Cases	15
3 Blade Filament Winding	25
3.1 Machine Building and Functionalities, Supplies Requirements	25
3.2 X-Winder Software Description	27
3.3 G-code File Analysis	32
3.4 Winding Materials Choice	33
3.5 Step-by-Step Winding Session Description	34
4 VAWT Blade Demonstrators Manufacturing	39
4.1 Custom Blades Data	39
4.1.1 NACA 0021	39
4.1.2 Optimized NACA 0015	40
4.2 Blade Structural Supports manufacturing	40
4.3 NACA 0021 Demonstrator Manufacturing	41
4.3.1 Mandrel Realization	41

4.3.2	Blade Winding	48
4.4	Optimized NACA 0015 Demonstrator Manufacturing	51
4.4.1	Demonstrator Challenges and Technology Limitations	51
4.4.2	Mandrel Realization	52
4.4.3	Blade Winding	54
4.5	Time-Costs overview	61
4.5.1	Qualitative Analysis	61
4.5.2	Quantitative Analysis	62
5	Conclusions	65

Abstract

A Vertical Axis Wind Turbine mounts a set of blades around a vertical shaft, which is transverse to the wind: the latter sets the rotors in motion, generating electrical energy via torque. The VAWT comes in different architectures, each with specific features and design criteria. We focused on a small-scale straight bladed H-Rotor type, in particular on the manufacturing of the blade itself. An efficient blade design and realization greatly enhances the turbine's performance. We considered a scenario involving the production of a number of differently shaped (*custom*) blades, representing specific performance needs. Such condition is hardly satisfied by traditional blade manufacturing processes, therefore we evaluated and proposed an Additive Manufacturing - Filament Winding process chain: a custom-designed straight blade is printed, employed as a rotating mandrel and wound as a fiber roving - epoxy resin composite.

We have relied on several tools during production: (i) "Patran/Nastran" and "Netfabb" for 3D blade modeling and preliminary design; (ii) *Dimension sst 1200es* "Catalyst EX" for .stl elaboration and printing; (iii) *X-Winder* "Designer" and "Executor" for blade winding. The desktop winding machine was specifically mounted in laboratory for this work.

To validate the process, we produced two demonstrators: the first has a typical NACA 0021 profile, the second an optimized NACA 0015 profile resulting from an aero-structural optimization analysis. Each blade was modularized in two smaller components, printed with *ad hoc* structural supports for effective mounting on the FW machine.

The key factors for an efficient blade realization were identified as: (i) minimal model and support printing volume through Skin-only, Lattice-less model; (ii) vertical printing orientation; (iii) blade modularization. The best component quality during winding phase is achieved by: (i) accurate fiber roving width and thickness measurement; (ii) post-winding curing via heat shrink tape and heat gun.

The NACA 0021 demonstrator successfully validates the process chain, showing feasibility potential for custom convex components. The optimized NACA 0015 blade, being of concave shape, could only be manufactured with a straightened pressure side. Though the final component differs from its design model, having lost the aerodynamic advantage it held compared to the simple NACA 0015 baseline, a structural gain was achieved nonetheless. This makes the sub-optimal blade economically desirable anyway, being comparable to its baseline in terms of production time and cost.

Abstract Italiano

Una turbina eolica ad asse verticale monta un sistema di pale su un albero verticale, trasversale al vento: quest'ultimo mette in moto i rotori, i quali generano energia elettrica tramite torsione. Le VAWT si presentano in diverse architetture, ciascuna con caratteristiche e criteri di design specifici. Ci siamo concentrati su una turbina di piccola scala di tipo H-Rotor con pale rettilinee, in particolare sulla manifattura di queste ultime. Un design e una realizzazione efficienti di pala, difatti, migliorano notevolmente le prestazioni di turbina. Abbiamo analizzato la produzione di un numero di pale a forma diversa (*customizzata*) corrispondenti a diverse esigenze di performance. Tale condizione risulta difficilmente soddisfatta da sistemi tradizionali di produzione di pale, indi abbiamo valutato e proposto una catena di processo Additive Manufacturing - Filament Winding: una pala rettilinea dal design customizzato viene stampata, utilizzata come mandrino rotante ed avvolta come composito di roving di fibra - resina epossidica.

Ci siamo affidati a diversi strumenti durante la produzione della pala: (i) "Patran/Nastran" e "Netfabb" per la modellazione 3D e il design preliminare; (ii) "Catalyst EX" (*Dimension sst 1200es*) per elaborazione del file .stl e stampa; (iii) "Designer" ed "Executor" (*X-Winder*) per l'avvolgimento. La macchina da desktop per avvolgimento è stata specificatamente montata in laboratorio per l'uopo.

Per validare il processo, abbiamo prodotto due dimostratori: il primo è caratterizzato da un tipico profilo NACA 0021, il secondo da un profilo NACA 0015 ottimizzato e risultante da un'analisi di ottimizzazione aero-strutturale. Ciascuna pala è stata modularizzata in due componenti più corti, stampati assieme a supporti strutturali *ad hoc* al fine di un montaggio efficace sulla macchina per avvolgimento.

I fattori chiave per una realizzazione di pala efficiente sono stati identificati come: (i) volume minimo di modello e supporto in fase di stampa, ottenuto tramite modello con sola Skin e nessun Lattice; (ii) orientazione di stampa verticale; (iii) modularizzazione di pala. La qualità componente migliore in fase di avvolgimento si è ottenuta tramite: (i) accurata misurazione di larghezza e spessore del roving di fibra; (ii) cura post-avvolgimento tramite nastro termorestringente e pistola a calore.

Il dimostratore NACA 0021 valida con successo la catena di processo, mostrando potenziale di fattibilità per componenti customizzati a forma convessa. La pala NACA 0015 ottimizzata, di forma convessa, è risultata realizzabile solo con intradosso raddrizzato. Nonostante il componente finale si discostasse dal modello di design, avendo perso il guadagno aerodinamico rispetto al NACA 0015 di base, nondimeno è stato possibile replicare il guadagno a livello strutturale. Ciò rende il modello sub-ottimale comunque economicamente desiderabile, essendo comparabile alla sua versione base per costi e tempi di produzione.

List of Symbols

E	Young's Modulus	[Pa]
ν	Poisson's Ration	[-]
ρ	Density	[kg/m ³]
σ_{max}	Maximum Allowable Stress	[Pa]
δ_{max}	Maximum Allowable Displacement	[mm]
ϵ^*	Elongation at Break	[%]
ϕ_{eq}	Equivalent Diameter	[mm]
V_F	Volume of Fibers	[%]
T_g	Glass Transition Temperature	[°C]

List of Acronyms

<i>VAWT</i>	Vertical Axis Wind Turbine
<i>HAWT</i>	Horizontal Axis Wind Turbine
<i>AM</i>	Additive Manufacturing
<i>FW</i>	Filament Winding
<i>FDM</i>	Fused Deposition Modeling
<i>FRP</i>	Fiber Reinforced Polymers
<i>GF</i>	Glass Fiber
<i>CF</i>	Carbon Fiber
<i>ABS</i>	Acrylonitrile Butadiene Styrene
<i>FEA</i>	Finite Element Analysis
<i>CAD</i>	Computer-Aided Design
<i>CAE</i>	Computer-Aided Engineering
<i>CBC</i>	Custom Boundary Conditions
<i>DH</i>	Delivery Head
<i>DHL</i>	Delivery Head Linear (arm)
<i>CW</i>	Clockwise
<i>CCW</i>	Counter-clockwise

List of Figures

1.1	Typical Darrieus Vertical Axis Wind Turbine configurations [1]. From left to right: H-type (Gyromill), V-type, Troposkien type, Gorlov (Helical) type.	2
1.2	Vacuum Assisted Resin Infusion Molding (VARIM) manufacturing technology.	3
1.3	Common Additive Manufacturing Technologies divided by application, materials and main manufacturers [2].	4
1.4	(a) FDM technology schematics; (b) <i>Dimension sst 1200es</i> FDM Printer (Stratasys Inc.).	5
2.1	1000 mm^3 cube rendering and Lattice-Surface regions example data in Within Optimization Utility. A well-repaired mesh will show a Mesh Quality flagged as Good.	9
2.2	1000 mm^3 cube built with: (a) Skin and Grid Lattice Topology; (b) Skin and Tetrahedron Lattice Topology. The Skin is 0.5 mm thick and the Lattice is made of $(x, y, z) = (3; 3; 3)$ mm cells with beam thickness of 0.25 mm	10
2.3	1000 mm^3 cube built with: (a) Skin and Hexa Grid Lattice Topology; (b) Skin and Random Endoskeleton Lattice Topology. The Skin is 0.5 mm thick and the Lattice is made of $(x, y, z) = (1; 1; 1)$ mm cells with beam thickness of 0.25 mm	11
2.4	Front view of a 1000 mm^3 cube, built with a 0.5 mm thick Skin and a Grid Lattice Topology with $(x, y, z) = (3; 3; 3)$ mm cells and beam thickness of 0.25 mm . The component is created with: (a) no kernels ; (b) a centered $(x, y, z) = (3; 3; 3)$ mm Spatial Lattice Kernel, with a peak of 3 mm	12
2.5	Load Case simulation of a Titanium Ti64 1000 mm^3 cube with a Fixed base and a $F_y = -1000 N$ Concentrated Force, distributed on the selected nodes.	13
2.6	FEA results for a non-optimized 1000 mm^3 cube subject to a custom-defined Load Case, in terms of: (a) Displacement ; (b) Stress.	14
2.7	Optimization process for a 1000 mm^3 cube with Grid Lattice Topology. The results are shown in terms of: (a) Displacement; (b) Stress.	16
2.8	Titanium Ti64 1000 mm^3 cube with optimized Skin and Grid Lattice Topology. The FEA resulted in local thickening of Skin and Lattice rods to achieve the best structural performance in respect to the given Load Case. An Advanced Surface Trim and a Lattice Fine Smoothing were also selected.	17
2.9	Simulation of a horizontally printed 6 cm sample NACA 0021 blade chunk through FDM technology - CatalystEX package information.	18

2.10	Simulation of a vertically printed 6 <i>cm</i> sample NACA 0021 blade chunk through FDM technology - CatalystEX package information.	18
2.11	Simulation of a horizontally printed 6 <i>cm</i> sample NACA 0021 blade chunk through Polyjet technology - Objet Studio package information.	19
2.12	Simulation of a vertically printed 6 <i>cm</i> sample NACA 0021 blade chunk through Polyjet technology - Objet Studio package information.	20
2.13	Printing procedure of a sample cylinder with radius $r = 10$ <i>mm</i> and height $h = 20$ <i>mm</i> - CatalystEX Software General tab.	21
2.14	Printing procedure of a sample cylinder with radius $r = 10$ <i>mm</i> and height $h = 20$ <i>mm</i> - CatalystEX Software Orientation tab.	21
2.15	Printing procedure of a sample cylinder with radius $r = 10$ <i>mm</i> and height $h = 20$ <i>mm</i> - CatalystEX Software Orientation tab with .stl elaboration. . .	22
2.16	Printing procedure of a sample cylinder with radius $r = 10$ <i>mm</i> and height $h = 20$ <i>mm</i> - CatalystEX Software Package tab.	22
2.17	Imported .stl models of two 3 <i>cm</i> long NACA 0021 blade chunks. The components are built with a (8;8;10) <i>mm</i> Grid Topology Lattice structure and 0.25 <i>mm</i> thick Skin and Lattice Beams. Both horizontal and vertical orientations were considered.	23
2.18	Elaborated .stl models of two 3 <i>cm</i> long NACA 0021 blade chunks. The components are built with a (8;8;10) <i>mm</i> Grid Topology Lattice structure and 0.25 <i>mm</i> thick Skin and Lattice Beams. Both horizontal and vertical orientations were considered.	23
2.19	Printing package of two 3 <i>cm</i> long NACA 0021 blade chunks. The components are built with a (8;8;10) <i>mm</i> Grid Topology Lattice structure and 0.25 <i>mm</i> thick Skin and Lattice Beams. Both horizontal and vertical orientations were considered. A great amount of Support material is required, about twice the Model material volume, because of horizontal configuration and Lattice structure.	24
2.20	Printed 3 <i>cm</i> long blade chunks. The components are built with a (8;8;10) <i>mm</i> Grid Topology Lattice structure and 0.25 <i>mm</i> thick Skin and Lattice Beams. Both horizontal (left) and vertical (right) orientations were considered. . . .	24
3.1	List of X-Winder 4-axis “4X-23” winding machine model.	26
3.2	DH rollers - from left to right: (i) default Steel roller; (ii) customly printed roller with approx 50% reduced middle section and same tip sections, compared to the default one; (iii) customly printed roller with approx 50% reduced middle section and double tip sections, compared to the default one.	27
3.3	(a) Mounted 4-axis Filament Winding machine utilized in the current work and (b) Axis electronic control system, with corresponding labels.	28
3.4	Detailed view of mounted NEMA 23 stepper motors with 60 <i>kg</i> holding torque: (a) carriage stepper. A limit switch is also mounted for carriage linear path control; (b) mandrel stepper.	28
3.5	Detailed view of mounted Delivery Head linear and rotary NEMA 17 stepper motors with 20 <i>kg</i> holding torque. Two limit switches are also mounted for DH linear and rotary path control.	29

3.6	Required supplies for a basic winding session yielding a high-quality component.	30
3.7	X-Winder Designer Software UI - 3-Axis Winding configuration. The four sub-sections are marked and labeled.	30
3.8	X-Winder Executor Software UI. The three sub-sections are marked and labeled.	32
3.9	X-Winder Settings window - General settings tab.	35
3.10	X-Winder Settings window - 4-Axis settings tab.	36
3.11	X-Winder Settings window - Speeds settings tab.	37
4.1	2D optimized profile, obtained from a baseline NACA 0015 profile through an aero-structural optimization code. The airfoil has a normalized chord.	40
4.2	NACA 0021 3D solid model created in Patran. The extruded blade is 0.4 <i>m</i> long and has a chord length $c = 0.05$ <i>m</i>	41
4.3	Repaired NACA 0021 blade, remeshed with triangular elements. Each element has angles $> 10^\circ$, thus FEA and Optimization may be conducted on the part.	42
4.4	NACA 0021 blade - Created Component data with Hollow tip surfaces, 1 <i>mm</i> thick lateral surface Skin and middle 2 <i>mm</i> thick reinforcement (from 0.06 <i>m</i> blade chunk).	43
4.5	NACA 0021 Within Simulation - Custom ABS Material and simplified, worst-case scenario Winding Load Case setup.	44
4.6	NACA 0021 Within Simulation - FEA results in terms of: (a) Stress; (b) Displacement.	45
4.7	NACA 0021 demonstrator - Netfabb design models and geometrical data for: (a) Blade; (b) Tip inserts (Patran was previously employed for the cylindrical rods extrusion).	46
4.8	0.2 <i>m</i> long NACA 0021 blade - CatalystEX elaborated .stl	46
4.9	0.06 <i>m</i> long NACA 0021 mid insert - CatalystEX elaborated .stl	47
4.10	0.024 <i>m</i> long NACA 0021 tip inserts - CatalystEX elaborated .stl	47
4.11	NACA 0021 blade components - CatalystEX printing package. The estimated total Model and Support material volumes are presented, together with an approximate building time.	48
4.12	Printed 0.2 <i>m</i> long NACA 0021 blades, together with the 0.06 <i>m</i> internal chunk.	49
4.13	Mounted 0.4 <i>m</i> long NACA 0021 blade. The junction between the two 0.2 <i>m</i> parts is reinforced with a 0.06 <i>m</i> internal chunk and sealed for enhanced rigidity.	49
4.14	X-Winder Designer data for the 0.4 <i>m</i> NACA 0021 blade.	50
4.15	GF/epoxy filament wound NACA 0021 VAWT blade demonstrator.	50
4.16	Optimized NACA 0015 3D solid model created in Patran. The extruded blade is 0.4 <i>m</i> long and has a chord length $c = 0.06$ <i>m</i>	52
4.17	Repaired optimized NACA 0015 blade, remeshed with triangular elements. Each element has angles $> 10^\circ$, thus FEA and Optimization may be conducted on the part.	53

4.18	Optimized NACA 0015 blade - Created Component data with Hollow tip surfaces, 1 <i>mm</i> thick lateral surface Skin and middle 2 <i>mm</i> thick reinforcement (from 0.06 <i>m</i> blade chunk).	53
4.19	Optimized NACA 0015 Within Simulation - Custom ABS Material and simplified, worst-case scenario Winding Load Case setup.	54
4.20	Optimized NACA 0015 Within Simulation - FEA results in terms of: (a) Stress; (b) Displacement.	55
4.21	Optimized NACA 0015 demonstrator - Netfabb design models and geometrical data for: (a) Blade; (b) Tip inserts (Patran was previously employed for the cylindrical rods extrusion).	56
4.22	0.2 <i>m</i> long optimized NACA 0015 blade - CatalystEX elaborated .stl	56
4.23	0.06 <i>m</i> long optimized NACA 0015 mid insert - CatalystEX elaborated .stl	57
4.24	0.024 <i>m</i> long optimized NACA 0015 top insert - CatalystEX elaborated .stl	57
4.25	0.024 <i>m</i> long optimized NACA 0015 bottom insert - CatalystEX elaborated .stl	58
4.26	Optimized NACA 0015 blade components - CatalystEX printing package. The estimated total Model and Support material volumes are presented, together with an approximate building time.	58
4.27	Printing summary for a 0.4 <i>m</i> optimized NACA 0015 demonstrator: two 0.2 <i>m</i> long blades, two internal tip inserts and one mid-section blade chunks.	59
4.28	X-Winder mandrel setup. The 0.4 <i>m</i> long optimized NACA 0015 blade fixing at the mandrel chucks is realized via the two tip inserts, while the internally reinforced mid section is sealed with tape.	59
4.29	X-Winder Designer data for the 0.4 <i>m</i> optimized NACA 0015 blade.	60
4.30	GF/epoxy filament wound optimized NACA 0015 VAWT blade demonstrator.	60

Chapter 1

Introduction

1.1 Vertical Axis Wind Turbines Description

A Wind Turbine is a mechanical system that transforms energy through rotors (blades). The blades are set in motion by the wind, turning it into mechanical energy via torque and then into electrical energy via generators. A turbine with a power capacity of up to 100 kW is defined as *small-scale*.

A Vertical Axis Wind Turbine (VAWT) is a class of Wind Turbine, mounting a set of blades rotating around the main rotor shaft (vertical pole) which is transverse to the wind. The main components, i.e. gearbox and electronics, are located at the base of the turbine. A typical power conversion efficiency is 20% ~ 40%.

Since G. J. M. Darrieus patented the first VAWT in 1931 [3], several VAWT architectures were developed (Fig.1.1), each with specific aims and design criteria. For example, a Troposkien type VAWT enhances both aerodynamic and structural performances, but has very little torque at the tips; a H-Darrieus type has straight blades and equally distributed torque, but is subject to heavier centrifugal loads and bending moments [4].

VAWT are also classified in regards to the aerodynamic force they mainly harness: (i) *Lift-type*: high aerodynamic efficiency, favourable blade surface requirement, high power output; (ii) *Drag-type*: low aerodynamic efficiency, high blade surface requirement, limited power output.

Unlike the more commercially widespread Horizontal Axis Wind Turbine (HAWT), a VAWT has several advantages, especially when designed for a urban landscape [5], [6]:

- Omni-directional, no need for wind tracking system (yaw control);
- Take advantage of turbulent and gusty winds;
- Gearbox and generator are easily accessible and less subject to fatigue;
- Can be grouped close to each other, e.g. on rooftops;
- Low-noise output.

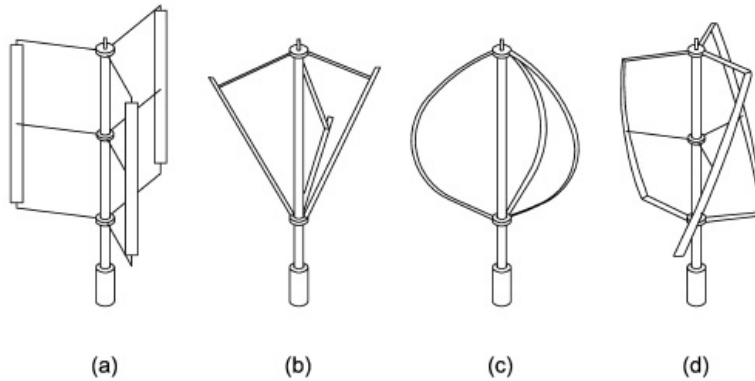


Figure 1.1: Typical Darrieus Vertical Axis Wind Turbine configurations [1]. From left to right: H-type (Gyromill), V-type, Troposkien type, Gorlov (Helical) type.

Given the rising demand of renewable energy in the worldwide economic scenario [7], [8], micro- and small-scale VAWT have been showing good potential especially as home-based energy system: design simplicity, easy installation and maintenance, low manufacturing and retail costs are key advantages [9], [10].

The present work focuses on such turbines, with particular attention to the manufacturing process of the blades: they represent a large fraction of the total VAWT cost and their quality reflects heavily on the turbine's performance [11].

1.2 Straight VAWT Blade Manufacturing Overview

We analyzed the manufacturing of a small-scale VAWT straight blade. In recent years several processes with metals, plastic and composite materials have been employed, focusing on both large and small scale economies.

Fernández et al. designed a VAWT with hydroformed metal blades, whose size and shape were determined via aerodynamic/structural analysis, showing potential competitiveness with fiber-reinforced composites and larger-scale productions [12]. Kong et al. presented a high-efficiency composite VAWT blade design, also manufacturing and testing a prototype made through hand lay-up of glass fabric-epoxy on a Styrofoam mold (cut via hot wire from steel templates) [13]. Khan and Rao focused on a low cost small H-Rotor with curry neem blades, analyzing its affordability for rural applications in India [14]. A more classic approach was followed by Brown and Brooks, designing and analyzing a thermo-plastic composite blade manufactured using a one-step vacuum moulding process [15]. Guerrero-Villar et al. developed small-scale VAWT models using the FDM technology, demonstrating that rapid prototyping may offer affordable and budget options in respect to composite blades [16].

In this work we focused on two technologies, representing different antithetic needs: (i) Thermoplastic Polymer 3D Printing: cheap, versatile prototyping at the expenses of blade performance; (ii) FRP processing: optimal performance but costly manufacture. The best process would ideally guarantee top aero-structural blade performances while keeping low manufacturing times/costs. The former can be achieved through composite materials, the latter through plastic Additive Manufacturing.

1.3 Blade Customization through Additive Manufacturing

Aforementioned VAWT blade manufacturing processes perform differently - economically speaking - based on the target blade. For example, Aluminum blade extrusion is convenient in producing commonly used blade airfoils (e.g. symmetrical NACA profiles): the process requires a die, whose cost can be well amortized with mass production. In case of a large number of blade with different profiles though, said technology would become unfavourable in terms of costs. The same holds true for processes requiring molds, such as Vacuum Resin Infusion (Fig.1.2): each different blade would require a corresponding mold.

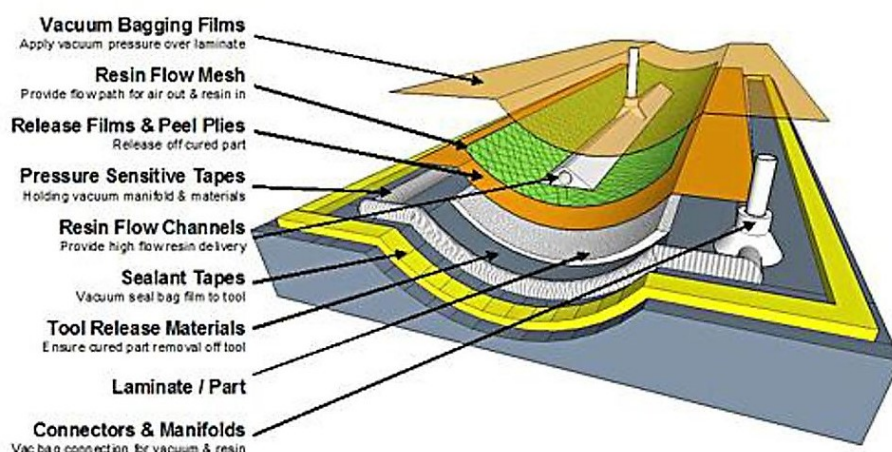


Figure 1.2: Vacuum Assisted Resin Infusion Molding (VARIM) manufacturing technology.

VAWT market competitiveness and diffusion rely on turbine performances (power output, blade fatigue life), which is enhanced by blades with optimized profile. Since optimization analysis depends on Boundary Conditions (turbine location, wind conditions, ...), optimized blades are intrinsically custom components. For example, VAWT mounted in different geographical locations would employ differently optimized airfoils to obtain the best performance.

A solution may come from Additive Manufacturing, allowing automated realization of geometrically versatile components without requiring a combination of different technologies and higher production costs [17], [18]. Many AM technologies are commercially available,

as shown in Fig.1.3. The most widely used is the plastic FDM (Fig.1.4), which is also typically the simplest and most affordable one. These features, combined with a great variety of available printing materials, make this technology ideal for cheap customization needs.

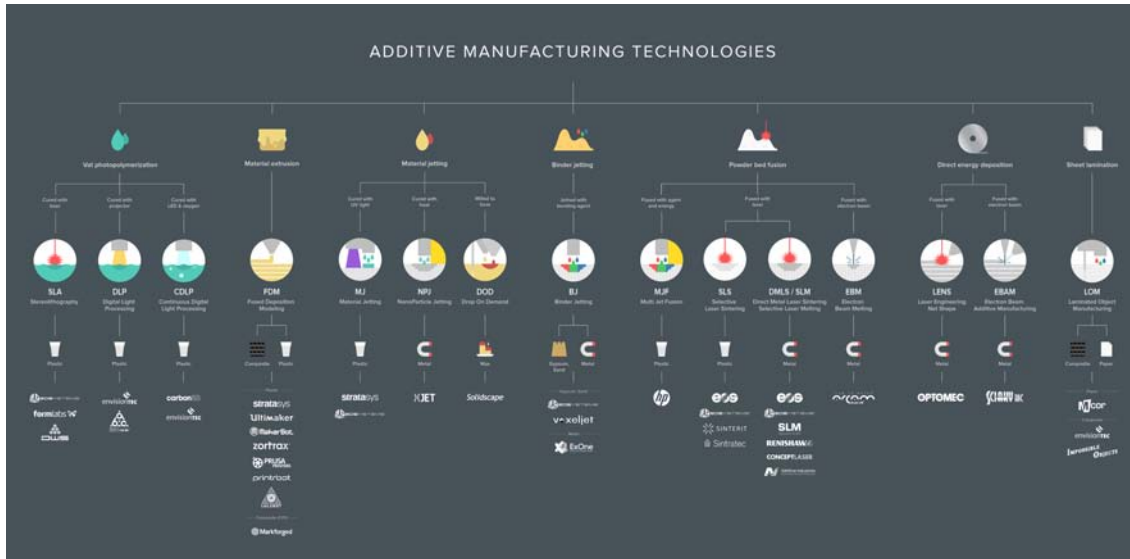


Figure 1.3: Common Additive Manufacturing Technologies divided by application, materials and main manufacturers [2].

1.4 Additive Manufacturing - Filament Winding Process Chain

Plastic Rapid Prototyping solves the geometrical customization issue, but that alone is insufficient: polymers are generally not suited for structural and aerodynamical components subject to relevant loads. Even resistant plastics (e.g. ABS) may be employed only on micro-scale turbines.

Satisfactory mechanical performances are generally guaranteed by materials such as metals and FRP, the latter especially desirable for their specific properties and design versatility. Typical FRP manufacturing technologies for VAWT blades are: (i) *Vacuum Resin Infusion*, where resin is pumped in a vacuum bag and wets the dry fibers positioned on a mold; (ii) *Resin Transfer Molding*, which employs a two-part, matching closed mold containing the fiber reinforcement: resin is injected in the mold under low-to-moderate pressure and the part is then cured; (iii) *Manual Lay-up*, a less industrial procedure involving a blade preform (usually made of foam or wood) on which the resin wetted fiber mats are manually positioned.

Said processes often involve high tooling and manpower costs, which may result economi-

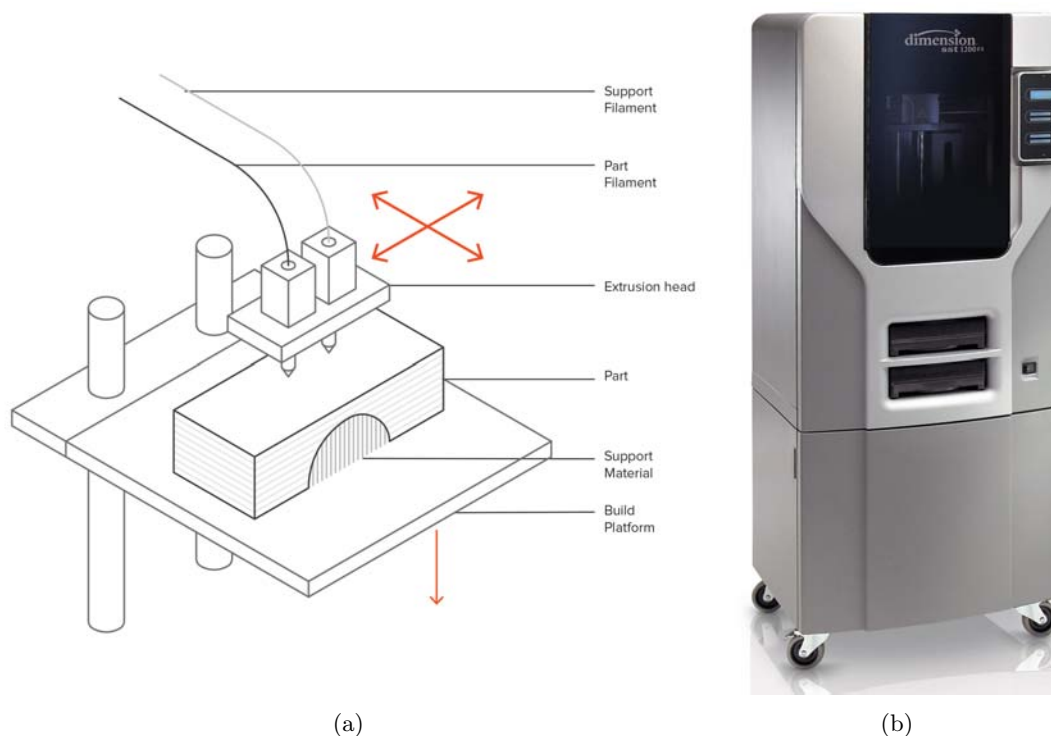


Figure 1.4: (a) FDM technology schematics; (b) *Dimension sst 1200es* FDM Printer (Stratasys Inc.).

cally unfavourable for small lot blade production. Aiming at lower costs without sacrificing component quality, Filament Winding (FW) was then considered. This automated technology involves an axial-symmetric rotating mandrel, over which wetted continuous fiber filaments are wound under tension; once the winding is complete, the part is cured. Based on the number of axis (Degrees of Freedom), complex geometries are also achievable. Typical FW application range from sporting gear to high-pressure vessels and missile casings. VAWT straight blades appear to be good candidates for FW manufacturing: both lightweighting and performance requirements may be satisfied, e.g. with GF/CF filaments wetted by Epoxy resin. Automation and commercial affordability (desktop-scale machines [19]) are also desirable features.

As an innovative way to manufacture small-scale VAWT straight blades, the current work proposes a new process chain to combine the advantages of Rapid Prototyping with the benefits of FRP: a custom-designed blade is printed through AM and subsequently employed as a rotating mandrel in a Filament Winding machine, realizing the axial-symmetric straight blade as a GF/CF - Epoxy composite. The objective is to detail and optimize said procedure, both conceptually and practically, as well as highlighting its potential applications and limitations through demonstrators.

Chapter 2

Mandrel Design and Printing

This chapter describes the first phase of the manufacturing process chain: 3D modeling, mesh manipulation, FEA optimization analysis and FDM printing. Various software were employed:

MSC Patran/Nastran - Patran is a pre-/post-processing FEA software providing solid modeling, meshing, analysis setup and results processing; Nastran is a versatile structural analysis solver for both linear and nonlinear problem solving [20];

Autodesk Netfabb - additive manufacturing and design software with features including CAD models import and mesh manipulation, AM machine environment simulation (layer-by-layer modeling, support material structuring) and parts packing. In its Ultimate version, it grants further control over the manufacturing process, as well as including advanced features such as lattice and topology optimization for lightweight designing through a Nastran solver [21], [22];

CatalystEX - additive manufacturing software working as interface for Stratasys FDM 3D printer, manages part orientation and printing parameters control, as well as manufacturing simulation and printing package management [23].

2.1 Netfabb - Model Design

The preliminary solid 3D modeling is covered by Patran, whose many features are out of this work's scope and won't be discussed in detail. Netfabb was then chosen for the control over the part's external and internal geometry; the main steps of this phase are: (i) 3D CAD model import; (ii) Part/mesh repair; (iii) Part orientation and spatial disposition. We start by creating a new project and importing a solid 3D model. An appropriate level of detail, i.e. mesh density, must be selected. There are 5 options, from Extra Low to Extra High, depending on the number of triangular finite elements representing the model surface. At this stage it is advised to adopt a Low-to-Medium level of detail, for two reasons: (i) to not encumber the PC processor, allowing quicker modeling; (ii) surfaces can be remeshed later through the *Repair* function.

The next important step is mesh manipulation. The imported model usually suffers from meshing problems (triangular elements with internal angles $< 10^\circ$), which need to be addressed if a FEA is to be conducted, e.g. during an optimization process. Therefore, the *Repair* function is launched, opening a sub-program granting the following controls of interest: (i) Single element and surface selection (whole, tolerance); (ii) Remeshing and node creation/position control; (iii) Edges Highlighting and FEA/optimization check.

In repairing the part, every model surface should be represented by triangular elements as regular as possible, with shape close to an equilateral triangle. The process is complete when *Status for Optimization Utility* shows a green tick: the FEA and subsequent component optimization will not flag any problems or ask for automatic re-triangulation of the part. The latter is undesirable, as it often brings unwanted modification to the geometry, such as edges smoothing or uneven surfaces.

2.2 Netfabb Within - Model Optimization

Having repaired the part, the Optimization Utility *Within* is run. Such application is exclusive part of the Netfabb Ultimate version. The utility is organized in different, consequential sections:

1. *Parts* - mesh quality check, skin and lattice definition in terms of geometrical properties, kernels creation;
2. *Simulation* - material and machine environment definition, FEA of selected part in terms of load case, global stress and displacement;
3. *Optimization* - Lattice and topological optimization of the part, given a series of constraints; skin and lattice thicknesses must be set as Variable;
4. *Component* - Summary of part's surface area, occupied volume etc..

A rendering of a sample 1000 mm^3 cube is shown in Fig.2.1: a successful Repair process will result in Mesh Quality flagged as "Good".

The first step involves the *Parts* section. Various regions must now be defined, according to the part's application and the printing technology capabilities (i.e. printing thickness machine threshold):

Lattice - periodic internal structure comprised of cells with customizable topology meant to substitute a solid body, thus reducing the component's weight while maintaining defined levels of global maximum stress and displacement. The cell's basic geometry is defined through its $x - y - z$ Unit Sizes, as well as Beam Thickness and Topology;

Skin - thin region covering the exterior of the part. It is defined by Thickness and triangular surface elements involved. Being solid, it generally has the greatest impact in the overall part's volume and therefore should be reduced as much as possible in a lightweight design;

Hollow region - region to be left empty.

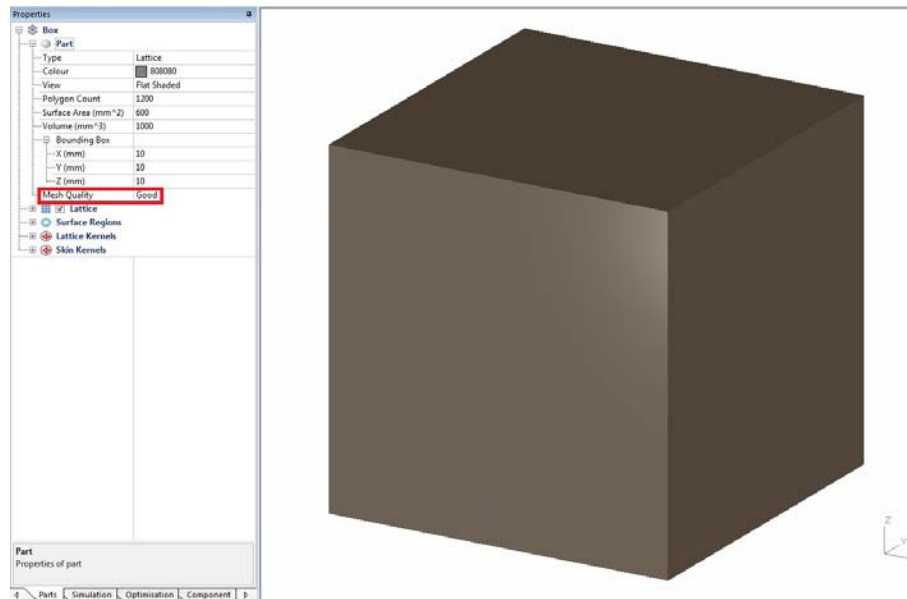


Figure 2.1: 1000 mm^3 cube rendering and Lattice-Surface regions example data in Within Optimization Utility. A well-repaired mesh will show a Mesh Quality flagged as Good.

Fig.2.2 and Fig.2.3 show four different Lattice Topologies, among the many available by default, each with structural characteristics and volume reduction coefficient that befit different materials and applications. For example, the Grid Topology works well for non-active components, a Tetrahedron Topology offers higher stiffness and impact resistance and a Random Endoskeleton Topology is best suited for medical applications [24]. A customized Lattice Topology may also be defined through the Netfabb Lattice Topology Utility.

While the internal geometry can conveniently be very complex, e.g. through topology randomization or spatial/density kernels usage (Fig.2.4), it is also important to realize simple yet efficient configurations in order to achieve: (i) faster design and computational times, especially during the optimization phase which is the most time-consuming operation in this process; (ii) shorter printing times and material usage. Preliminary considerations should be made regarding the part's functions and material as a built component. There are several options in the *Create Component* function. It is advised to start building the component with the *Minimum Thickness* option: an optimization process would then thicken the skin and the lattice locally and where needed, making it easier to visualize the difference between optimized and unoptimized component.

Having created the component with first-attempt regions, the *Simulation* tab is selected. The linear elastic material properties, i.e. Young's Modulus and Poisson's Ratio, need to be defined in the *Parts* menu either by choosing from default AM Printing Machine Environments or by Custom Machine Environment and Material.

Next, a Load Case must be defined via direct data input or via CBC file import (e.g. NAS-TRAN .bdf file). Either way, the FEA simulation only allows for Linear Static Analysis,

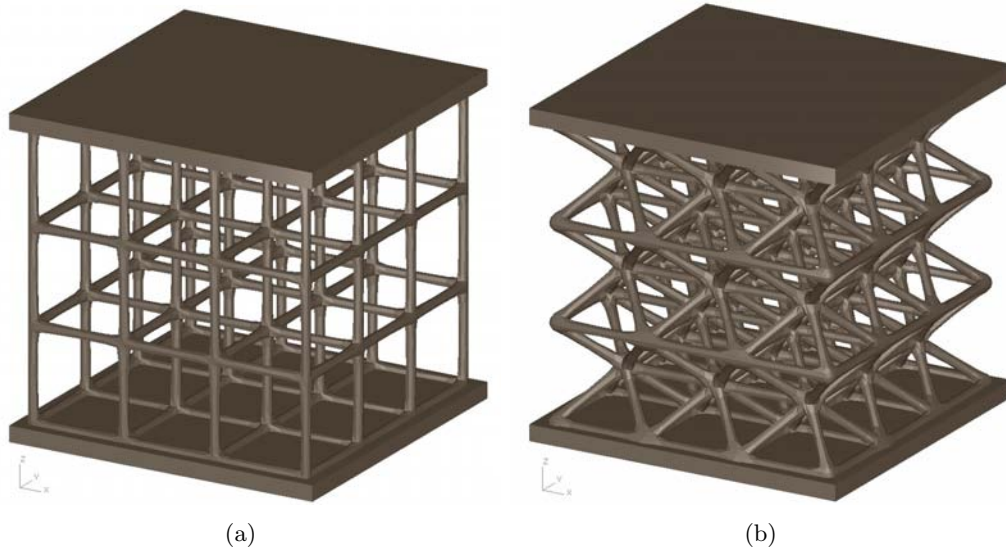


Figure 2.2: 1000 mm^3 cube built with: (a) Skin and Grid Lattice Topology; (b) Skin and Tetrahedron Lattice Topology. The Skin is 0.5 mm thick and the Lattice is made of $(x, y, z) = (3; 3; 3) \text{ mm}$ cells with beam thickness of 0.25 mm .

which imposes time and spatial constant Boundary Conditions. The available options are: Concentrated Force, Distributed Load, Restraint.

Aforementioned limitations to analysis capabilities may be problematic, especially for the current work which relies on a following Filament Winding process, which forces both time and spatial dependant loads on the wound part. To overcome this problem, a simplified Load Case should be evaluated. Once the Simulate Component button is selected and the FEA is over, the Stress and Displacement graphs are available. These help highlighting the maximum value σ_{max} and δ_{max} of both, as well as a qualitative amount of elements subject to such values. Fig.2.6 shows an example of such graphs for the 1000 mm^3 sample cube with the aforementioned Boundary Conditions.

If σ_{max} and δ_{max} are over acceptable thresholds, different solutions are viable:

1. Proceed with the optimization process through the corresponding tab, allowing *Within* to iterate on the component and its Skin-Lattice thicknesses in order to reach the desired levels of stress and displacement;
2. Create a new component with second-attempt Lattice Topology;
3. Create a new component with thicker Skin or Lattice.

The first solution, being the only one not imposing a complete part overhaul, represents the last major step in the optimization process. *Within* operates a FEA iterative sequence, trying to achieve or maintain a low model volume (e.g. minimal at 0 mm^3) while keeping the stress and displacement under the set threshold values. Many options are available, the most important being: maximum time and number of iterations, "keep"

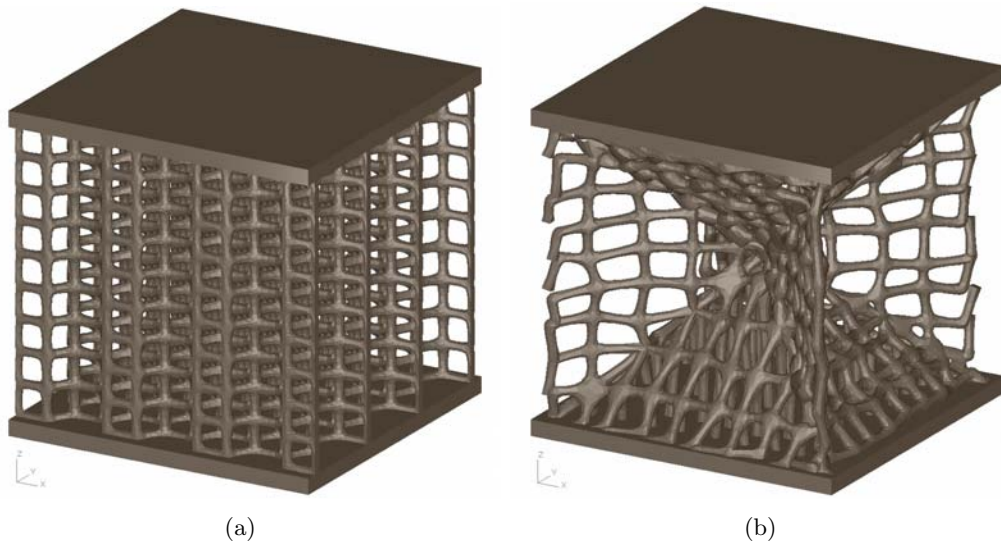


Figure 2.3: 1000 mm^3 cube built with: (a) Skin and Hexa Grid Lattice Topology; (b) Skin and Random Endoskeleton Lattice Topology. The Skin is 0.5 mm thick and the Lattice is made of $(x, y, z) = (1; 1; 1) \text{ mm}$ cells with beam thickness of 0.25 mm .

criteria, lattice and skin importance (weight).

Fig.2.7 shows the optimization process for the above sample cube built with a Grid Lattice Topology. As the process runs, a series of graphs are build as a function of the iteration number, showing: Estimated Volume, Skin and Lattice Stress Ratios, Linear Buckling Safety Factor, Skin and Lattice Displacement, Skin and Lattice Thicknesses. The blue continuous line represents the instantaneous value of the analyzed figure, while the dashed green line represents the custom set threshold. The most successful outcome would see the blue line always under the green line. The Estimated Volume is an exception, since the starting part already represents the Minimum Volume (if such option was selected during component creation).

Multiple optimization runs can be conducted in sequence, if the first results are not satisfactory. The optimized 1000 mm^3 cube with Grid Lattice Topology is shown in Fig.2.8: *Within* has locally thickened both Skin and Lattice to better withstand the given loads. The *Parts* tab grants the finishing touch on the optimized component. A few commonly used options involve Surface Trimming and Lattice-Skin Modification (smoothing). These functions can be run by selecting *Create Component* again, without losing the optimization results.

The part is ready for printing and is exported as component from *Within* to Netfabb, where it is saved as .stl file.

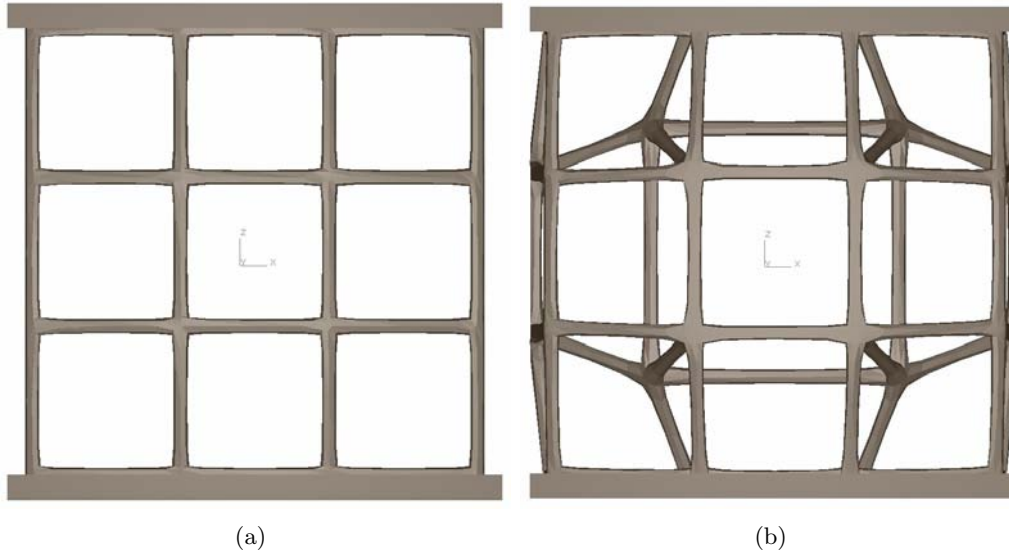


Figure 2.4: Front view of a 1000 mm^3 cube, built with a 0.5 mm thick Skin and a Grid Lattice Topology with $(x, y, z) = (3; 3; 3) \text{ mm}$ cells and beam thickness of 0.25 mm . The component is created with: (a) no kernels ; (b) a centered $(x, y, z) = (3; 3; 3) \text{ mm}$ Spatial Lattice Kernel, with a peak of 3 mm .

2.3 Printing technology - FDM versus Polyjet

The final step towards mandrel manufacturing is its 3D printing. In this particular work, only polymer printing machines were considered. This implies lower costs for both machine and material, as well as major setup commercial availability.

Two printing technologies from *Stratasys Inc.* were readily available in laboratory and thus analyzed:

FDM - layer-by-layer printing via plastic filament, unwound from a coil and delivered on a tray through a nozzle. The material (e.g. ABS) is pulled by rollers, then heated and liquefied before deposition. A support material is also loaded in the machine and delivered from the same nozzle. Its function is structural and, being soluble, it is removed via an appropriate bath when the part is printed;

PolyJet - jetting of layers of curable liquid photopolymer onto a build tray. Typically more accurate and resolute than FDM, but also more expensive, prints in different materials (e.g. VeroWhitePlus RGD835) and utilizes a supporting material removable via high-pressure water jets.

Several aspects were taken into consideration to choose the most suitable mandrel printing technology:

1. Component's printed surface quality: the printed part will become a mandrel in a FW process, therefore its outer surface will represent the final wound component's inner surface, which does not need to be of high quality;

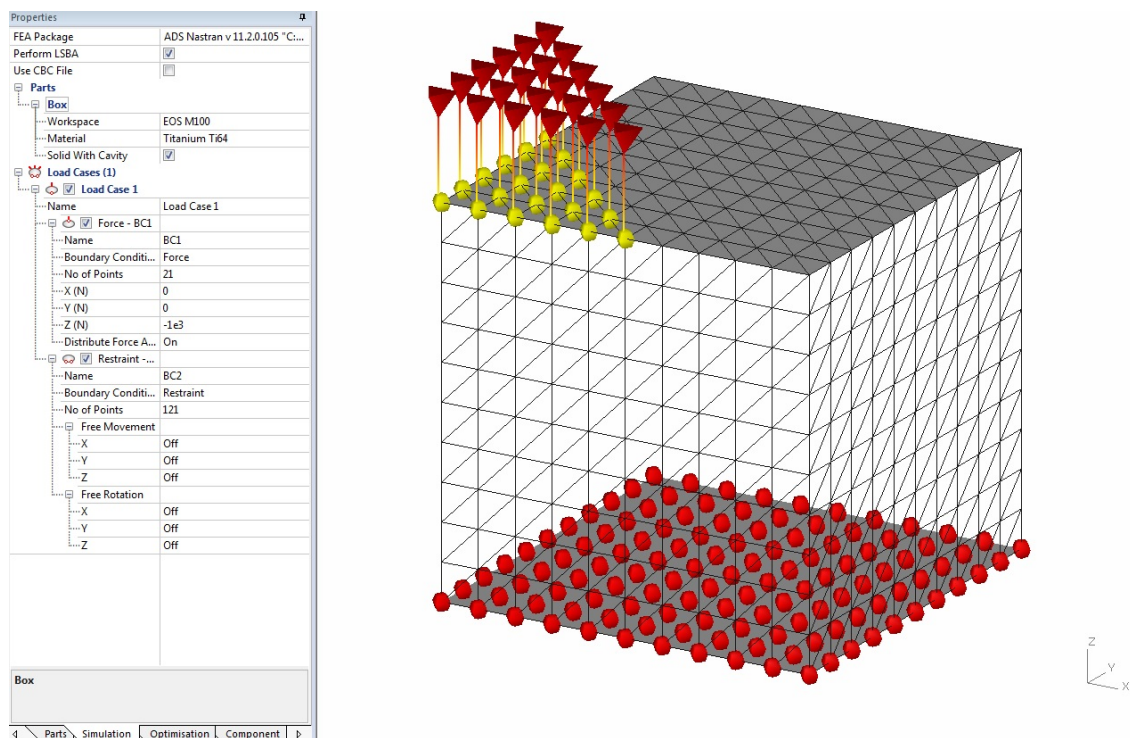


Figure 2.5: Load Case simulation of a Titanium Ti64 1000 mm^3 cube with a Fixed base and a $F_y = -1000 \text{ N}$ Concentrated Force, distributed on the selected nodes.

2. Printing time: inversely proportional to productivity, it highly influences the final product's cost;
3. Printing material: material mechanical performances and batch cost are key factors, the former during the following FW phase specifically while the latter contributes to the product's economical competitiveness.

Based on the aforementioned criteria, a simulated printing session was conducted on a 6 cm sample NACA 0021 blade chunk. The component printing was evaluated through FDM's *CatalystEX* and Polyjet's *Objet Studio* software. The blade was automatically oriented for both simulations, but since FDM favours vertical printing whereas Polyjet favours horizontal printing, both configurations were considered. The results are shown in Figs.2.9,2.10 for the FDM printer and in Figs.2.11,2.12 for the Polyjet. The chosen material for the FDM technology was ABS, whereas we considered VeroWhitePlus for the Polyjet. Both materials have comparable batch costs, but the former is given for a 1000 cm^3 cartridge and the latter for a 1 kg one. Considering similar support material costs as a simplifying approximation, calculations show that ABS material is about 3-to-4 times cheaper than VeroWhitePlus. Lastly, the Polyjet printer conducts frequent cleaning purges, especially when changing printing model material, thus gradually consuming up to 20% of the total cartridge; this mechanic is absent in the FDM apparatus.

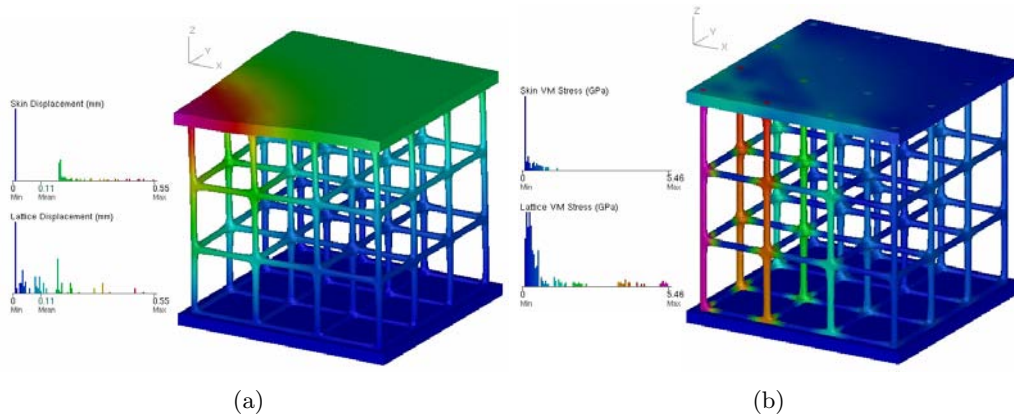


Figure 2.6: FEA results for a non-optimized 1000 mm^3 cube subject to a custom-defined Load Case, in terms of: (a) Displacement ; (b) Stress.

Combining advantageous material cost with FDM printing times about half the Polyjet ones, we chose FDM as AM mandrel printing technology and ABS as material.

2.4 CatalystEX - 3D Model Printing

The FDM printer chosen for the current work is the Stratasys Inc. *Dimension sst 1200es*, with a maximum printing volume of $254 \times 254 \times 305$ mm.

Starting the *CatalystEX* program, an .stl input file is required. The software interface includes many option, the most important of which are divided in four different tabs:

- General - part overview and printing properties selection, such as layer-support density plastic filament thickness;
- Orientation - control over part positioning inside the printing volume, as well as layer-by-layer visualization (once stl elaboration is completed);
- Package - part positioning on the 2D build tray and time/cost estimates in terms of printing and model/support material usage;
- Printer Status - review of printing process and status updating.

To successfully print the part, a procedure similar to the one shown in Figs.2.13-2.16 must be completed.

Before launching a building process, a few rules of thumb are:

1. *Support material costs almost as much as printing material*: parts should be oriented and designed so that support material volume is minimal. This benefits post-printing processes, effectively reducing extra times such as support material removal which may be comparable to the printing time itself;
2. *Printing is based on planar, horizontal layers*: mechanical properties of built part rely heavily on layer deposition (a vertically printed component will resist shear,

horizontal stresses worse than horizontally printed ones). Oblique, thin parts may also risk falling during printing, as the building tray is subject to relevant vibrations;

3. *Printing time depends on part orientation and build tray positioning*: a vertically FDM built part will take shorter printing times than a horizontally built one. Also, the top-right quarter of the build tray is the closest to the delivery nozzle, therefore positioning parts in that region will further cut the building times;

Once the part has been printed, it can be manually removed from the tray. The last step involves support material removal through a cleaning cycle inside an $H_2O + NaOH$ bath. The process is automatic and only requires appropriate time and temperature settings. An *SCA 1200* cleaning system was chosen as reference in this work.

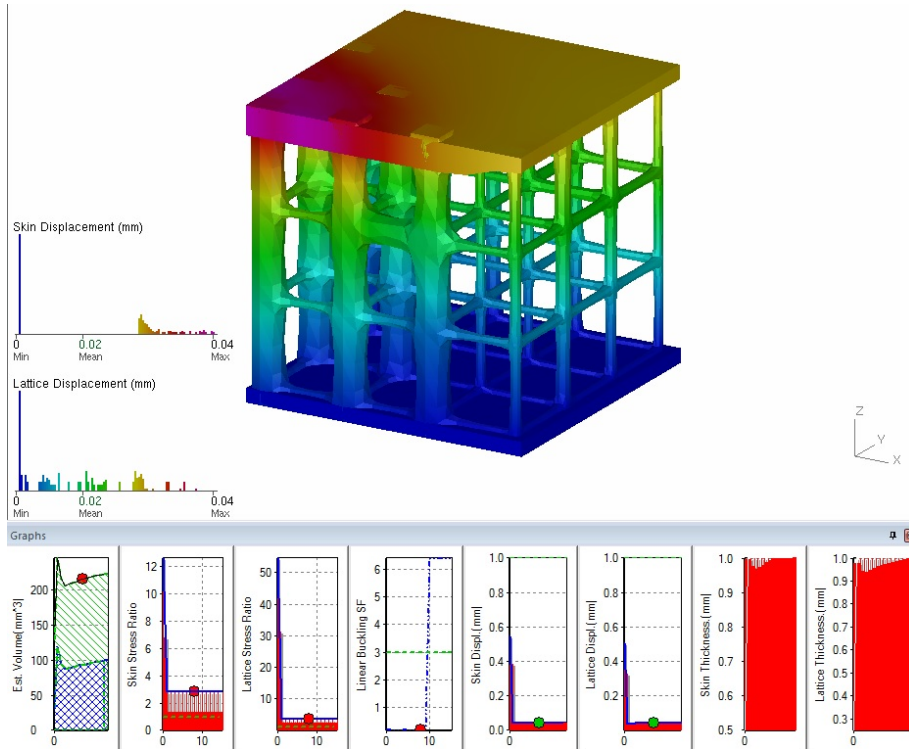
2.5 Preliminary Printing Test Cases

Before printing full-length blades, we tested out the FDM technology through small, 3 cm long NACA 0021 blade chunks. To evaluate the resulting printing quality as widely as possible, we considered both vertical and horizontal printing orientation, paired with a simple (8; 8; 10) mm Grid Topology Lattice structure. The chunks are made with 0.25 mm thick Skin and Lattice Beams, i.e. the smallest printing thickness available on the *Dimension sst 1200es* machine.

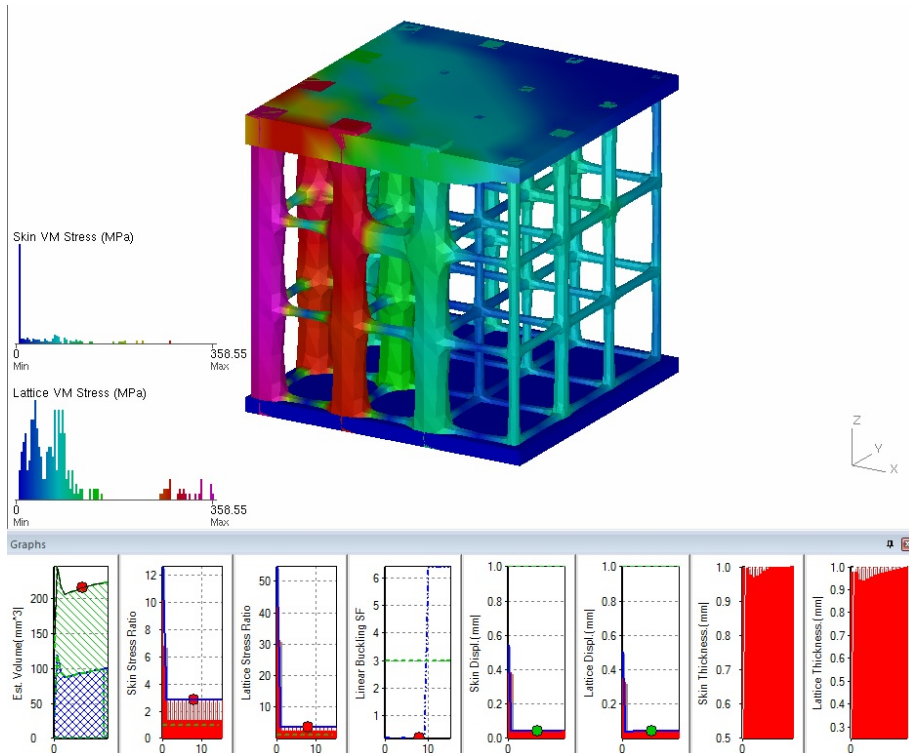
The .stl models were prepared via Netfabb Within, then imported in the *CatalystEX* software interface (Fig.2.17). An .stl elaboration followed, showing the Support material filling the entire internal volume of both chunks; in particular, the horizontally oriented one required even more for building the support base (Figs.2.18,2.19).

Fig.2.20 shows the two printed chunks. The left one, being horizontally printed, presents both Skin and Lattice thicknesses more adherent to the printing settings but at the same time its mechanical resistance is very low. On the contrary the right one, vertically printed, forced the printer to deposit a thicker layer (thus employing more volume) of model material; the support material volume is lower though, and the mechanical properties are much greater compared to the horizontal print.

Generally speaking, a vertical orientation is preferable for both resulting shape as well as total consumed material volume. Also, a Lattice is to be considered unfavourable for small-scale components because of excessive part filling.



(a)



(b)

Figure 2.7: Optimization process for a 1000 mm³ cube with Grid Lattice Topology. The results are shown in terms of: (a) Displacement; (b) Stress.

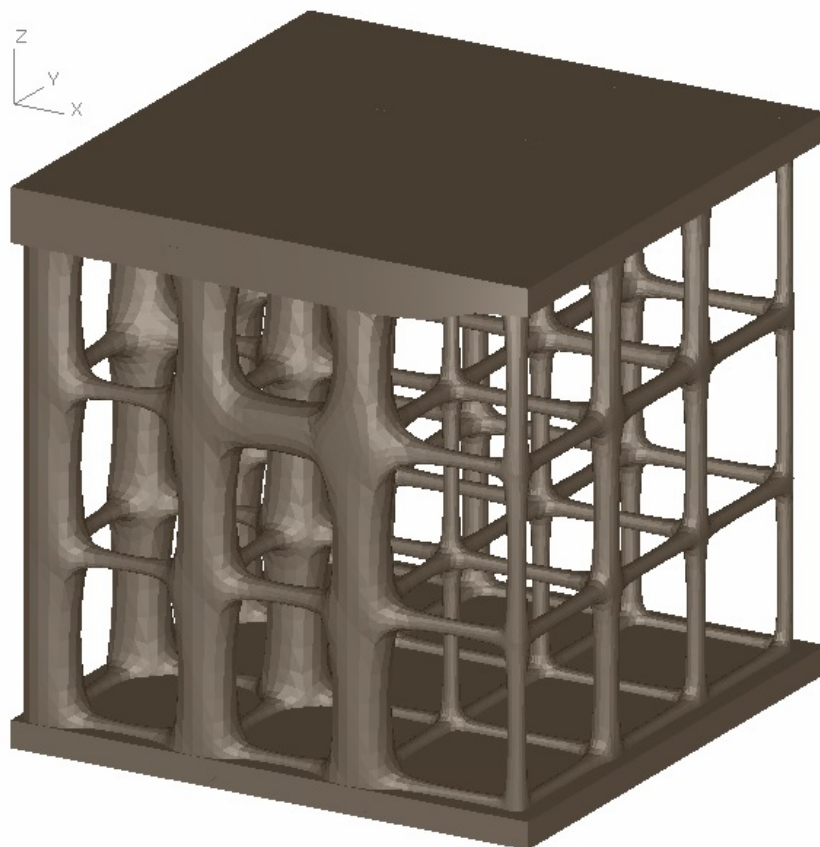


Figure 2.8: Titanium Ti64 1000 mm^3 cube with optimized Skin and Grid Lattice Topology. The FEA resulted in local thickening of Skin and Lattice rods to achieve the best structural performance in respect to the given Load Case. An Advanced Surface Trim and a Lattice Fine Smoothing were also selected.

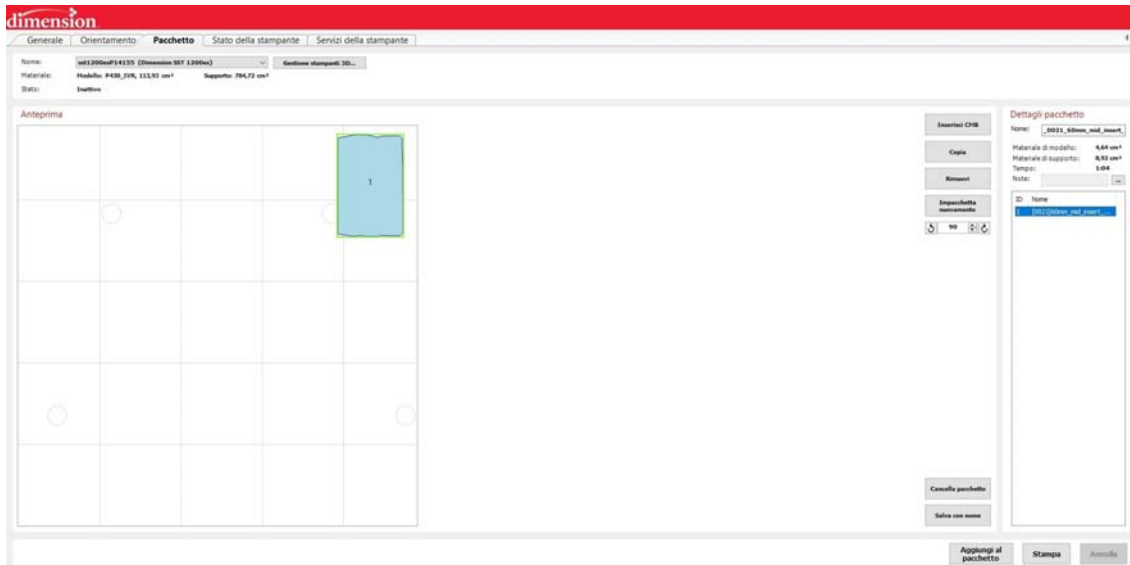


Figure 2.9: Simulation of a horizontally printed 6 *cm* sample NACA 0021 blade chunk through FDM technology - CatalystEX package information.

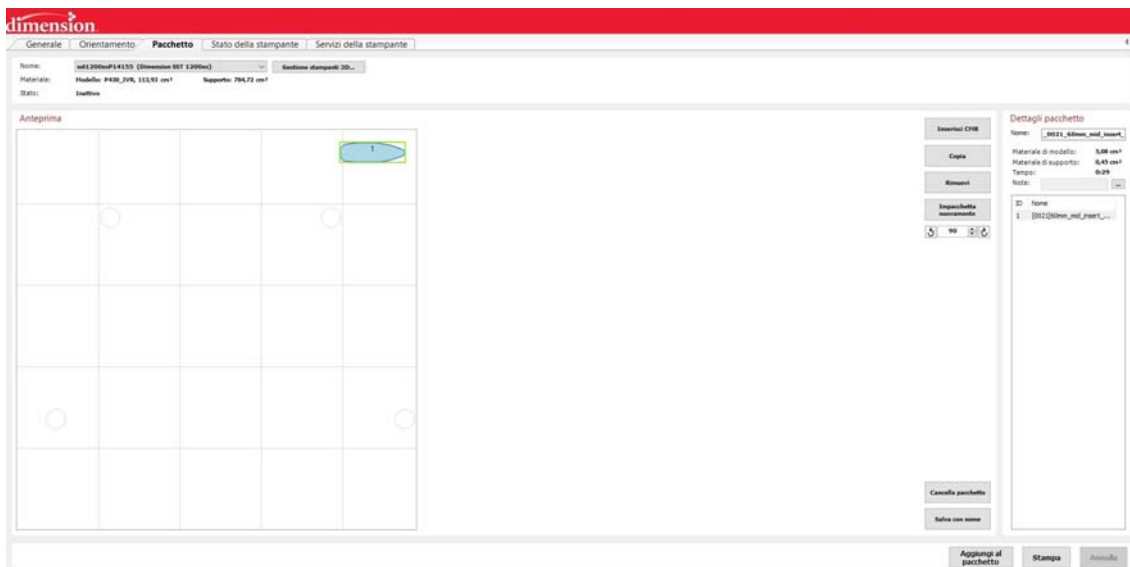


Figure 2.10: Simulation of a vertically printed 6 *cm* sample NACA 0021 blade chunk through FDM technology - CatalystEX package information.

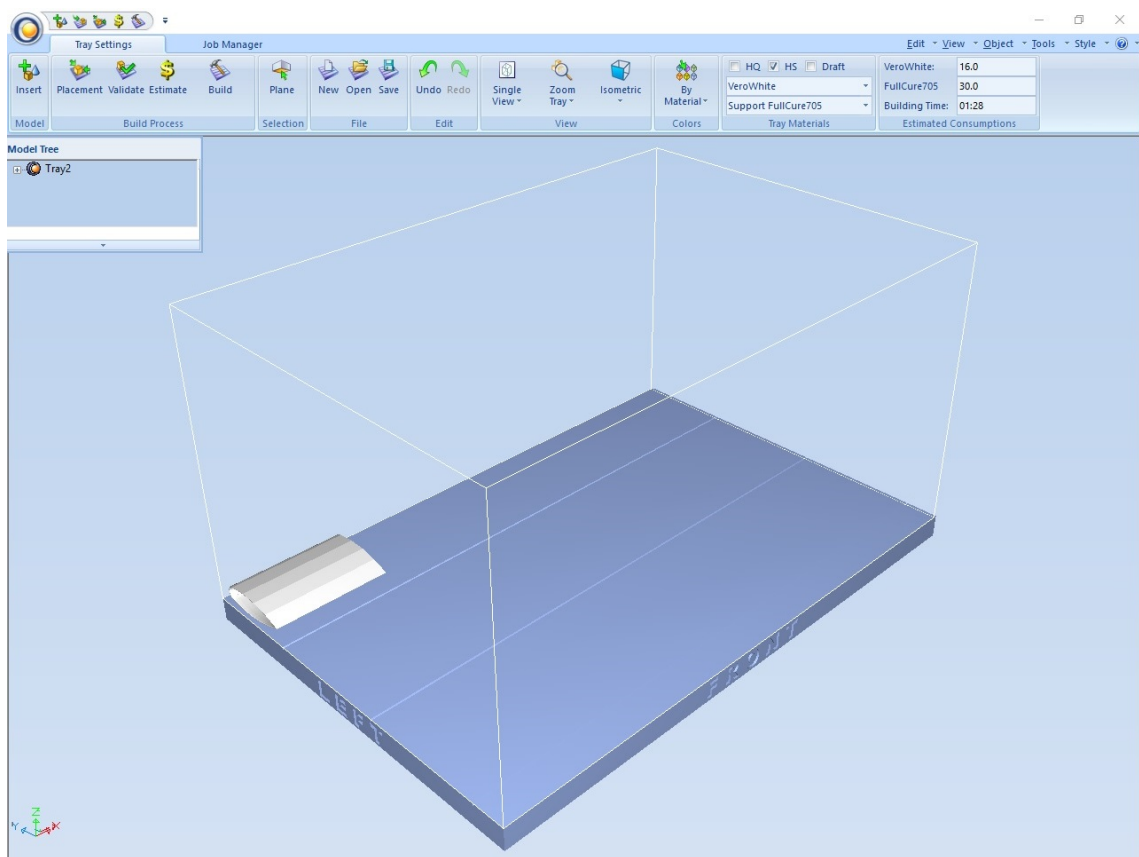


Figure 2.11: Simulation of a horizontally printed 6 cm sample NACA 0021 blade chunk through Polyjet technology - Objet Studio package information.

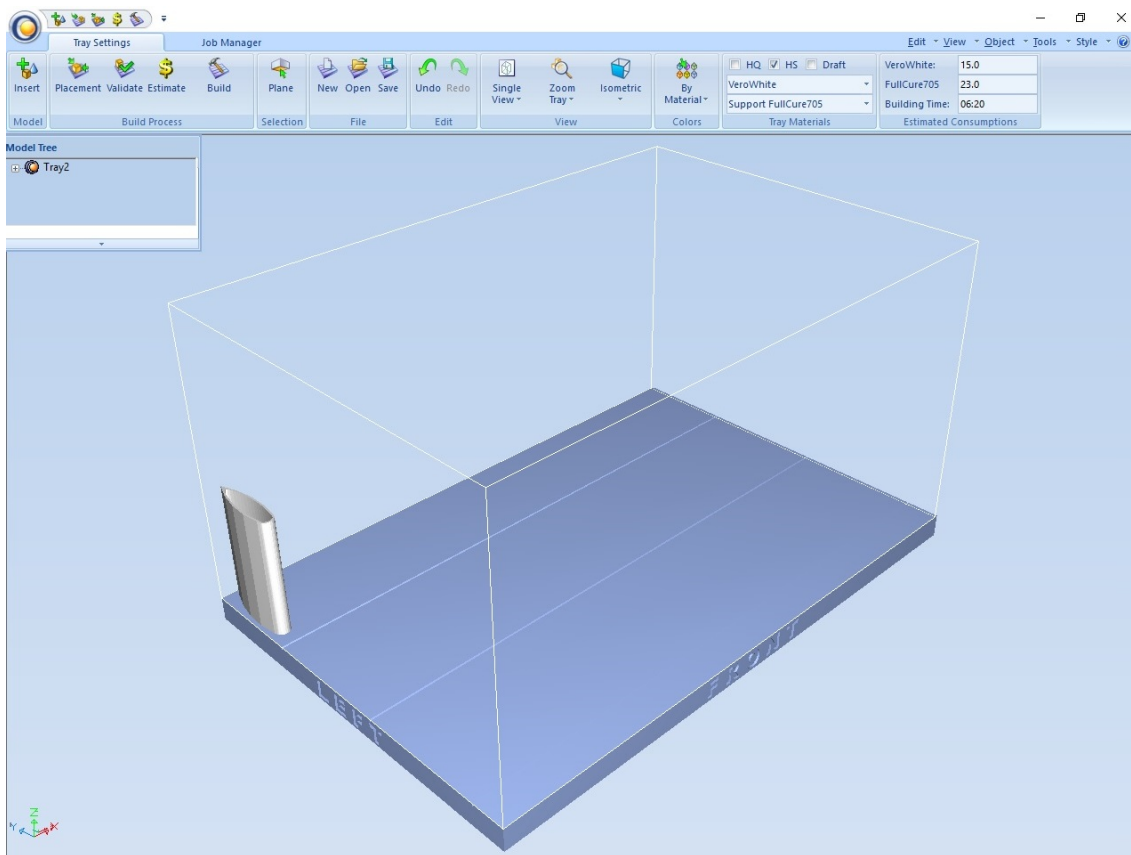


Figure 2.12: Simulation of a vertically printed 6 cm sample NACA 0021 blade chunk through Polyjet technology - Objet Studio package information.

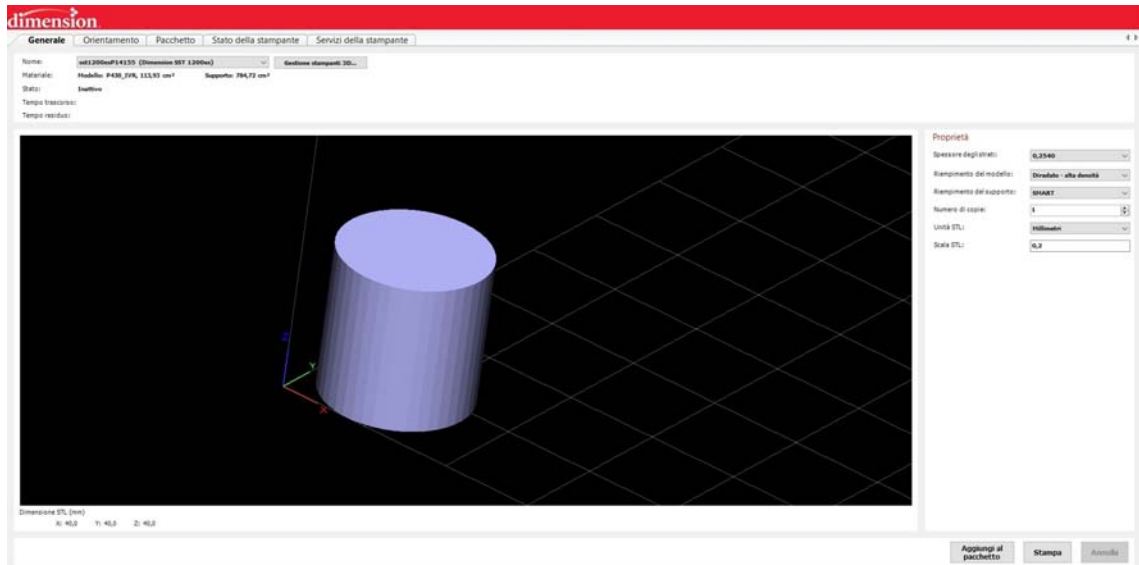


Figure 2.13: Printing procedure of a sample cylinder with radius $r = 10 \text{ mm}$ and height $h = 20 \text{ mm}$ - CatalystEX Software General tab.

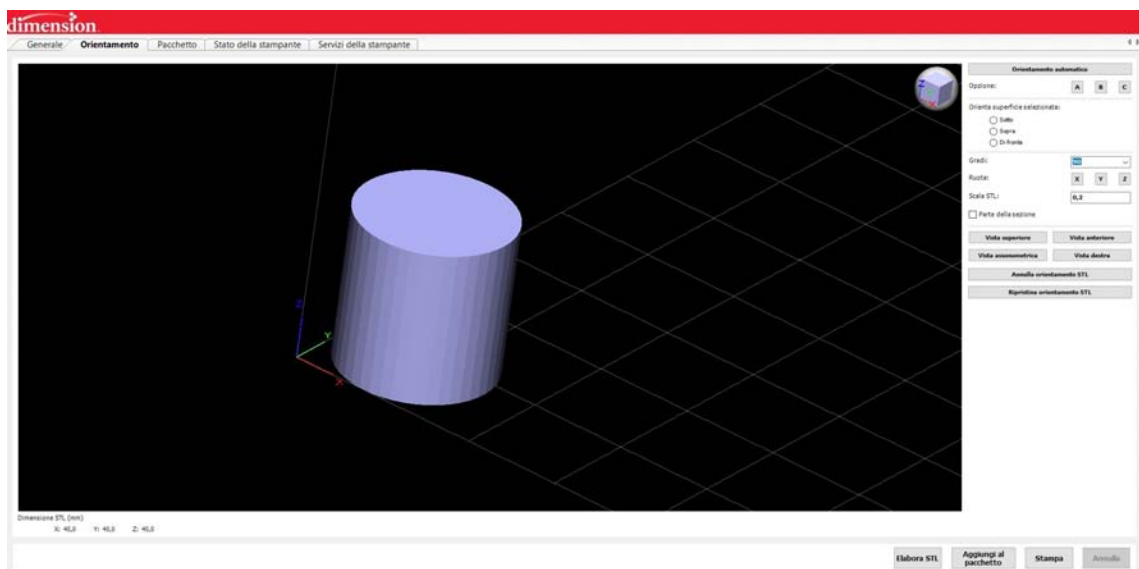


Figure 2.14: Printing procedure of a sample cylinder with radius $r = 10 \text{ mm}$ and height $h = 20 \text{ mm}$ - CatalystEX Software Orientation tab.

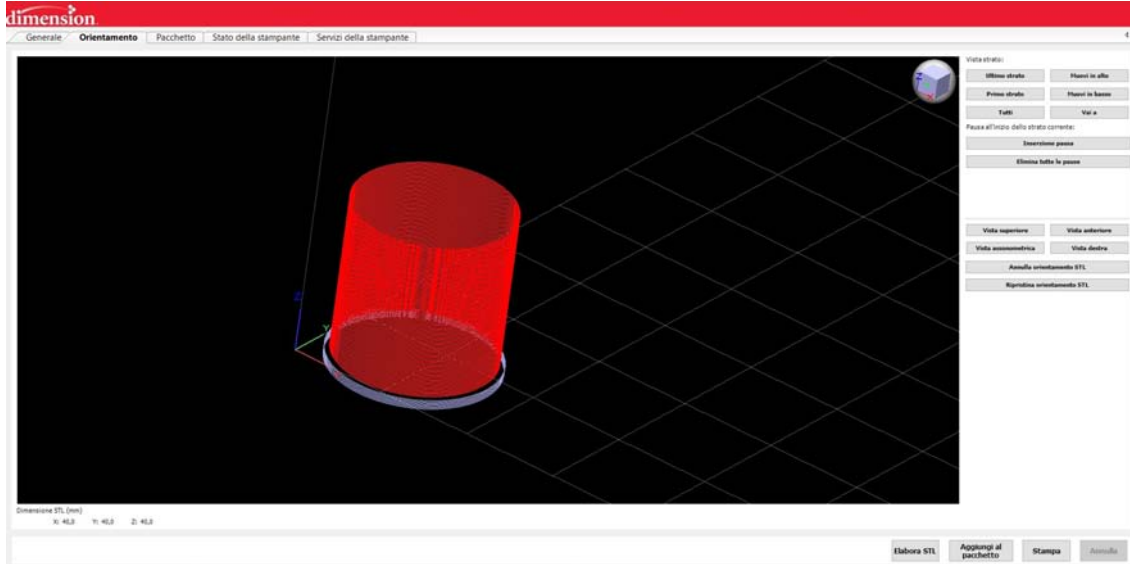


Figure 2.15: Printing procedure of a sample cylinder with radius $r = 10 \text{ mm}$ and height $h = 20 \text{ mm}$ - CatalystEX Software Orientation tab with .stl elaboration.

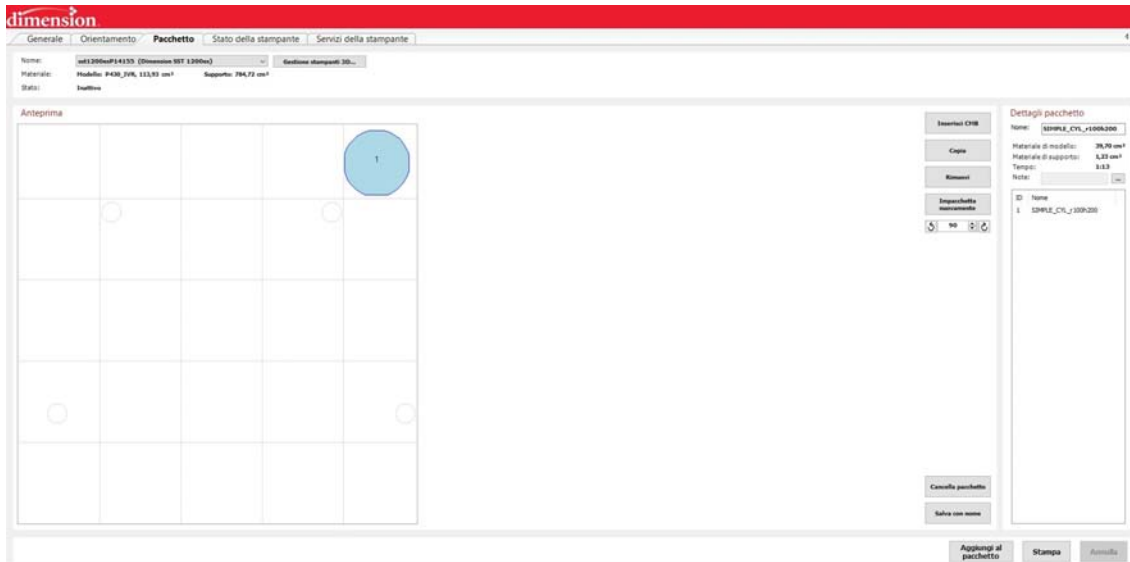


Figure 2.16: Printing procedure of a sample cylinder with radius $r = 10 \text{ mm}$ and height $h = 20 \text{ mm}$ - CatalystEX Software Package tab.

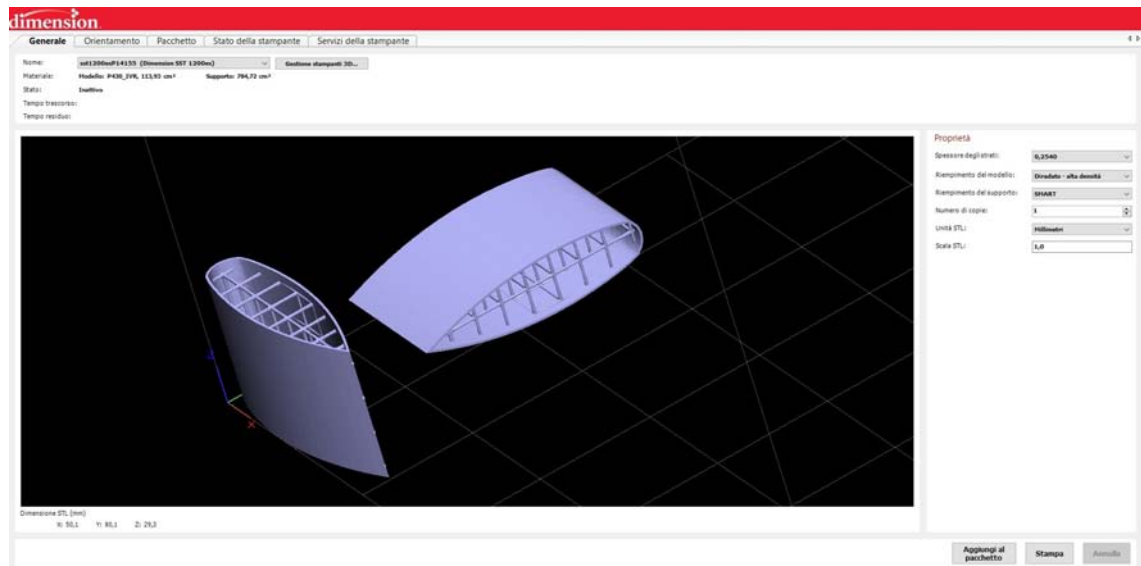


Figure 2.17: Imported .stl models of two 3 cm long NACA 0021 blade chunks. The components are built with a (8; 8; 10) mm Grid Topology Lattice structure and 0.25 mm thick Skin and Lattice Beams. Both horizontal and vertical orientations were considered.

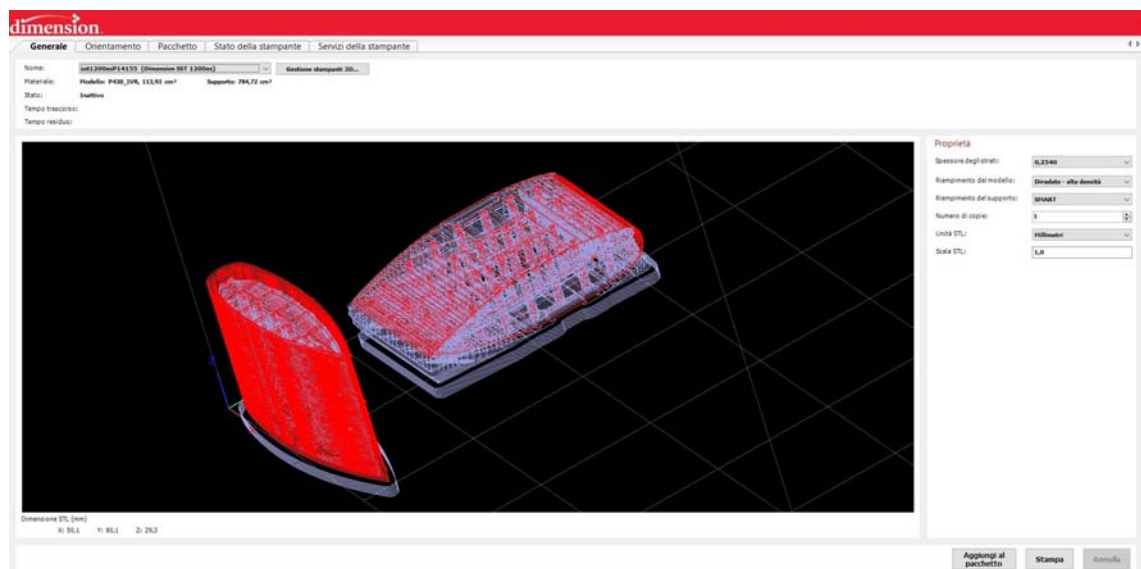


Figure 2.18: Elaborated .stl models of two 3 cm long NACA 0021 blade chunks. The components are built with a (8; 8; 10) mm Grid Topology Lattice structure and 0.25 mm thick Skin and Lattice Beams. Both horizontal and vertical orientations were considered.



Figure 2.19: Printing package of two 3 *cm* long NACA 0021 blade chunks. The components are built with a (8; 8; 10) *mm* Grid Topology Lattice structure and 0.25 *mm* thick Skin and Lattice Beams. Both horizontal and vertical orientations were considered. A great amount of Support material is required, about twice the Model material volume, because of horizontal configuration and Lattice structure.

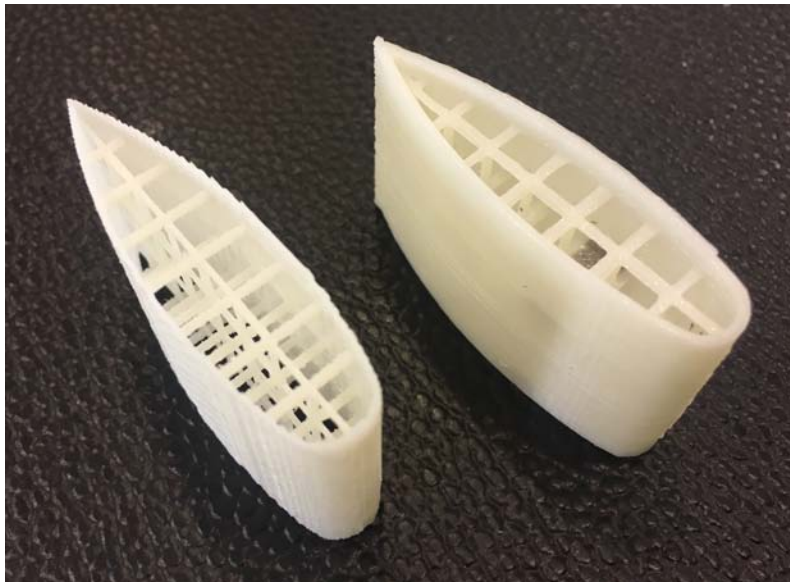


Figure 2.20: Printed 3 *cm* long blade chunks. The components are built with a (8; 8; 10) *mm* Grid Topology Lattice structure and 0.25 *mm* thick Skin and Lattice Beams. Both horizontal (left) and vertical (right) orientations were considered.

Chapter 3

Blade Filament Winding

The aim of the current work is to illustrate an affordable yet reliable blade manufacturing process chain, employing non industrial-level machinery. The Filament Winding apparatus normally represents a huge capital investment, therefore the *X-Winder* - a Desktop Filament Winder - was chosen for its good degree of product quality paired with a reduced initial investment [19].

This chapter is meant as a guide describing the machine and software employed (detailed functionalities, material and supplies requirements), as well as presenting a simple step-by-step winding procedure.

3.1 Machine Building and Functionalities, Supplies Requirements

A FW machine works with a dry spool of fibers, wetted in a resin bath and positioned on a rotating mandrel. This is achieved through coordinated machine movements, controlled by a series of axis. The *X-Winder* comes in two configurations: 2-axis “2X-23” and 4-axis “4X-23”. The former, being the cheapest and simplest, allows for axial-symmetrical parts winding only; the latter represent the direct evolution of the 2-axis version, employing a Delivery Head for two additional degrees of freedom (forward/backwards translation, CW/CCW rotation): this widens the winding capabilities of the machine, including polar and hemispherical parts. For the current work’s scope, a 2-axis model would suffice; we chose the 4-axis nonetheless, favouring greater geometric versatility. A detailed list of the 4-axis model specs is shown in Fig.3.1.

The apparatus is divided in several parts, each with specific functions:

Fiber spool and traction system - dry fibers (e.g. GF, CF) to be wetted in the resin bath and delivered to the rotating mandrel. The latter pulls the fibers and in doing so is aided by a roller and compressed springs;

Resin bath - plastic container for thermoset resin (e.g. epoxy), previously mixed with appropriate hardener (e.g. formulated amine). A series of roller and a pressing steel blade help removing excess resin from the fibers, while passing them straight to the delivery head;



4-AXIS MODEL 4X-23

\$3,795.00

Weight:
56.00 LBS

PRODUCT DESCRIPTION

4X-23 Specs:

- **Frame and Carriage:** standard 1" aluminum extrusions
- **Length:** up to 20 feet (3m) - Long Bars **NOT** Included (see [Long Bars](#))
- **Mandrel width:** up to 8" (200mm) in width
- **Mandrel Max. RPM:** 90
- **Carriage Max. Speed:** 8in/s (200mm/s)
- **Electrical Power:** 110v/220v AC with 24V/3A DC to the stepper motors
- **Mandrel & Carriage Motors:** geared NEMA 23 stepper motors with 800 oz-in (60 kg cm) holding torque
- **Delivery Head Motors:** geared NEMA 17 stepper motors with 250 oz-in (20 kg cm) holding torque
- **Drive Belts:** "L" type 1/2" (12mm) wide for carriage and mandrel and "XL" belts for delivery head
- **Filament Tension:** adjustable strap friction mechanism
- **Reel Holder:** single reel standard or dual reel option (see [dual reel](#))
- **Resin Bath:** 6 fluid ounce resin bath (170 cc*3)
- **Carriage Wheels:** custom dual bearings with 8mm axle
- **Electronics:** switch controller box and 4 axis controller boxes with USB cables (not sold separately)
- **Software:** X-Winder Designer program and Executor software packages standard (not sold separately)

Note: X-Winder ships with "L" size belt of 18 feet (5.6m) long - enough for about an 8 foot long (2.5m) X-Winder. For additional length, you'll need a [longer L-Belt](#).

Figure 3.1: List of X-Winder 4-axis "4X-23" winding machine model.

Rotating mandrel - the first axis supporting the wound component, rotating and pulling the fibers from the spool. In the current work, the mandrel is custom-made and is a product of the AM phase illustrated in Chapter 2;

Linear carriage - the second axis, translating back and forth covering the part's length during winding process. It is mounted on aluminum bars of arbitrary length;

Delivery head - the third and fourth axis, it manages the winding angle and distance from the mandrel. It ends with a freely rotating concave roller guiding wet fibers deposition according to the process parameters.

The *X-Winder* apparatus comes with a default steel DH roller. To enhance and better control the fiber delivery though, especially at angulated turns by the mandrel tips, a custom-designed DH roller may also be designed and printed. In comparison to the default one, the printed roller would be more concave: smaller middle section, larger tip sections. Two sample DH rollers were tested and are shown in Fig.3.2 close to the default steel one for better comparison. The rightmost one was later employed for VAWT blade winding.

The mounted machine, a detailed view of the 4-axis control system and stepper motors (with limit switches) are shown in Figs.3.3,3.4,3.5.

The supplies required for a typical winding session are shown in Fig.3.6. Though only the fiber spool and the resin are needed for the actual part manufacturing, the rest of the supplies help achieving a better part quality: the heat gun enhances the curing process of the wound part and, together with the heat shrink tape, provides the best results in term of superficial quality and fiber-to-resin ratio (removing excess resin from the part during



Figure 3.2: DH rollers - from left to right: (i) default Steel roller; (ii) customly printed roller with approx 50% reduced middle section and same tip sections, compared to the default one; (iii) customly printed roller with approx 50% reduced middle section and double tip sections, compared to the default one.

shrinkage). Cash register and cellophane tapes allow for multiple usage of a removable mandrel, effectively separating the wound part from the latter, while also maintaining a good internal surface quality of the finished product.

3.2 X-Winder Software Description

The *X-Winder* product comes with a built-in software which is articulated in 2 autonomous, consequential programs:

Designer - graphically guides the design of a wound part through numerous pre- and post- winding phases (such as pre-wrap and heat gun curing) and parameters. It generates an output *G-code* file to be processed in the Executor program;

Executor - works both in manual control and with a *G-code* input file. It allows control over the winding phase via graphical winding interface, process start/stop/pause buttons and step-by-step *G-code* log visualization;

Inside both programs, the user may define various Settings which are required before starting a winding session. The *Designer* interface is particularly straight-forward, as Fig.3.7 shows for a 3-Axis Winding configuration. The window can be divided in 4 major sub-sections which include many different process parameters:

- Left: measurement unit selection (inches, millimeters), 2- and 4-axis (3 sub-configs) winding configurations, number of layers, filament width and thickness, winding rate;

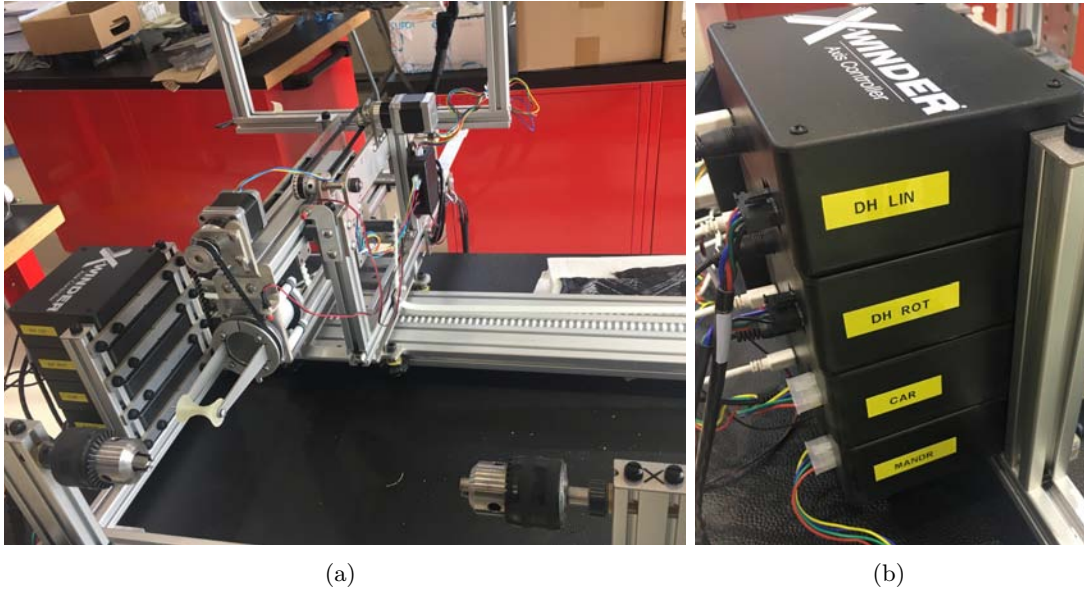


Figure 3.3: (a) Mounted 4-axis Filament Winding machine utilized in the current work and (b) Axis electronic control system, with corresponding labels.

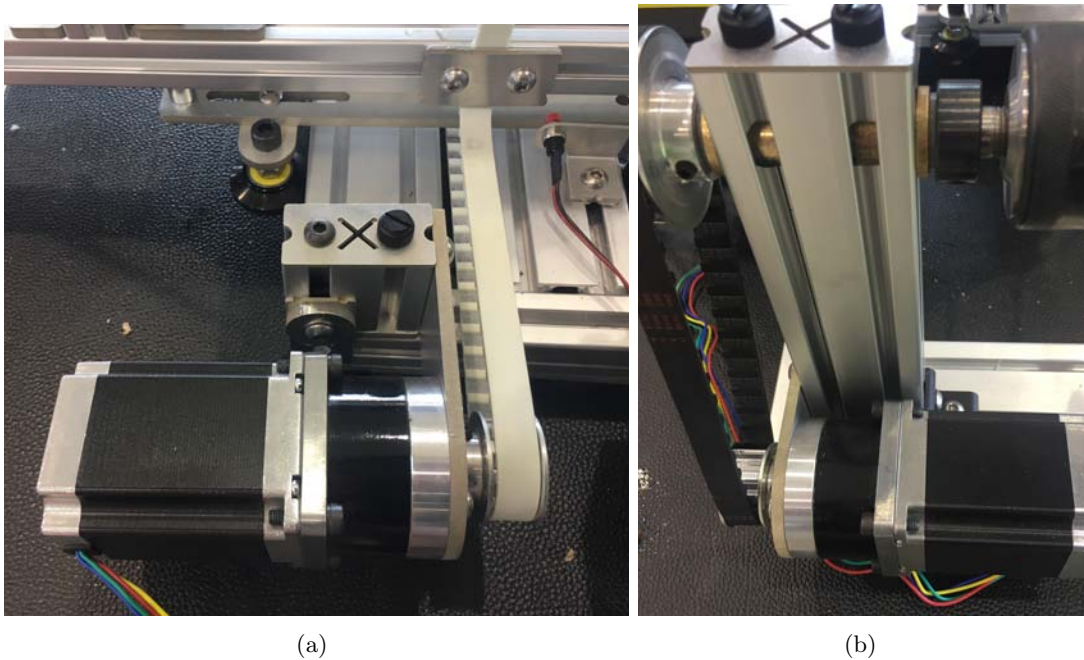


Figure 3.4: Detailed view of mounted NEMA 23 stepper motors with 60 *kg* holding torque: (a) carriage stepper. A limit switch is also mounted for carriage linear path control; (b) mandrel stepper.

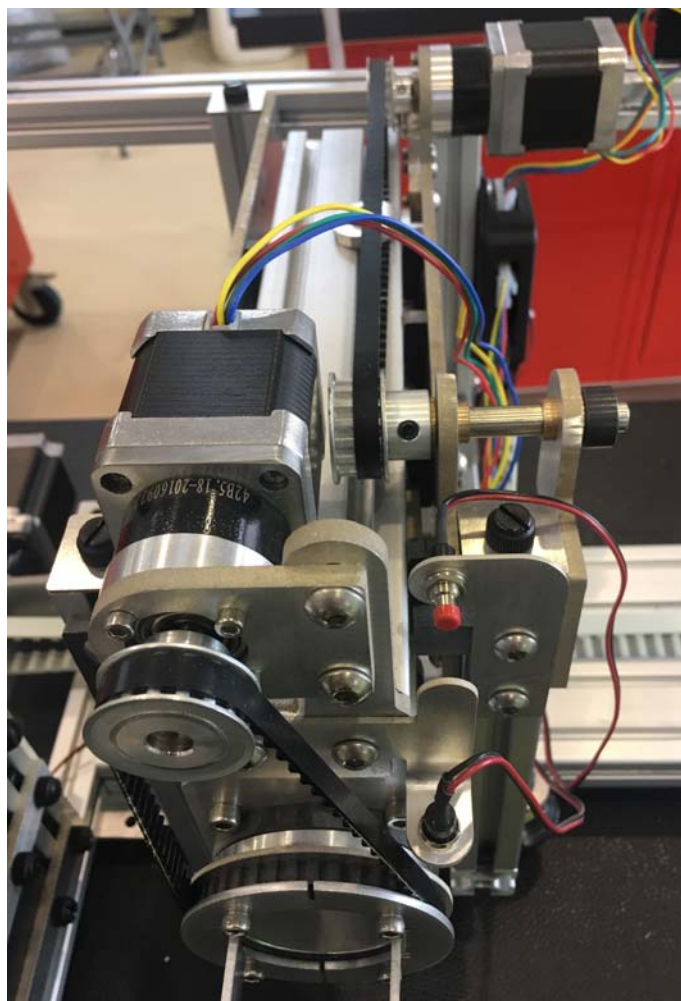


Figure 3.5: Detailed view of mounted Delivery Head linear and rotary NEMA 17 stepper motors with 20 *kg* holding torque. Two limit switches are also mounted for DH linear and rotary path control.

Supplies		
	<p>Various Tapes Cash Register Tape, Packing Tape, Cellophane Tape, Elec. Tape</p>	<p>Office Supply Store Hardware Store</p>
	<p>Heat Gun + Paper Towels ~ 1,500 Watt Heat Gun and Wet Wipes or Paper Towels</p>	<p>Office Supply Store Hardware Store</p>
	<p>Epoxy Resin and Hardener West Epoxy, AeroPoxy, EZ-Poxy, etc. with Pot Life Greater Than Build Time</p>	<p>Composite Supply Store</p>
	<p>High Tensile Strength Continuous Filament</p>	<p>ACPComposites, Zoltek, eBay Vendors, Ixperial, BasaltFiberWorld, Haufler and Many Others</p>

Figure 3.6: Required supplies for a basic winding session yielding a high-quality component.

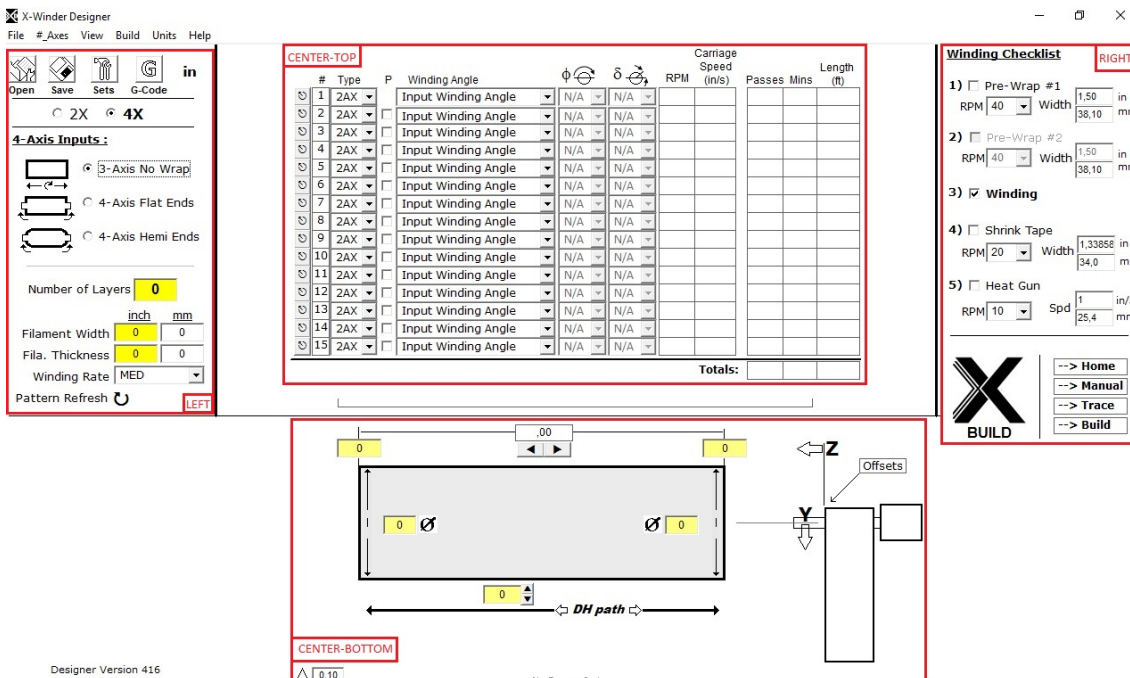


Figure 3.7: X-Winder Designer Software UI - 3-Axis Winding configuration. The four sub-sections are marked and labeled.

- Center-Top: layer-by-layer settings in terms of type (2-axis, hoop), ϕ and δ angles (4-axis mode only), mandrel RPM and carriage speed, number of passes/minutes/filament length required for layer processing;
- Center-Bottom: graphical UI for geometrical mandrel settings, including tip diameters, z-coordinates, DH path and polar winding parameters (4-Axis only);
- Right: Winding controls (BUILD, Home, Manual, ...) and phases checklist with corresponding figures, i.e. mandrel RPM, tapes width, carriage speed;

Each space must be filled for proper winding, the only exception being the optional DH path. The mandrel section needs not be circular: *X-Winder* is able to wind around many geometrically different sections, in which case ϕ in the Center-Bottom UI must be calculated as *equivalent diameter*: $\phi_{eq} = \frac{2p}{\pi}$, where $2p$ =perimeter of the section.

During several test cases, few software bugs were discovered¹:

- Too small mandrel diameters (lesser or about 10 *mm*) are incompatible with the machine algorithms and will yield unforeseeable results;
- The millimeters measurement unit will sometimes fill the UI figures spaces with random, physically impossible numbers;
- Low mandrel speeds (< 5 *RPM*), combined with low carriage speeds (< 1 *in/s*), stop the carriage itself from moving but do not stop the mandrel from rotating;

To avoid such process-breaking problems, it is advised to employ the inches measurement unit, to work with mandrels with diameters larger than 1 *in* and run carriage speeds above > 2 *in/s* and mandrel rotation speeds above > 5 *RPM*.

When the Design phase is completed correctly, the *Totals* row will show the estimated summary of Passes, Minutes and Length (ft) required for the winding process. A *G-code* file can also be visualized and modified.

The *Executor* interface is simpler than the *Designer* one, as the former only needs to launch an input *G-code* file (*Designer*-made or custom-made). Fig.3.8 shows the interface and three major sub-section of the *Executor* program:

- Center-Top: Hardware and Limit Switch checking lights, paired with corresponding Control System Board ID number;
- Center-Bottom: graphical UI visualizing linear carriage position and speed as well as mandrel RPM. An highlighting process checklist is also available;
- Right: *G-code* line log visualizer;

Before launching any process, a small Motor Amperage Setting window must be opened ("A" button on Fig.3.8), set and verified compatibly with the employed stepper motors. The correct maximum amperage must be determined in order not to prematurely overheat the motors and compromise the winding process.

¹Verified for Designer 416 version.

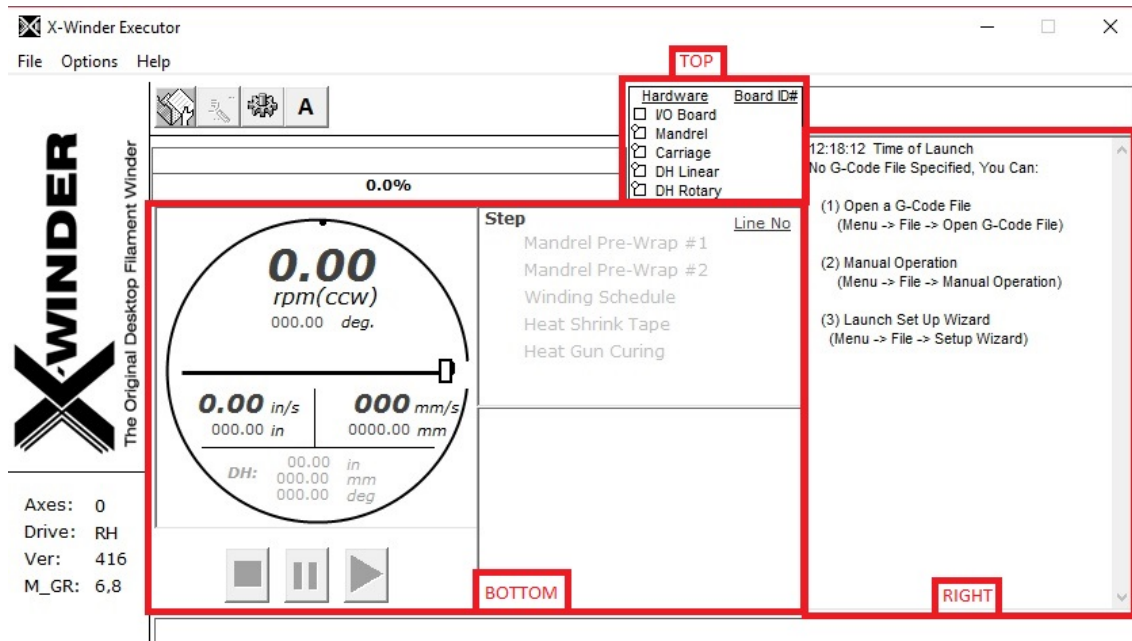


Figure 3.8: X-Winder Executor Software UI. The three sub-sections are marked and labeled.

3.3 G-code File Analysis

This section illustrates the most important *G-code* commands that are usually generated by the *Designer* program and that may require user modification, in case of customly tailored winding operations. Three tables summarize a group of commands and their corresponding description.

Table 3.1 shows the first group of commands, involving *Machine Setup* non-movement type commands.

Command	Description
[...]	Comment, ignored by executor
D0	Comment followed by data (layer, winding angle, ...)
CC1, CC0	Decimal format (comma) EU, English standard
G20, G21	Inches (in) and millimeters (mm) measurement unit
G28	Send "Home" (to Limit Switch)
G90	Absolute Positioning
M711H...M...S...	Estimated Time of Operation in hours, minutes, seconds
M17, M18	ables (current, voltage) or disable motor steppers
XV...T2(T4)Z...	Software Version, Winding Type (2-axis, 4-axis), z-offset

Table 3.1: Machine Setup, non-movement G-code commands.

Table 3.2 shows the next group of commands, dealing with layer-building movement commands. Some of these commands (marked here with a *) are coordinated, so that everything following them will be executed at the same time. This is particularly important for 4-Axis winding.

Command	Description
<i>G1</i>	Linear (x, y, z) non-coordinated movement
<i>G4</i>	Pause/Carriage hold position, waiting next command
<i>G2</i>	(*) DHL and carriage move towards mandrel with CW rotation on DH polar ellipses path
<i>G5</i>	(*) DH moves away from mandrel with CCW rotation
<i>G3</i>	(*) DHL and carriage move towards mandrel with CCW rotation on DH polar ellipses path
<i>G6</i>	(*) DH moves away from mandrel with CW rotation
<i>M0</i>	Pause Executor and wait for Resume button pressing
<i>M5</i>	Mandrel stop

Table 3.2: Layers Processing, movement G-code commands.

G2 – *G5* and *G3* – *G6* commands are coupled, as they represent the forward/backward movements of the DH on its polar elliptic path.

Table 3.3 does not show commands, instead illustrates the Letter Designation of instructions following commands of Table 3.1 and 3.2.

Geometric Entity	x-axis	y-axis	z-axis
Position ($[in]$, $[mm]$)	X	Y	Z
Linear Rate ($[in/s]$, $[mm/s]$)	D	E	F
Linear Acceleration ($[full/100]$)	I	J	K
Angle ($[^\circ]$)	A	B (DH)	C (mandrel)
Angular Rate ($[RPM]$)	Q	R	S
Angular Acceleration ($[full/100]$)	N	O	T

Table 3.3: Letter Designation in a G-code file.

The A letter may also designate the cumulative mandrel angular rotation. In such case, the letter will be located at the end of the row, before a [...] command. Lastly, both the Angle and the Angular Rate represent positive quantities and follow the Right-hand rule.

3.4 Winding Materials Choice

As previously illustrated (Fig.3.6), many fiber rovings are commercially available and usable in a winding session. Among those, VAWT blades typically employ Glass or Carbon fibers for excellent specific mechanical properties. The former are the cheapest solution and the most widespread; the latter represents top performances at a higher cost.

Considering that the VAWT analyzed in the current work is a small-scale one, we favoured the Glass fibers for reduced cost combined with satisfying performances. Tab.3.4 shows

typical 2400 tex GF roving properties. As a pairing resin material we chose a mixture of *Epoxy* and *Formulated Amine* (100:25 ratio). The choice criteria is yet again that of typically employed VAWT composite blade materials. Tab.3.5 summarizes the resin mixture properties.

Property	Value
Tensile Strength [<i>MPa</i>]	2700 – 2900
Tensile Modulus [<i>GPa</i>]	86 – 89
Density [<i>kg/m</i> ³]	2580
Filament Diameter [μ <i>m</i>]	17
Tensile Strength @ $V_F = 60\%$ [<i>MPa</i>]	1120
Tensile Modulus @ $V_F = 60\%$ [<i>GPa</i>]	46
Transverse Tensile Strength [<i>MPa</i>]	30
Interlaminar Shear Strength [<i>MPa</i>]	64

Table 3.4: 2400 tex GF- Main physical and mechanical properties of fiber (upper part) and epoxy infused roving (lower part).

Property	Value
Density [<i>g/ml</i>]	1.10
Viscosity [<i>mPas</i>]	450
Pot Life (150 <i>g</i>) [<i>min</i>]	30
Gel Time (150 <i>g</i>) [<i>min</i>]	40
Exothermal Peak [$^{\circ}$ <i>C</i>]	220
Tensile Strength [<i>MPa</i>]	67.2
Elongation at Break [%]	9.3
Linear Shrinkage [%]	0.08
T_g [$^{\circ}$ <i>C</i>]	93

Table 3.5: Epoxy Resin + Formulated Amine 100:25 mixture - Main physical and mechanical properties.

3.5 Step-by-Step Winding Session Description

A generic winding session is divided in different steps, which will be briefly described in this section.

STEP 1 - Settings Preliminary settings are the basic of a quality winding and must be set correctly before proceeding. They come in different tabs, which are found both via *Designer* and *Executor* programs.

The first tab, as shown in Fig.3.9, is the *General* one, including global parameters that involve both winding and pre-/post- processes. The most important parameter is the Linear Carriage moving speed.

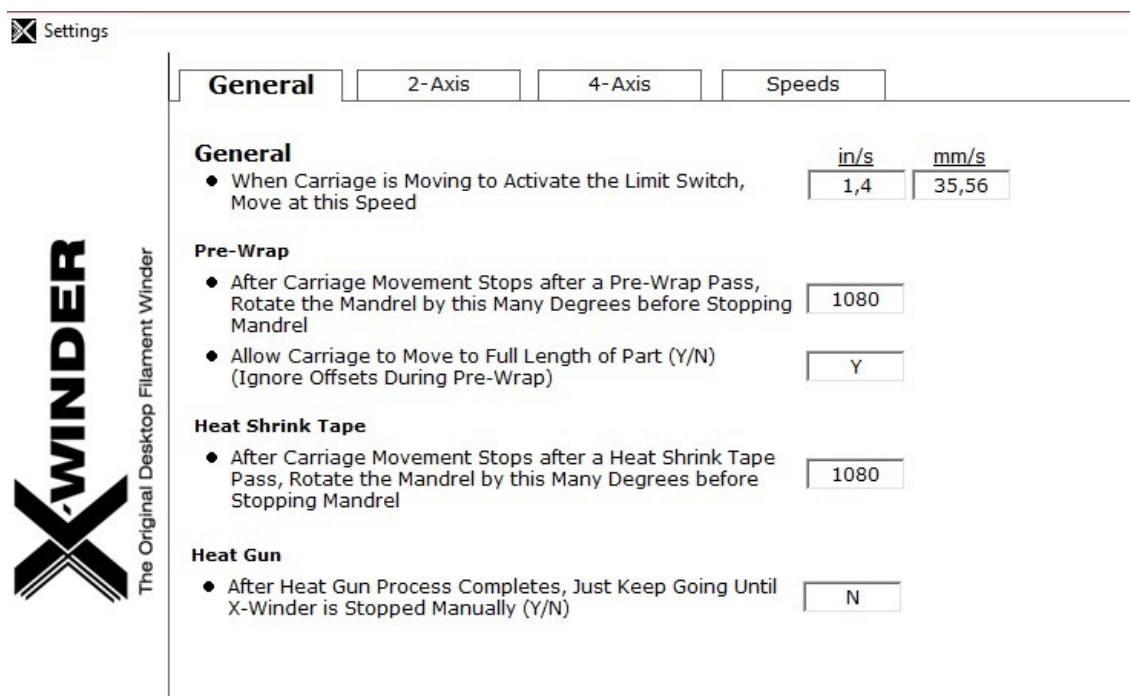


Figure 3.9: X-Winder Settings window - General settings tab.

The following two tabs, namely *2-Axis* and *4-Axis* (Fig.3.10), are crucial for a proper winding. Fig.3.10 shows the 4-Axis tab and its parameters that, once set, automatically fill the 2-Axis tab which represent a subset of the 4-Axis one. The *Geometry* parameters are the most important figures, allowing the winding machine to correctly consider the geometrical distances of interest: (i) DH distance from mandrel central axis; (ii) DH total width; (iii) DH mid-section z-axis offset from the mandrel post.

To determine such parameters, the machine default reference frame must be considered: *z-axis* corresponding to the mandrel central axis, pointing away from the mandrel motor; *y-axis* pointing orthogonally from the mandrel central axis to the DH; *x-axis* completing the frame; center point located at the mandrel post start.

The last tab deals with the *Speeds* settings, as in Fig.3.11. Both the mandrel and carriage speeds can be chosen in terms of 3 configurations: Slow, Medium, Fast. Having greater speeds allows for shorter winding sessions, therefore shorter overall manufacturing times, but it also implies higher electricity costs and heavier motor loading (i.e. they tend to overheat faster). Lastly, slower process speeds allow better control over the winding phase.

STEP 2 - Designer software Following Section 2, the *Designer* program is now run. All material (filament), mandrel (geometry, layers) and pre-/post- phases parameters (speeds) must be set. A *G-code* output file is produced and may also be manually

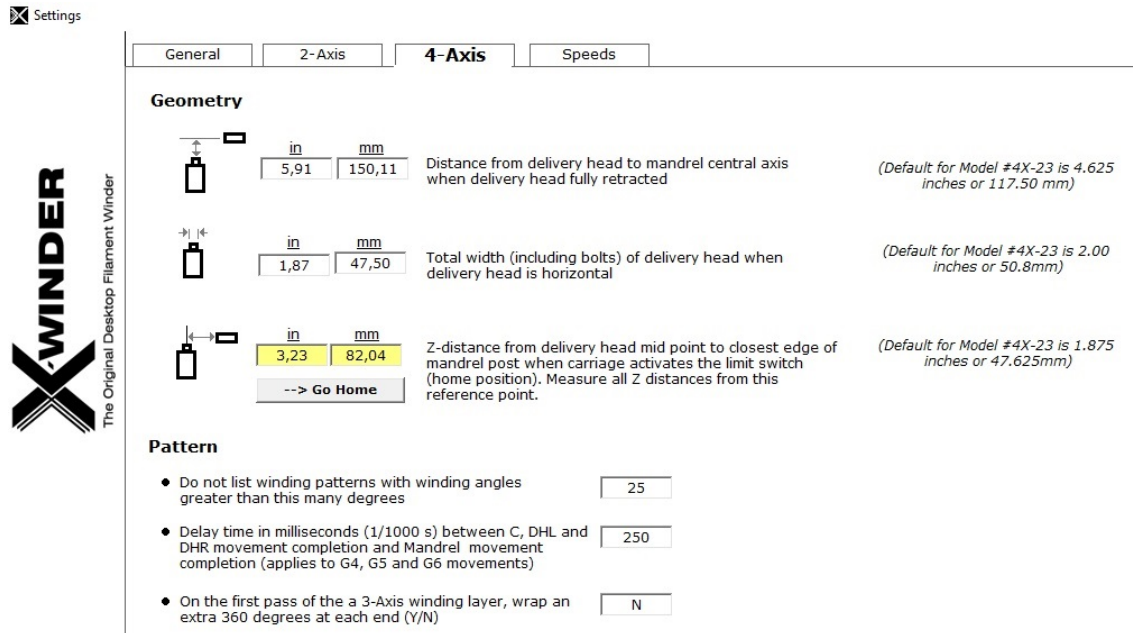


Figure 3.10: X-Winder Settings window - 4-Axis settings tab.

modified before the next step.

STEP 3 - Machine setup Before running the *Executor*, the *X-Winder* machine must be prepared. This involves a few elements:

- Filament/supply material: the spool should be mounted and the tip guided through the delivery plastic cylinders right before the resin bath zone;
- Mandrel: may need cash register and cellophane pre-wrapping (manual or automatic), in case of post-curing extraction;
- Resin bath: the chosen resin should be mixed with its hardener at appropriate ratio; after a few minutes, the mixture should be poured insides the plastic resin bath.

Lastly, the filament tip should be wetted in the resin bath and passed through the plastic cylinders, fixing it at the mandrel with at least one revolution. This will guarantee a correct Winding Angle at process start.

It is important to have the filament pulled enough to adhere to the DH cylinder. This should avoid problems such as excessive slipping of the filament on the latter.

STEP 4 - Executor software Once the machine is ready and the *G-code* is produced, the *Executor* program is run following the previous section's indications.

STEP 5 - Curing Though unnecessary, a curing process via heat gun is always advised. This will enhance the wound part's quality and mechanical properties. A wrapping

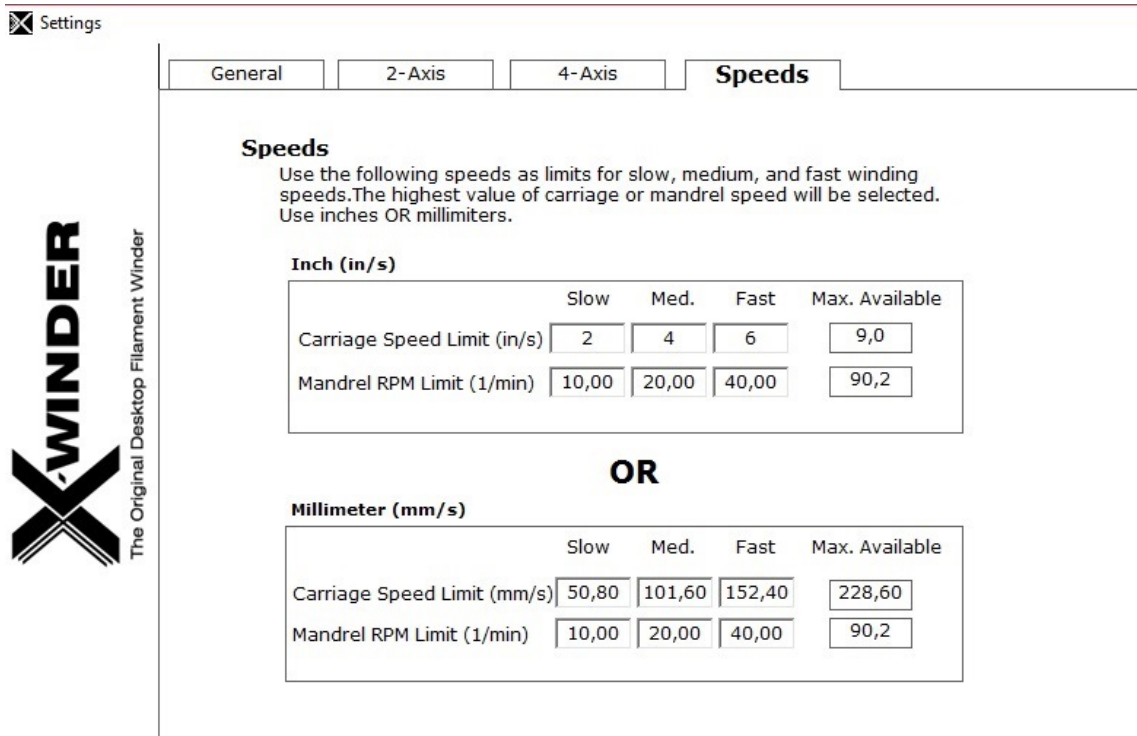


Figure 3.11: X-Winder Settings window - Speeds settings tab.

with heat shrink tape further promotes the outer surface quality. Both post-wrapping phases may be manual or automatic. In any case, a correct distance of the heat gun from the rotating mandrel must be set to avoid overheating and thermal damage/distortion.

Chapter 4

VAWT Blade Demonstrators Manufacturing

This chapter presents the detailed manufacturing of straight VAWT blade demonstrators, considering two different airfoils:

NACA 0021 - typical symmetrical airfoil, validating the proposed process chain through a custom length and chord blade;

Optimized NACA 0015 - aero-structural optimization output and evolution of the common NACA airfoils, pushing the process chain to its limits.

The first part reviews the process chain described in Chapters 2 and 3, applying it to the aforementioned airfoils. Small-scale prototypes were also produced in laboratory.

The last section presents a manufacturing time-cost overview, both qualitative and quantitative, for both demonstrators.

4.1 Custom Blades Data

In the following sections, $L = 0.4 \text{ m}$ long blade demonstrators will be considered and realized. As evident from Chapters 2 and 3 though, the adopted AM and FW machines do not allow blade processing with length $L > 0.35 \text{ m}$. A compromise was found in manufacturing two pieces of $L_{1/2} = 0.2 \text{ m}$ length each, bonded together and fixed to the mandrel through appropriate, custom-made structural supports. Since the main objective is to analyze the feasibility of customized component manufacturing, said design choice allows the validation of the proposed process chain by producing small whilst modular components and showing potential productivity for larger pieces.

4.1.1 NACA 0021

The profile shape is fixed and parametric in terms of the chord length, which was set at $c = 0.05 \text{ m}$. A reference VAWT mounts three 1 m long blades with said profile, an approximate radius $r = 1 \text{ m}$ and a pitch angle $\alpha = 0^\circ$.

4.1.2 Optimized NACA 0015

The baseline 2D airfoil is that of a NACA 0015. In respect to that, the optimized one enhances aerodynamic performances by about 3% and structural performances by about 10%. Geometrically speaking, it is slightly concave on the pressure side while maintaining a slim trailing edge (Fig.4.1).

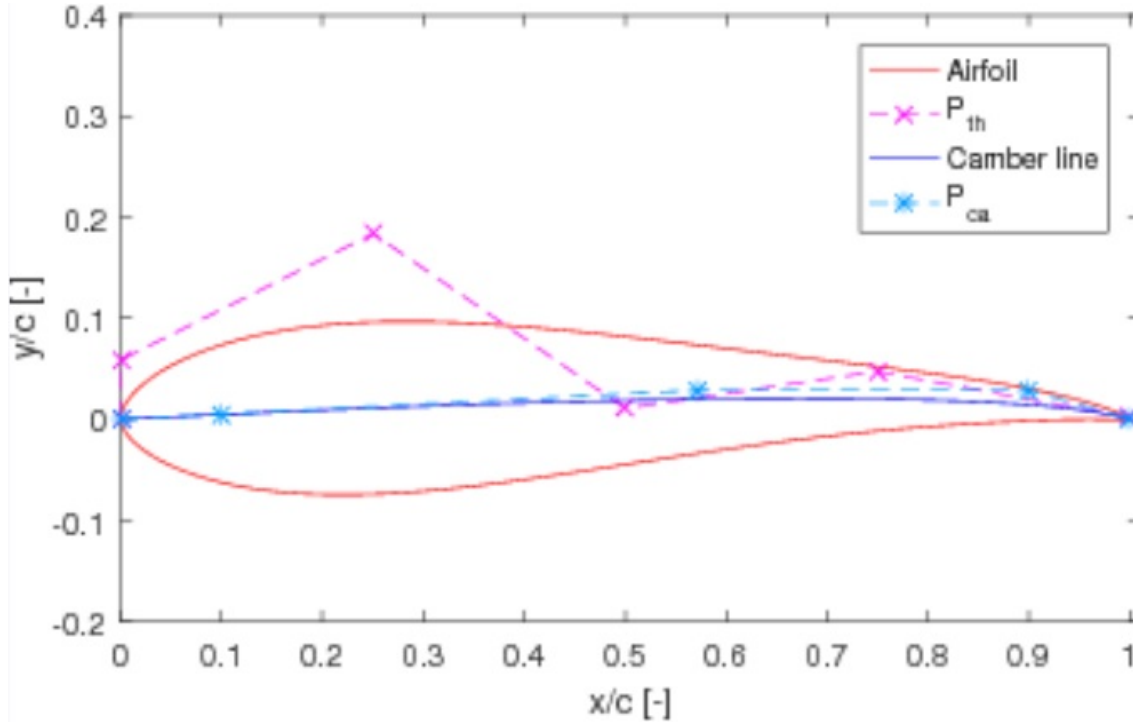


Figure 4.1: 2D optimized profile, obtained from a baseline NACA 0015 profile through an aero-structural optimization code. The airfoil has a normalized chord.

A reference VAWT blade with said profile has a chord length $c = 0.06 \text{ m}$ and a total length of approximately 1 m . The corresponding turbine would have two blades mounted with a radius $r = 0.6 \text{ m}$ and a pitch angle $\alpha = 0^\circ$ [25].

4.2 Blade Structural Supports manufacturing

As stated in the previous section, smaller parts modularization is required to manufacture long mandrels. A proper fixing solution between the modular parts must be identified, designed and manufactured. A way to correctly fix the mandrel to the FW machine is also needed.

The proposed solution consists of two different mandrel supports: (i) Tip mandrel inserts, with cylindrical end rods; (ii) Middle-section blade chunks. The first two pieces allow easy part fixing with the mandrel chucks and are put inside the tips of the mandrel; the second are needed for blade modularization and are put between two smaller mandrels to allow a

longer blade winding without excessive bending.

The advantage of such choice lies in its quick design and manufacturing potential: the 3D solid models and .stl files of the two supports are prepared through Patran and Netfabb by modifying the blade model, i.e. sub-scaling the blade and cutting it at the appropriate height. The mid chunk is 0.06 m long and the tip inserts are 0.024 m long, equally divided between blade chunk and cylindrical rod. In both cases, the blade-shaped part is obtained from the original blade through simple cut, whereas the rods are created in Patran through *Extrusion*.

4.3 NACA 0021 Demonstrator Manufacturing

4.3.1 Mandrel Realization

Patran Modeling

The 2D geometry of a NACA 0021 airfoil, being standard, may be easily generated as a series of points: we chose an open-source online generator to create a .txt file containing an arbitrary number of said points, given the chord length $c = 0.05\text{ m}$ [26].

Having imported the file inside Patran, the baseline 2D airfoil was created through *Curve-Arc3Point* option. An appropriate Surface was also created through *Surface-Break* involving an arbitrary complanar Surface and the 2D profile Curve. The solid 3D blade geometry was then created through the *Solid-Extrude* function, starting from the 2D airfoil surface and for a total length $L = 0.4\text{ m}$. The result is shown in Fig.4.2.

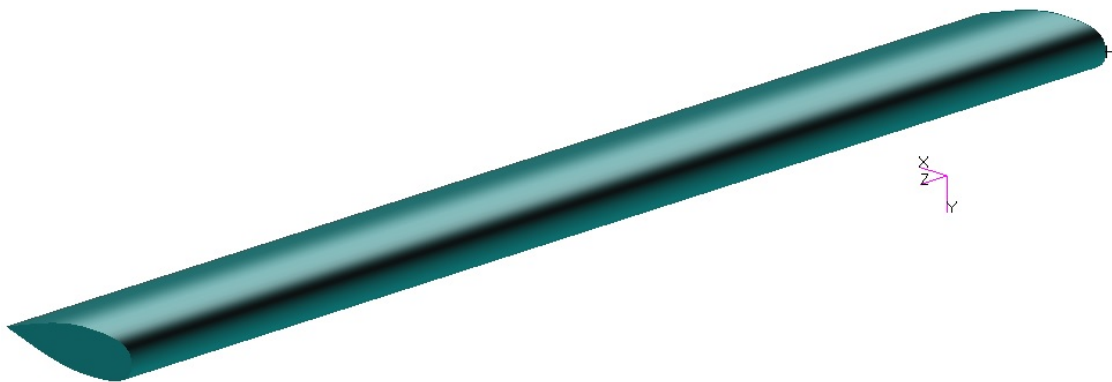


Figure 4.2: NACA 0021 3D solid model created in Patran. The extruded blade is 0.4 m long and has a chord length $c = 0.05\text{ m}$.

The 3D model was finally exported as .stl (ASCII) file, in preparation to the Netfabb design phase.

Netfabb Design

The model .stl file was imported as a new part in Netfabb through the *Import CAD file* function. A Detail Level of Low was also selected. The Repair Script was launched on

the part and the blade mesh was adjusted until Status for Optimization Utility showed a green tick (element smallest angle $> 10^\circ$), as demonstrated in Fig.4.3.

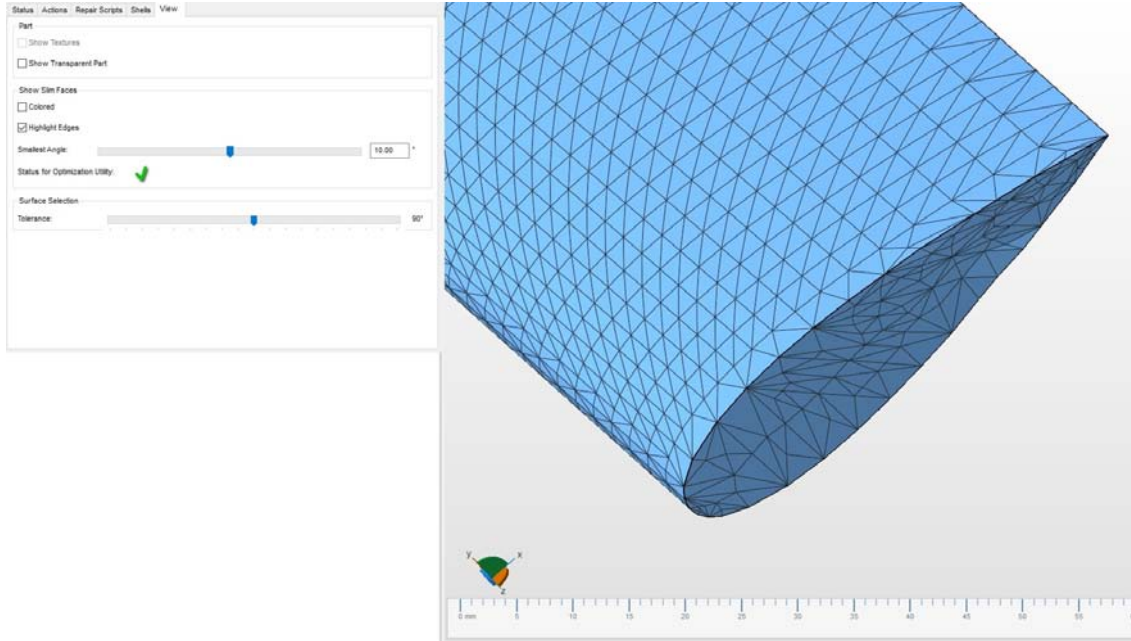


Figure 4.3: Repaired NACA 0021 blade, remeshed with triangular elements. Each element has angles $> 10^\circ$, thus FEA and Optimization may be conducted on the part.

The part was passed onto the *Within* Optimization Utility. A first-attempt structure built with a variable thickness Skin is created. Its minimum thickness was set at $t_{min} = 1 \text{ mm}$ (above *Dimension sst 1200es* printer thickness threshold) and its maximum thickness at $t_{max} = 2 \text{ mm}$. The Regions were defined as follows: (i) Hollow region, including only the 2D tip surfaces; (ii) Skin region, covering the lateral blade surface. The central part has double the thickness of the other portions, representing the 0.2 m blades connected and reinforced through the 0.06 m internal chunk. No Kernels were created and the Component was built using the *Minimum Thickness* option. The component is shown in Fig.4.4.

The Load Case on the blade, acting as mandrel during the following FW process, is that of a polymeric fiber pull: its application points vary with time and its modeling as Force is non-trivial. Since *Within* only supports Linear Static solutions with a simple LC, a trade-off Load Case was considered, representing a simplified worst-case scenario winding condition:

- the load is simulated as concentrated force from fiber pull, applied to a small group of points located at the middle section of the blade's Trailing Edge;
- the force is orthogonal to the trailing edge direction, pointing to the pressure side and thus resulting in maximum bending moment on the blade tips (restrained in

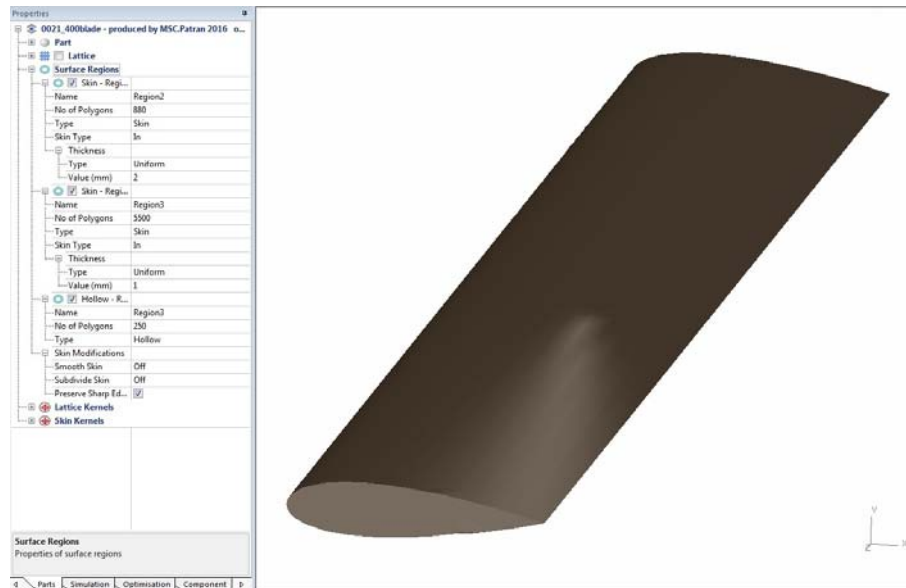


Figure 4.4: NACA 0021 blade - Created Component data with Hollow tip surfaces, 1 mm thick lateral surface Skin and middle 2 mm thick reinforcement (from 0.06 m blade chunk).

x-y-z directions) and maximum displacement on the mandrel middle section;

- a force modulus estimate of 10 N (Distribute Force Across Node flag ON) was set and based on the fiber traction of the *X-Winder* FW machine;
- the pull is considered at winding start, when the blade has no fiber-resin reinforcement on its surface.

Were the blade to resist such load, no critical event should occur during the whole winding process.

Material properties are those of ABS: $E = 3200 \text{ KSI}$, $\nu = 0.35$. Typical mechanical properties are: Elongation at Break $\epsilon^* = 20\%$, Tensional Yield Strength $Y_{tens} = 42 \text{ MPa}$, Flexural Yield Strength $Y_{flex} = 62 \text{ MPa}$. A Maximum Displacement Threshold $\delta_{max}^{thres} = 2 \text{ mm} = 0.5\%$ of total length and a Maximum Stress Threshold $\sigma_{max}^{thres} = 40 \text{ MPa} < Y_{tens}$ were chosen as safe indicators of structural resistance.

The Simulation setup, together with the resulting Stress and Displacement, are shown in Fig.4.5,4.6.

To decide whether an optimization process should follow or a second-attempt component should be created, several considerations were made:

1. the maximum stress is below chosen threshold but the maximum displacement is slightly over;
2. a thinner skin may not be desirable also because: (i) approaching the printing threshold yields poorer results; (ii) the part would be even less resistant against later filament winding gripping and cure heating;

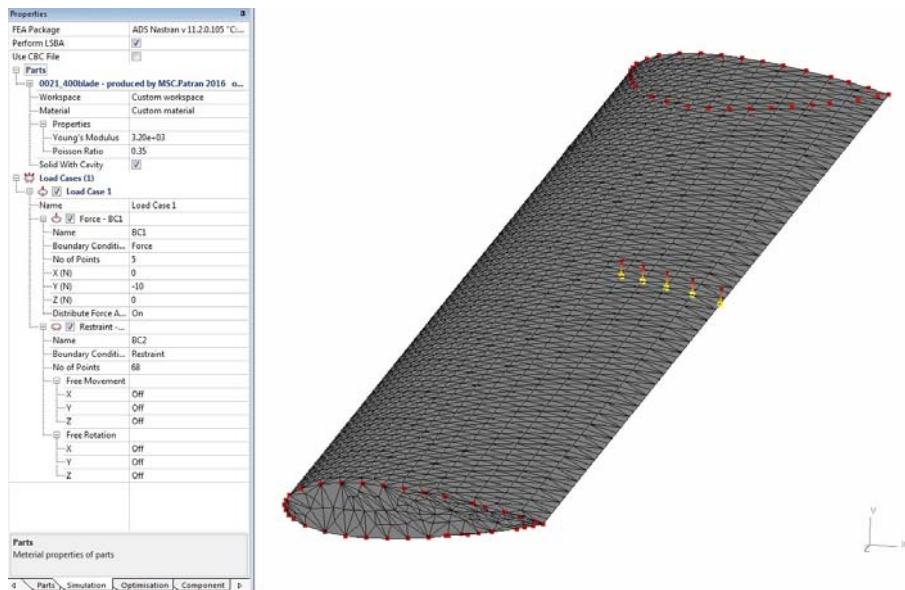


Figure 4.5: NACA 0021 Within Simulation - Custom ABS Material and simplified, worst-case scenario Winding Load Case setup.

3. the component is small: a Lattice internal structure, even with large cells, would result in a part completely filled by support printing material. This implies major printing costs and longer printing and support removal times;
4. optimization processes require specific trial-and-error setting, as well as a lot of computational time.

As a result, the 0.4 m blade was exported to *Netfabb as-is*, without any further optimization. The part was then cut in half and a single 0.2 m blade was saved as .stl file. Fig.4.7(b) shows the final blade and tip structural supports design in Netfabb.

Blade Printing

The blade .stl file was imported to the *CatalystEX* software. The .stl elaborated components are presented in Figs.4.8,4.9,4.10 through a series of *CatalystEX* screenshots.

In the *General* tab, the following properties were set: layer thickness of 0.2540 mm, Model Interior "Sparse - High Density", Support Fill "SMART". In the *Orientation* tab, the blade was vertically oriented: this allows minimum support volume printing and minimum machine pathing, therefore minimum printing and post-processing (support removal) times. In the *Package* tab, the parts were put in the upper right corner of the printing trail: it is the closest position to the nozzle, therefore making the machine move less and translating in shorter production times.

The printing package is shown in Fig.4.11. The two printed blades, together with the mid section reinforcement chunk, are presented in Fig.4.12.

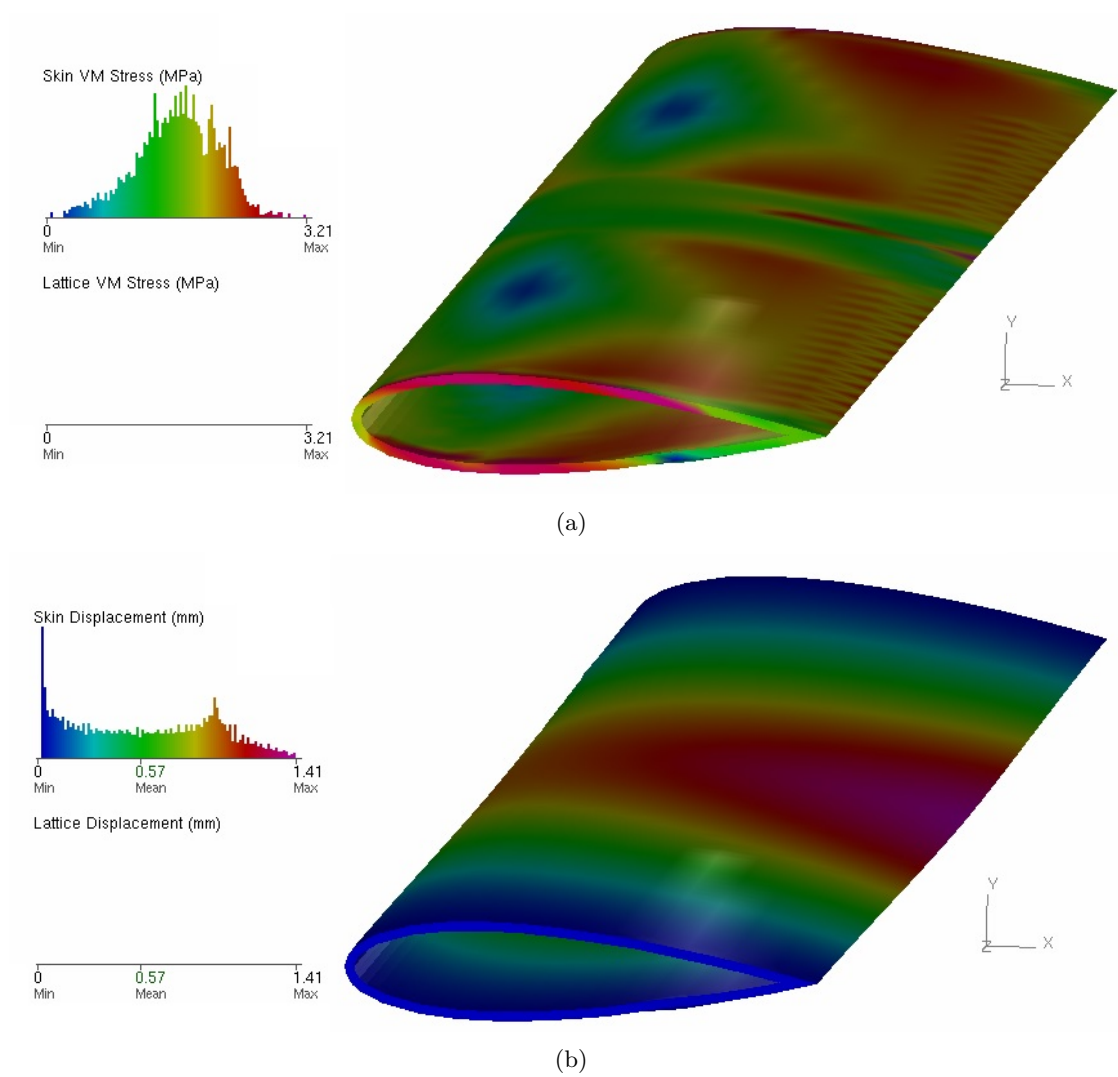


Figure 4.6: NACA 0021 Within Simulation - FEA results in terms of: (a) Stress; (b) Displacement.

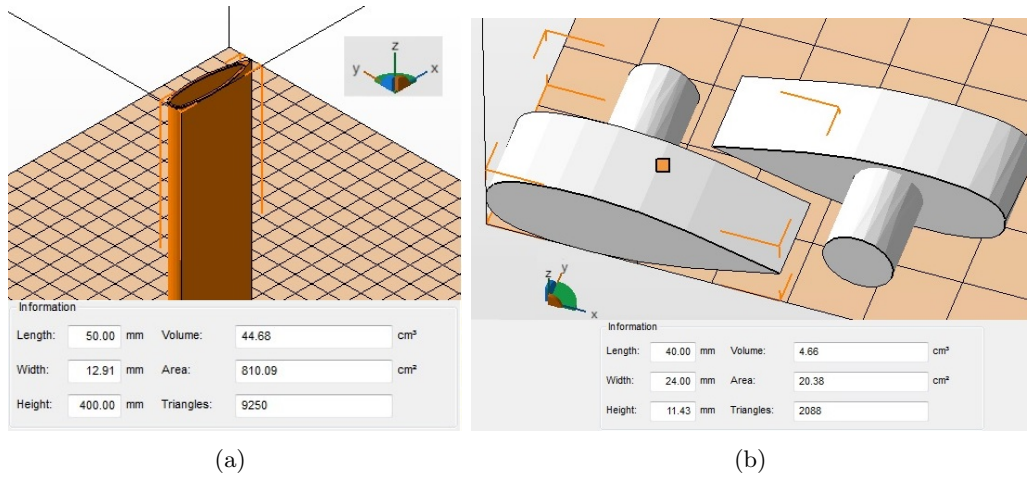


Figure 4.7: NACA 0021 demonstrator - Netfabb design models and geometrical data for: (a) Blade; (b) Tip inserts (Patran was previously employed for the cylindrical rods extrusion).

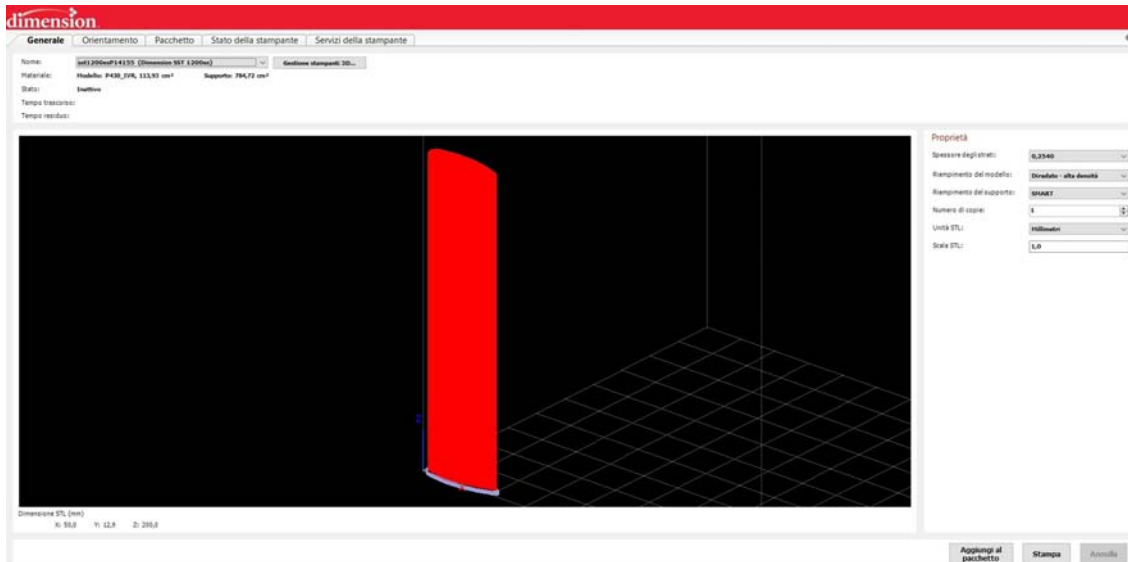


Figure 4.8: 0.2 m long NACA 0021 blade - CatalystEX elaborated .stl .

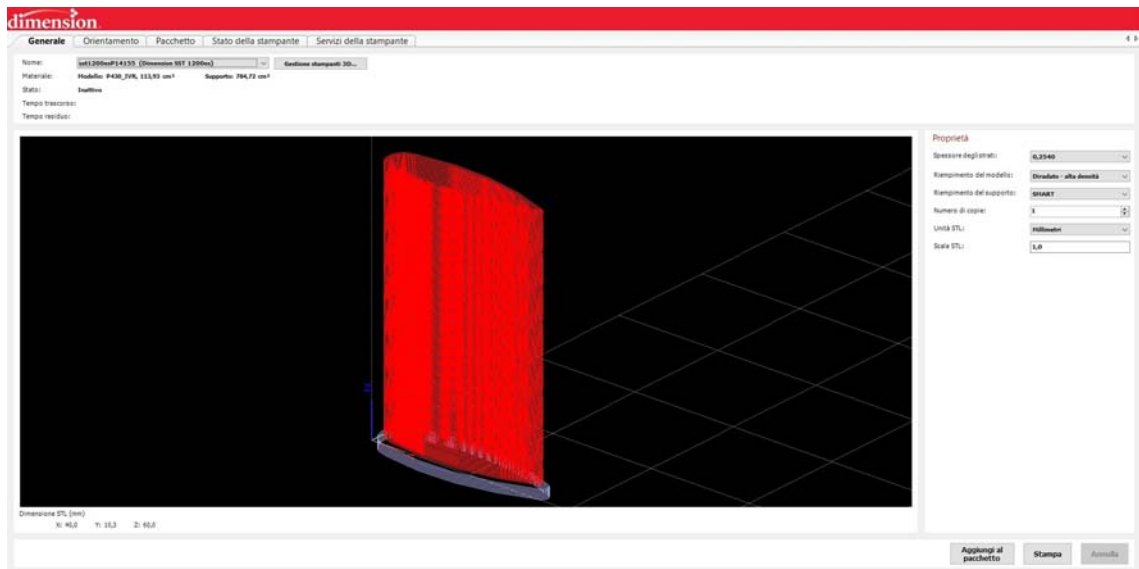


Figure 4.9: 0.06 m long NACA 0021 mid insert - CatalystEX elaborated .stl .

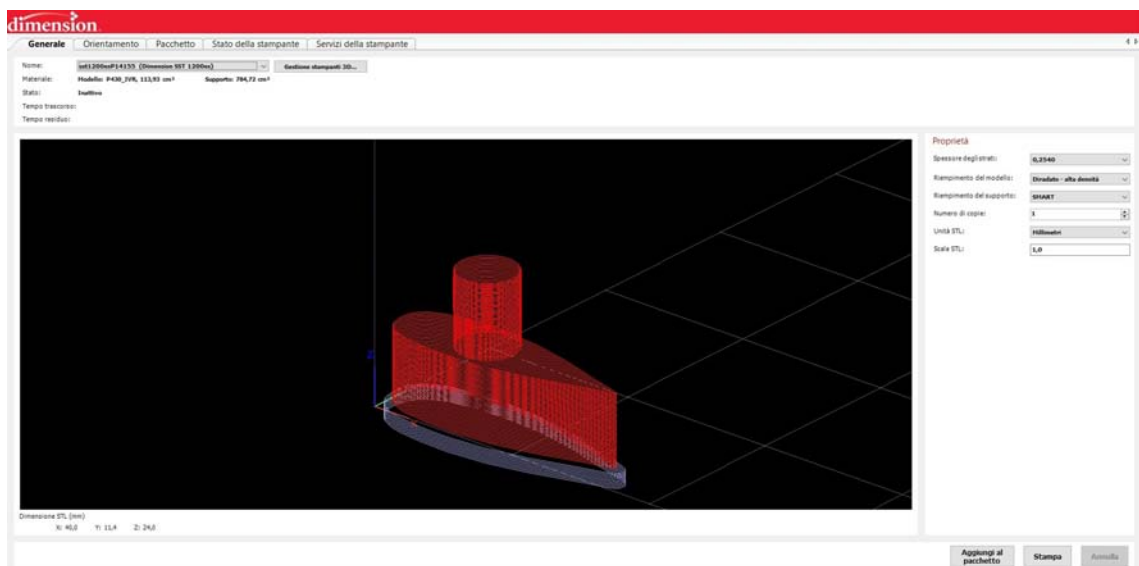


Figure 4.10: 0.024 m long NACA 0021 tip inserts - CatalystEX elaborated .stl .

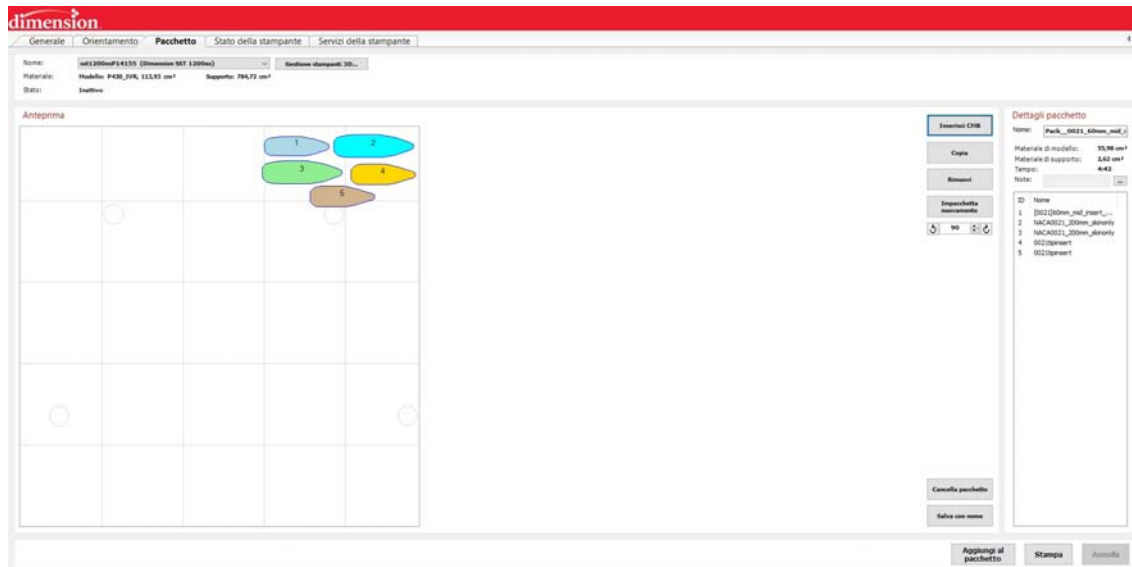


Figure 4.11: NACA 0021 blade components - CatalystEX printing package. The estimated total Model and Support material volumes are presented, together with an approximate building time.

4.3.2 Blade Winding

The full 0.4 m blade is shown in Fig.4.13, just before its mounting on the FW machine. Two paper discs were also cut and positioned on the cylindrical part of the tip inserts, to better contain the fibers inside the mandrel zone during the winding session. The blade, being a small-scaled part, was wound in respect to a $[0^\circ; +45^\circ, -45^\circ]_2$ laminate: this pattern represents a typical VAWT composite blade configuration, as described in previous works [13], [15], [27]. The aforementioned laminate structure, achievable only for fiber mats, was translated as a Hoop (90°) Winding followed by a 45° Winding in the *X-Winder Designer Software*.

Following the procedure outlined in Chapter 3, the Settings are those presented in Figs.3.9, 3.10 and 3.11. In particular, a SLOW speed configuration of 25,4 mm/s Carriage Speed and 10 RPM Mandrel Speed was chosen. This increased manufacturing times but allowed greater control during the winding process.

The *Designer* software data are shown in Fig.4.14. The GF filament was measured to be 6.5 mm wide and 0.3 mm thick: these values were taken considering a small lateral shrinkage of the filament as a consequence of the mandrel pull.

Once the winding is complete, a Heat Shrink Tape of 25 mm width was used to cover the entire blade. A manual Heat Gun curing process followed, lasting 10 to 15 minutes: the part was uniformly heated until the excess resin started to drop from the tape. Great care was taken, not to overheat the blade and cause the ABS mandrel to deform. The part was then left to cure at room temperature for about 12h. The demonstrator is shown in Fig.4.15.

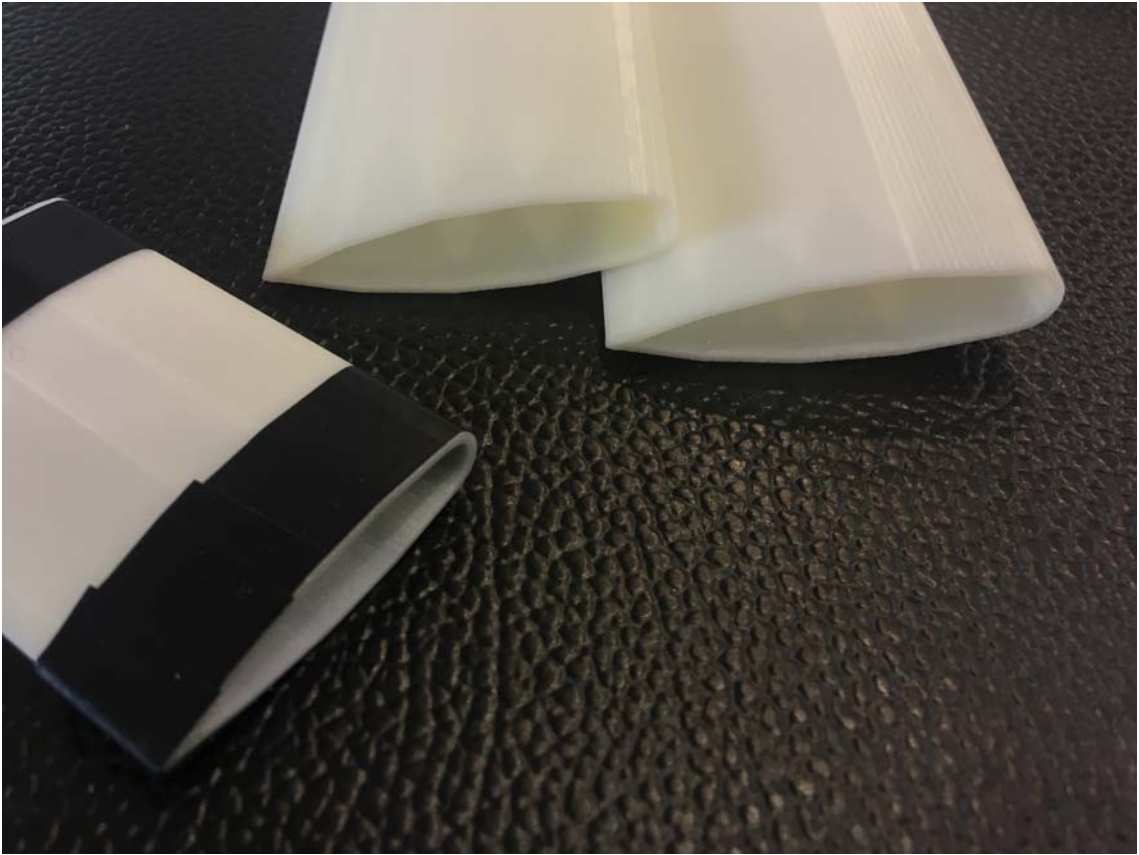


Figure 4.12: Printed 0.2 *m* long NACA 0021 blades, together with the 0.06 *m* internal chunk.



Figure 4.13: Mounted 0.4 *m* long NACA 0021 blade. The junction between the two 0.2 *m* parts is reinforced with a 0.06 *m* internal chunk and sealed for enhanced rigidity.

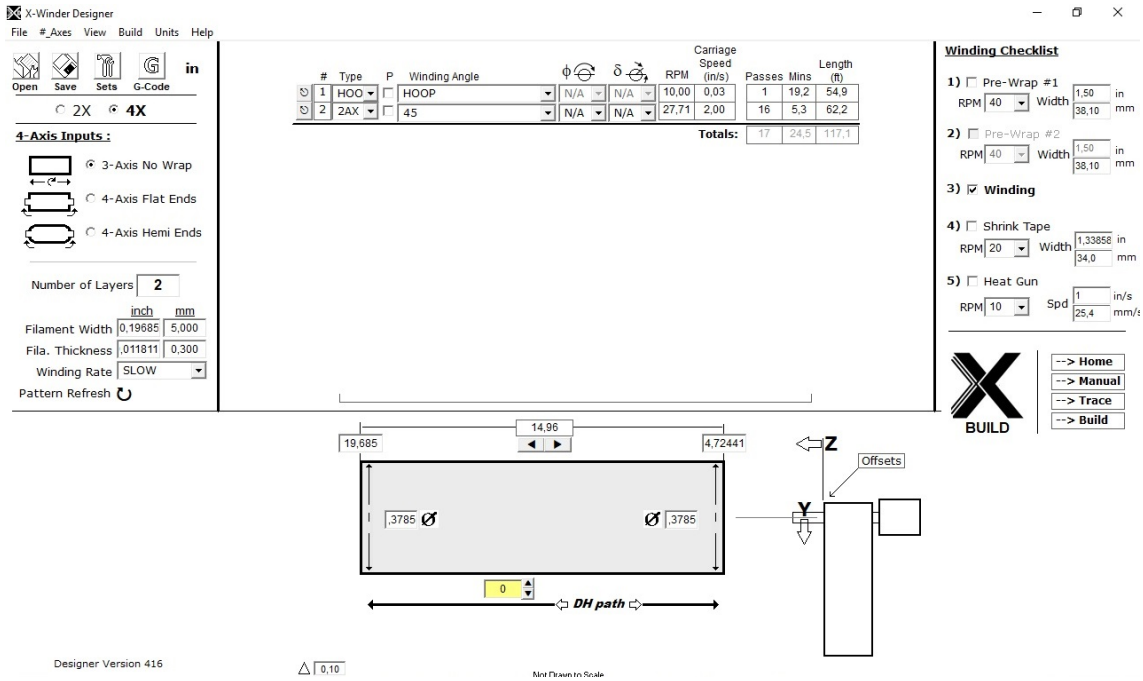


Figure 4.14: X-Winder Designer data for the 0.4 m NACA 0021 blade.

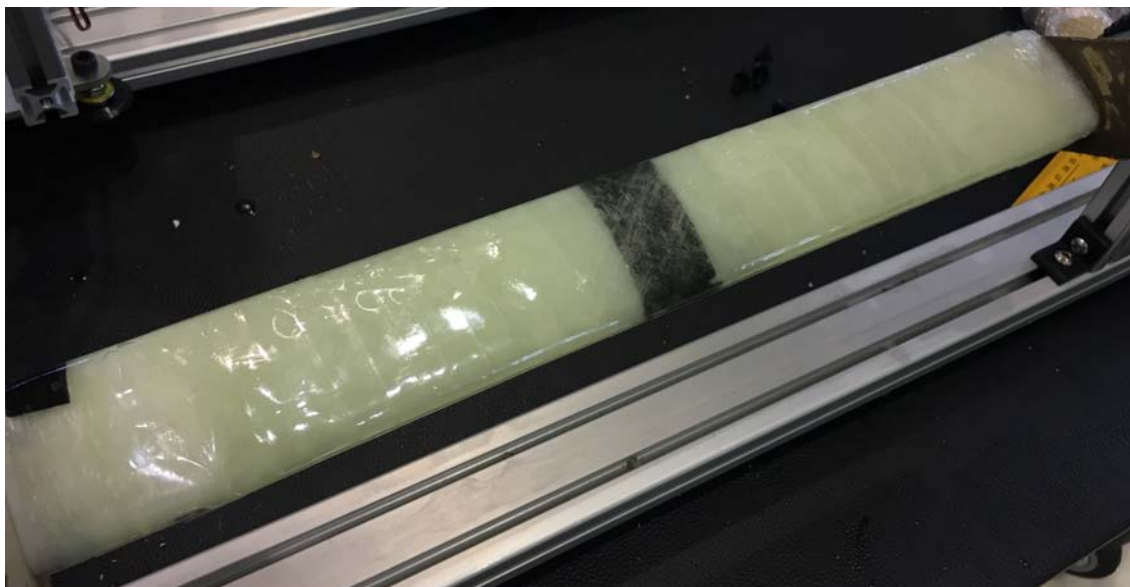


Figure 4.15: GF/epoxy filament wound NACA 0021 VAWT blade demonstrator.

With the exception of short, potentially removable tip zones, the blade shows a satisfactory manufacturing quality: the expected winding patterns were verified, no excessive resin gradients were observed and the wound thickness is uniform over the blade's full length.

4.4 Optimized NACA 0015 Demonstrator Manufacturing

4.4.1 Demonstrator Challenges and Technology Limitations

Differently from the NACA 0021 demonstrator, the optimized NACA 0015 one presents a specific challenge: the pressure side is slightly concave. Said feature poses a problem, as the automatic Filament Winding technology only handles straight or convex surfaces. To overcome this intrinsic limitation, several procedures were considered:

1. External, post-winding coating of stucco/AM-printed material: an additional rigid layer, to be put on the outer blade surface in a post-cure phase, would grant the theoretical profile shape which could not be processed during winding;
2. Smaller sized mandrel and external coating: same as the first procedure, but resizing the initially printed mandrel to maintain a final blade geometry closer to the theoretical one;
3. Post-winding, pre-cure rigid element, pressed on the concave pressure side: a removable or disposable element which forces the pressure side fibers against the mandrel, with a major contribution from the the heat shrink tape constricting action.

Every solution poses critical problems though: the first forces the blade's final geometry to be too different from the theoretical one; the second overcomes the limitations of the first but employs a smaller sized mandrel and wound blade, thus granting mechanical performances worse/other than the ones expected from the initial design; the last solves the geometric issue but introduces pre-loading on the pressure side fibers, risking compromised post-cure mechanical performances.

A trade-off solution comes from considering the sub-optimal NACA 0015 blade (straight pressure side) and analyzing its aero-structural performances through the same code that generated the optimal one. The results showed that the sub-optimal blade, confronted with the baseline NACA 0015 and the optimal one, loses most of its aerodynamic gain while approximately maintaining its structural one.

Since the manufacturing procedure (in terms of time and costs) for baseline, optimal and sub-optimal blades is the same, in the following sections we chose to consider an optimized NACA 0015 blade and attempt to manufacture the corresponding blade as close to the optimal shape as possible.

4.4.2 Mandrel Realization

Patran Modeling

The 2D geometry of the optimized NACA 0015 airfoil was generated as a series of points listed in a .txt file, output of the previous aero-structural optimization process¹.

The profile, being normalized at unitary chord length, was imported in Patran and subsequently rescaled to obtain the target chord length $c = 0.06 \text{ m}$. The 2D airfoil was then created through *Curve-Arc3Point* option. An appropriate Surface was also created through *Surface-Break* involving an arbitrary complanar Surface and the 2D profile Curve. The solid 3D blade geometry was then created through the *Solid-Extrude* function, starting from the 2D airfoil surface and for a total length $L = 0.4 \text{ m}$. The result is shown in Fig.4.16. The 3D model was finally exported as .stl (ASCII) file, in preparation to the

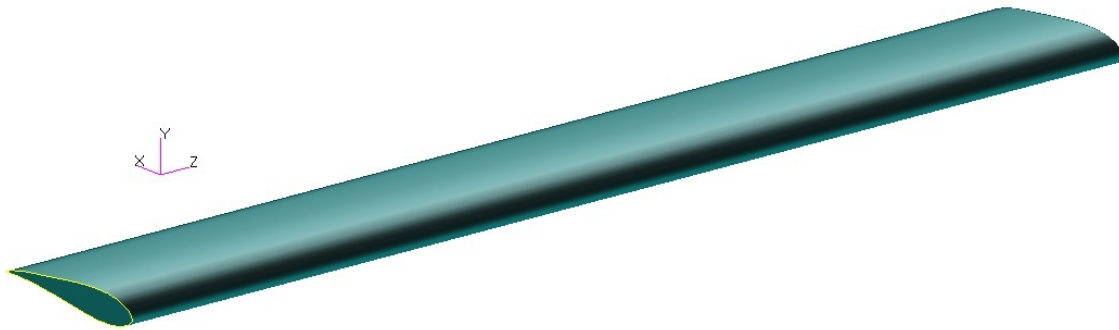


Figure 4.16: Optimized NACA 0015 3D solid model created in Patran. The extruded blade is 0.4 m long and has a chord length $c = 0.06 \text{ m}$.

Netfabb design phase.

Netfabb Design

Following the same procedure adopted for the NACA 0021 blade, the .stl file was imported as a new part, a Detail Level of Low was selected and the part was repaired until Status for Optimization Utility showed a green tick (Fig.4.17). The part was passed onto the *Within* Optimization Utility where a first-attempt “Skin-only” component was created, similarly to the NACA 0021 blade (Fig.4.18).

The Load Case on the blade is the same as the NACA 0021. Material properties are also the same, as well as mechanical properties and target maximum stress-displacement thresholds. The Simulation setup, together with the resulting Stress and Displacement, are shown in Fig.4.19,4.20.

Analogous considerations made for the NACA 0021 demonstrator led to a direct Component export in Netfabb, saving the part as .stl file. Fig.4.21 shows the final blade and tip structural supports design in Netfabb.

¹Not detailed in the current work.

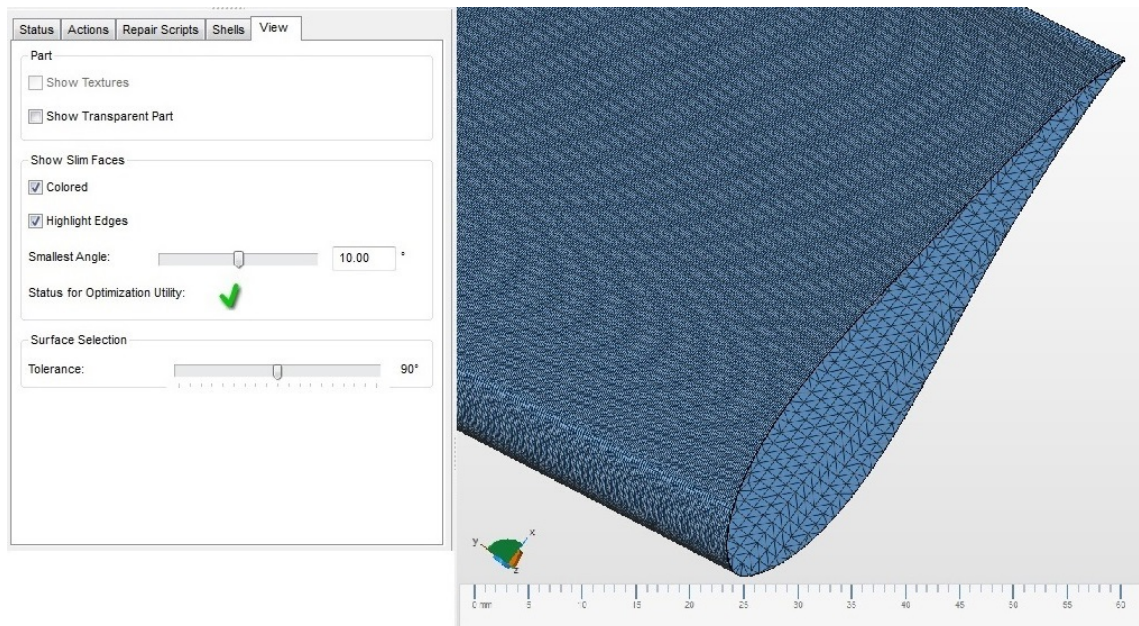


Figure 4.17: Repaired optimized NACA 0015 blade, remeshed with triangular elements. Each element has angles $> 10^\circ$, thus FEA and Optimization may be conducted on the part.

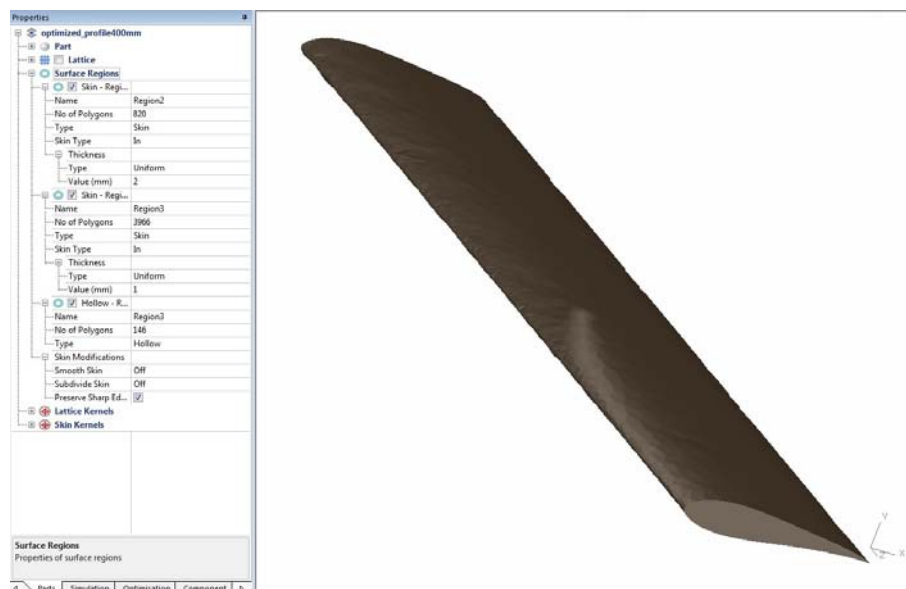


Figure 4.18: Optimized NACA 0015 blade - Created Component data with Hollow tip surfaces, 1 mm thick lateral surface Skin and middle 2 mm thick reinforcement (from 0.06 m blade chunk).

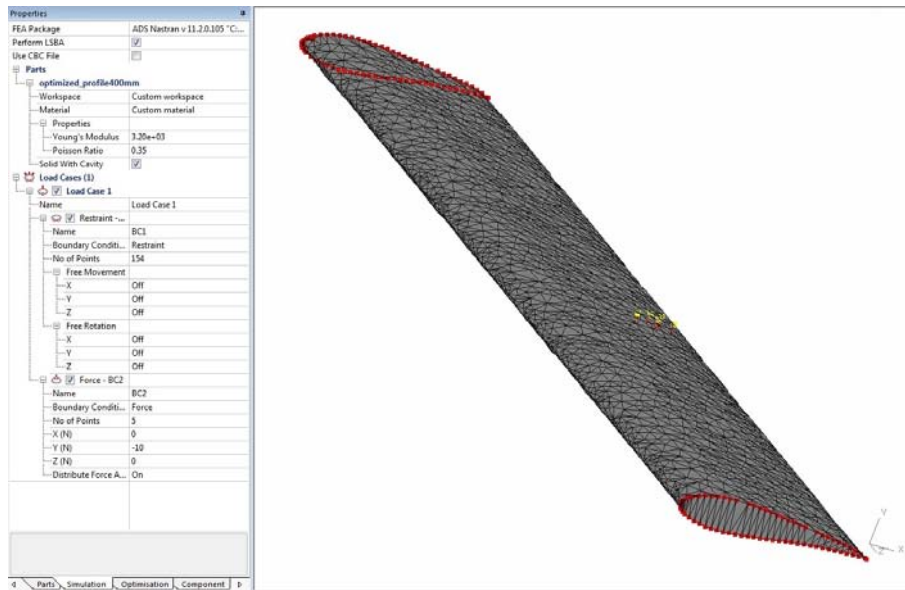


Figure 4.19: Optimized NACA 0015 Within Simulation - Custom ABS Material and simplified, worst-case scenario Winding Load Case setup.

Blade Printing

The *CatalystEX* software settings were the same as the NACA 0021 blade: layer thickness of 0.2540 mm, Model Interior "Sparse - High Density", Support Fill "SMART". The elaborated .stl component models are shown in Figs.4.22-4.25. It should be noted that, differently from the NACA 0021 blade, the top and bottom tip inserts have mirrored shape because of the non-symmetrical blade profile of the optimized NACA 0015 blade. Therefore, they were elaborated and presented separately.

The printing session is reported in Fig.4.26, whereas the total number of components printed is shown in Fig.4.27.

4.4.3 Blade Winding

Fig.4.28 shows the X-Winder mandrel setup before the winding procedure.

The reference laminate composition is yet $[0^\circ; +45^\circ, -45^\circ]_2$. The *X-Winder Designer* software interface is shown in Fig.4.29, where a 6.5 mm wide and 0.3 mm thick GF filament was considered. The Settings adopted for the NACA 0021 demonstrator were maintained.

The demonstrator in its cure phase is shown in Fig.4.30. As expected, the winding process resulted in a straight pressure side.

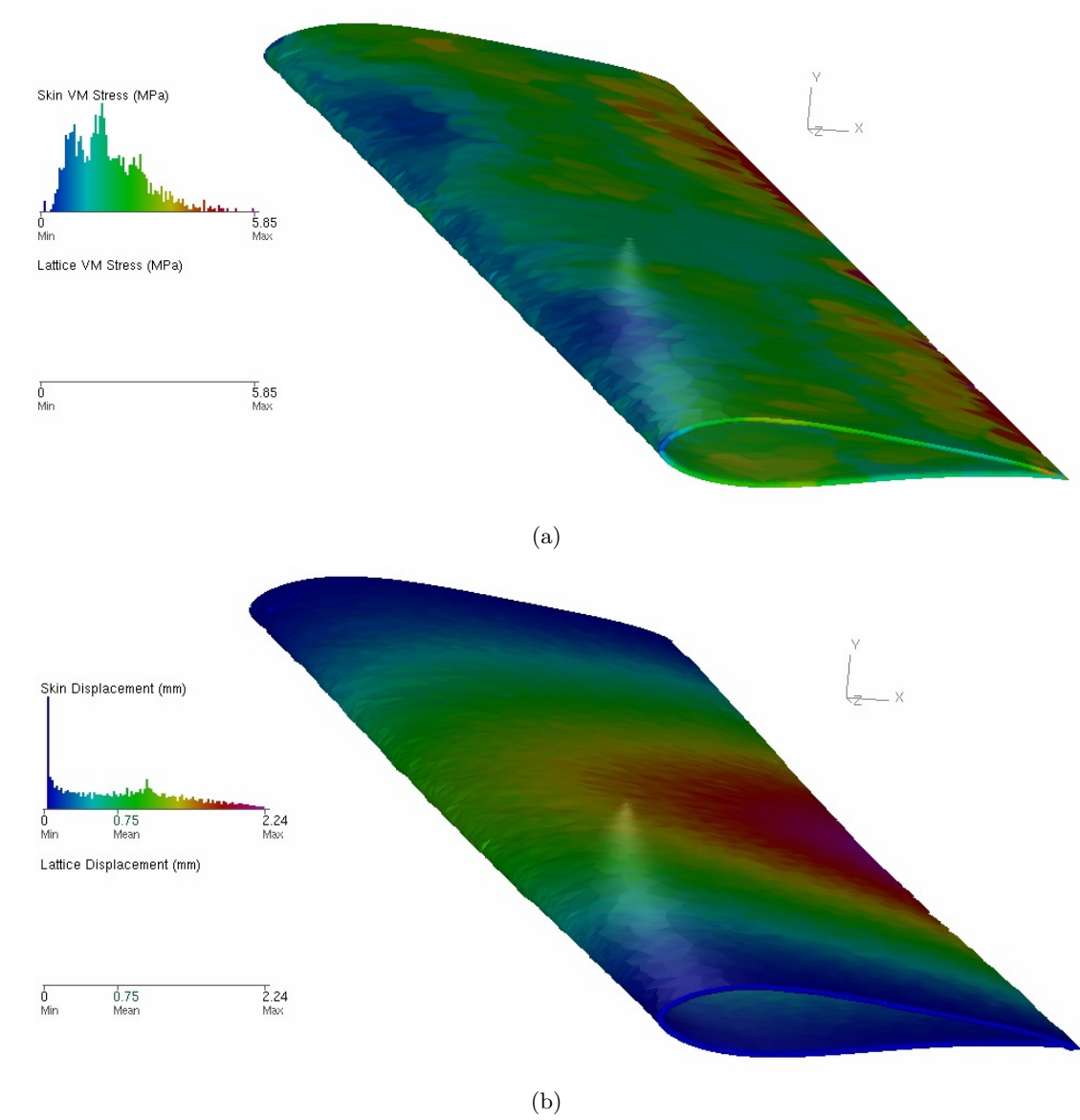


Figure 4.20: Optimized NACA 0015 Within Simulation - FEA results in terms of: (a) Stress; (b) Displacement.

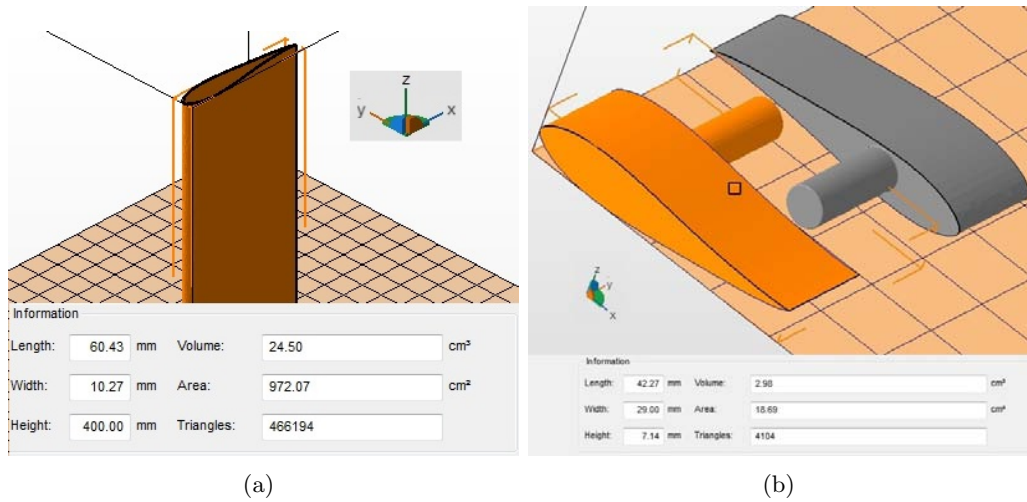


Figure 4.21: Optimized NACA 0015 demonstrator - Netfabb design models and geometrical data for: (a) Blade; (b) Tip inserts (Patran was previously employed for the cylindrical rods extrusion).

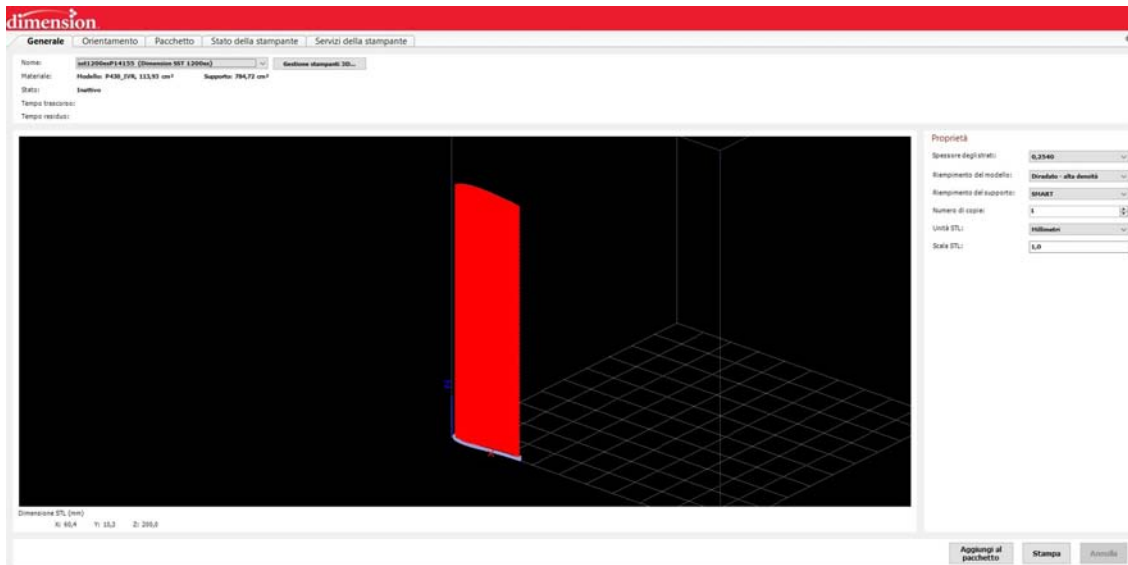


Figure 4.22: 0.2 m long optimized NACA 0015 blade - CatalystEX elaborated .stl .

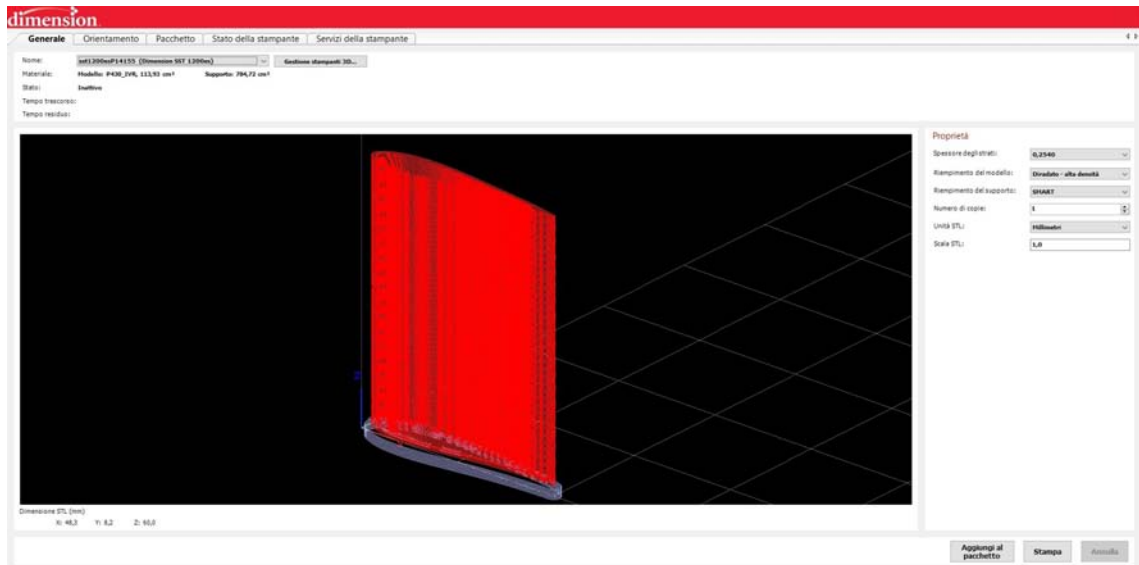


Figure 4.23: 0.06 *m* long optimized NACA 0015 mid insert - CatalystEX elaborated .stl .

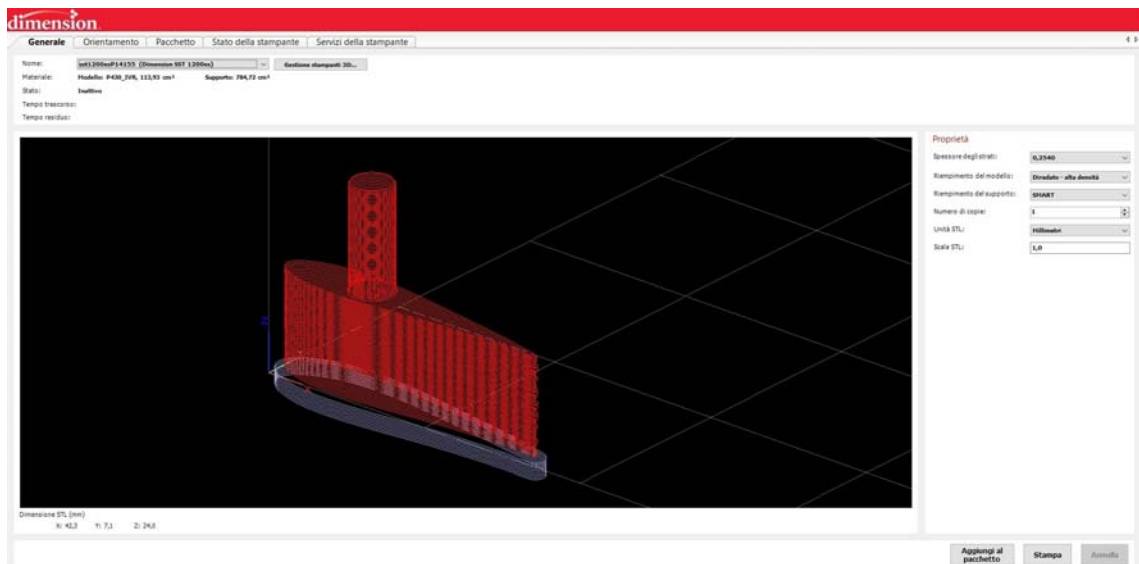


Figure 4.24: 0.024 *m* long optimized NACA 0015 top insert - CatalystEX elaborated .stl .

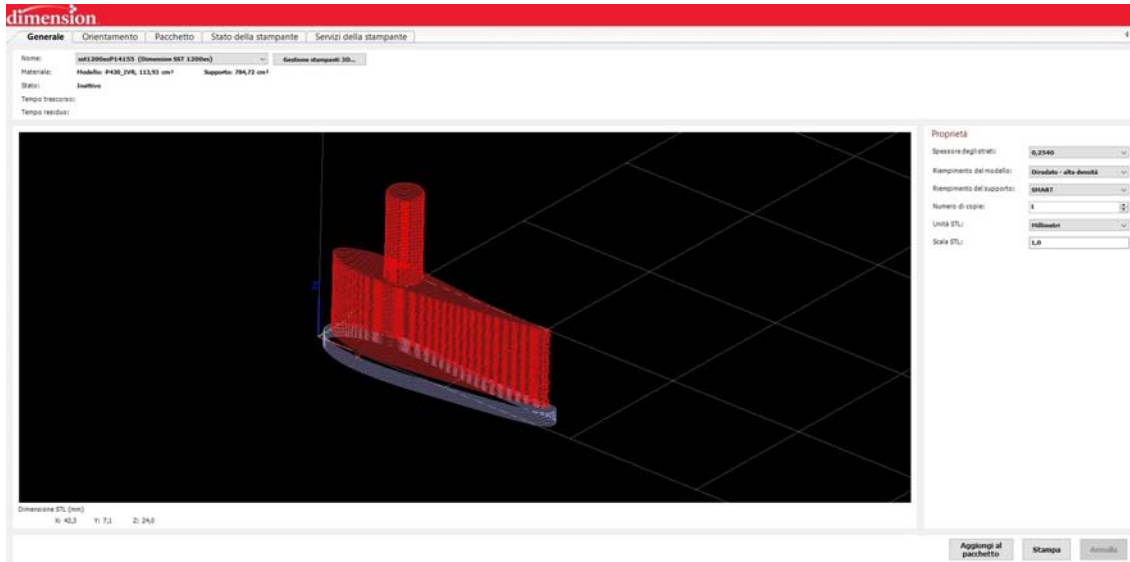


Figure 4.25: 0.024 m long optimized NACA 0015 bottom insert - CatalystEX elaborated .stl .

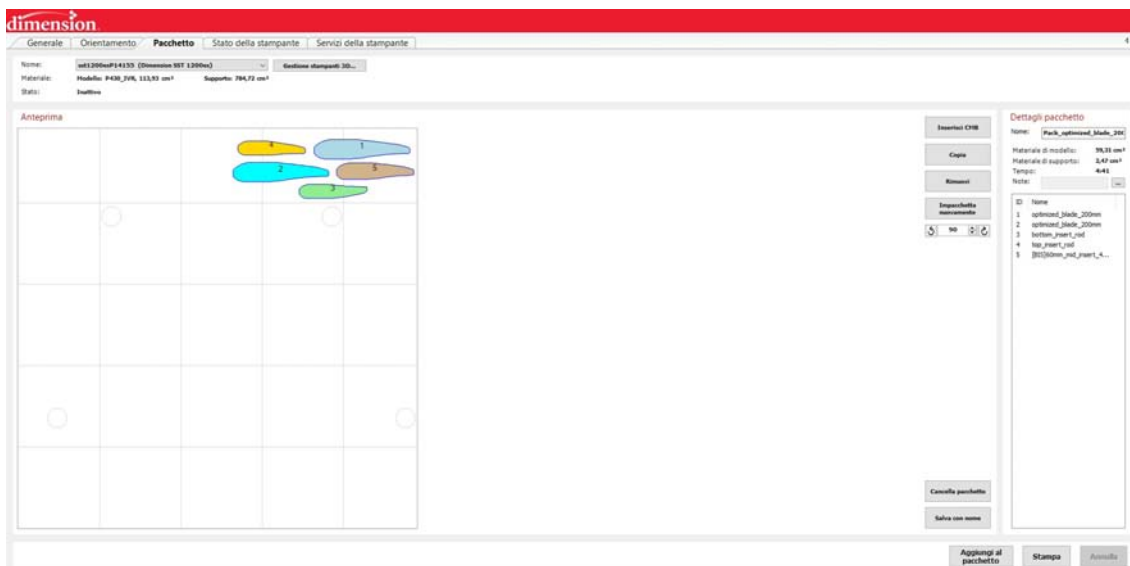


Figure 4.26: Optimized NACA 0015 blade components - CatalystEX printing package. The estimated total Model and Support material volumes are presented, together with an approximate building time.

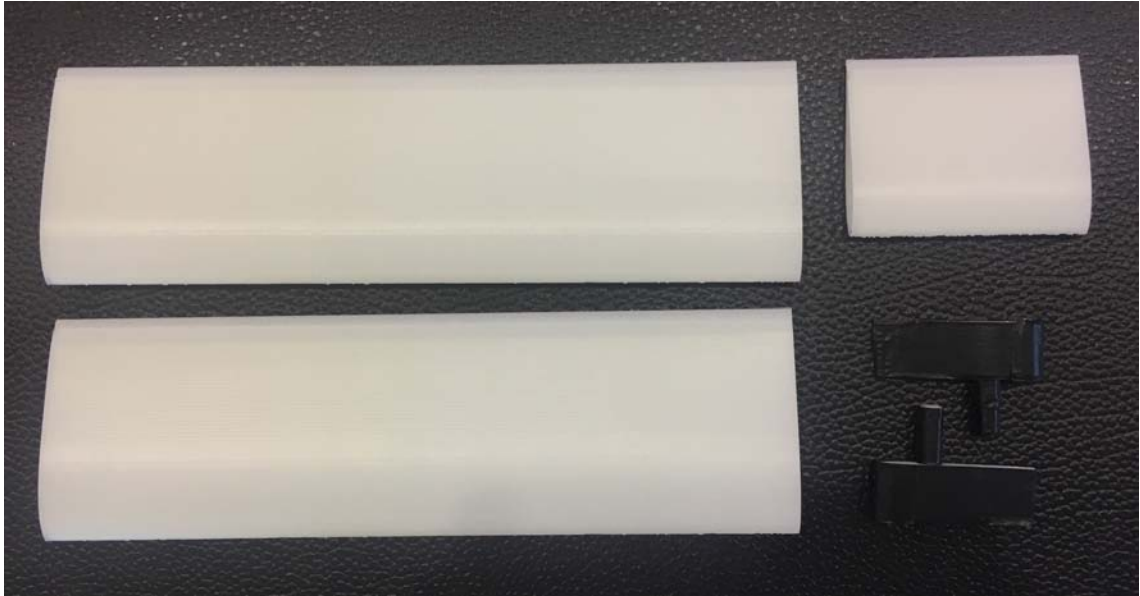


Figure 4.27: Printing summary for a 0.4 *m* optimized NACA 0015 demonstrator: two 0.2 *m* long blades, two internal tip inserts and one mid-section blade chunks.

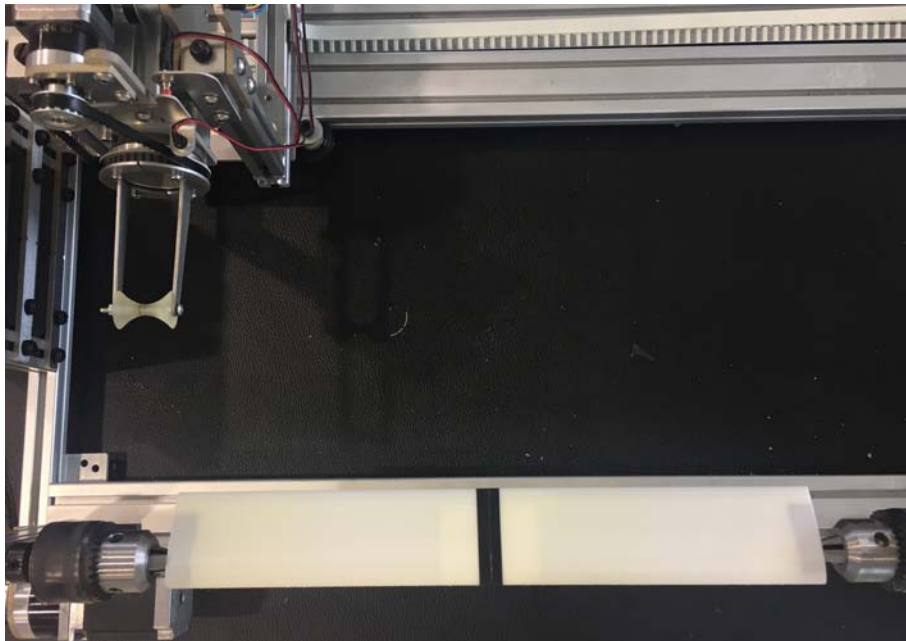


Figure 4.28: X-Winder mandrel setup. The 0.4 *m* long optimized NACA 0015 blade fixing at the mandrel chucks is realized via the two tip inserts, while the internally reinforced mid section is sealed with tape.

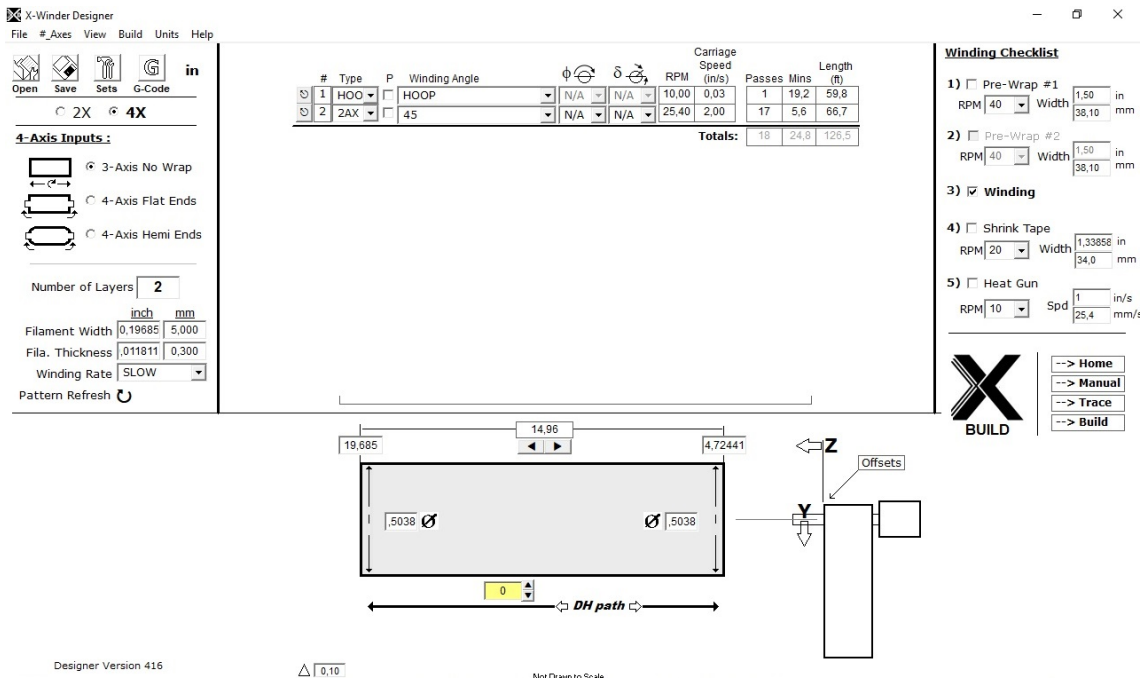


Figure 4.29: X-Winder Designer data for the 0.4 m optimized NACA 0015 blade.



Figure 4.30: GF/epoxy filament wound optimized NACA 0015 VAWT blade demonstrator.

4.5 Time-Costs overview

4.5.1 Qualitative Analysis

A qualitative cost breakdown for a custom VAWT blade consists of variable, semivariable and fixed items²:

A - Design Process

B - Materials

B.1 - Printing material (ABS, support)

B.2 - Fiber roving

B.3 - Resin (epoxy + amine mixture)

C - Manpower

C.1 - Technician/Main operator

C.2 - Assistant(s)

D - Machines and Tools

D.1 - FDM printing machine (*Dimension sst 1200es*)

D.2 - FW machine (*X-Winder - 4X-23 Model*)

D.3 - Terminals

D.4 - Software (*Patran/Nastran, Autodesk Netfabb - Ultimate Version, CatalystEX, X-Winder Designer and Executor*)

D.5 - Other accessories and laboratory tools

E - Properties

E.1 - Laboratory (part manufacturing)

E.2 - Storage³

F (EXTRA) - Testing and Examinations (CE certification)

G (EXTRA) - General Expenses

H (EXTRA) - Company Profit

Some of these factors, e.g. Materials, are volumes direct functions and can be easily evaluated; others are inverse functions instead, such as Design Process (better amortized the higher the number of manufactured parts). Finally, items like Manpower hourly cost require caution and represent a particular challenge.

The manufacturing process of a custom VAWT blade demonstrator involves several steps, which can be summarized as follows:

²The items marked as "EXTRA" represent cost factors not directly involved in the component realization.

³May be part of laboratory space.

1. Design phase: from .txt file to .stl file modeling;
2. AM phase: from .stl file to mandrel printing;
3. FW phase: from mandrel winding to finished product.

A more detailed cost and time breakdown of the process is shown for each aforementioned phase, characterized by several factors:

Design - 2D-to-3D modeling, mesh repair, skin/lattice structure iterations (lattice topology, kernels, ...), LC modeling and preliminary FEA, structural optimization;

AM - .stl model preparation, model orientation, model and support material volumes, post-printing support removal, printing;

FW - winding machine preparation, fiber roving and resin choice, part winding and curing, post-winding machine cleanup.

4.5.2 Quantitative Analysis

We focused on the Materials and Machine/Tools factors (A, B, D items of the qualitative analysis) and Tab.4.1 shows the batch costs of employed resources, obtained via retail/online services. In addition, the *Dimension sst 1200es* FDM printer cost is that of the 30000 – 34000 euros order, whereas the *X-Winder 4X-23* Desktop Filament Winder model is about 3800 dollars (\sim 3000 euros).

Item	Quantity	Cost [Euro]
2400 tex GF roving	30 <i>mt/lin</i>	8.50
Epoxy + Formulated Amine	1 <i>kg</i>	25.50
ABS (mandrel, supports)	1000 <i>cm</i> ³	230
Support printing material	1000 <i>cm</i> ³	230
25 <i>mm</i> wide Heat Shrink Tape	50 <i>m</i>	\sim 9
RS Pro Heat Gun	1	52.30

Table 4.1: Batch costs of materials and supplies employed in the demonstrator manufacturing.

In respect to Tab.4.1, the detailed time and cost expenses for the NACA 0021 and the optimized NACA 0015 demonstrators manufacturing are presented in Tab.4.2,4.3.

Item	Quantity	Cost [Euro]	Time
Mandrel - Model material	56 cm^3	12.88	
Mandrel - Support material	2.62 cm^3	0.60	
GF Roving	20 mt/lin	5.70	
Epoxy + Formulated Amine Resin	0.1 kg	2.60	1 min (mixing)
Heat Shrink Tape	3.8 m	0.68	3 min (post-winding)
Dimension sst 1200es - Mandrel Printing			4 h 42 min
X-Winder - Preliminaries			~5 min
X-Winder - Winding (2 Layers)			~15 min
X-Winder - Heat Gun and Ambient Curing			~12 h
TOTAL		~ 22.50	~17 h 6 min

Table 4.2: Estimated NACA 0021 demonstrator time and cost breakdown, in respect to resources batch costs presented in Tab.4.1.

Item	Quantity	Cost [Euro]	Time
Mandrel - Model material	59.31 cm^3	13.64	
Mandrel - Support material	2.47 cm^3	0.57	
GF Roving	25 mt/lin	7	
Epoxy + Formulated Amine Resin	0.1 kg	2.60	1 min (mixing)
Heat Shrink Tape	3.2 m	0.58	3 min (post-winding)
Dimension sst 1200es - Mandrel Printing			4 h 41 min
X-Winder - Preliminaries			~5 min
X-Winder - Winding (2 Layers)			~15 min
X-Winder - Heat Gun and Ambient Curing			~12 h
TOTAL		~ 24.40	~17 h 5 min

Table 4.3: Estimated optimized NACA 0015 demonstrator time and cost breakdown, in respect to resources batch costs presented in Tab.4.1.

Chapter 5

Conclusions

We have proposed and detailed a manufacturing process chain for customized, straight VAWT blades employing a two-step FDM - Filament Winding processing. Each phase was conceptually built, optimized and described for generic components, as well as for two distinct blade profiles: (i) typical NACA 0021 airfoil; (ii) specific, optimized NACA 0015 airfoil generated from a precedent aero-structural optimization code. The former was chosen to validate the manufacturing process by considering a component with basic level of customization; the latter was considered to further analyze the customization capabilities of the process and highlighting the technology's applications and limitations. The conceptual process chain analysis led to the following results:

- The most influential design factors, in terms of process costs and time, are identified as: (i) component structural design (skin, lattice, hollow, solid regions); (ii) part orientation and build tray positioning during FDM printing; (iii) Printing material and Fiber-Resin choice;
- The most efficient design for small scale straight VAWT blade is that of a vertically oriented component, built as a thin Skin with no internal Lattice structure; the latter would need too much support material during the FDM phase, filling the whole blade and *de facto* turning it into a solid (economically unfavourable);
- FDM printing volume limits the maximum dimension of manufactured components, but this can be partially overcome through modularization: longer parts can be subdivided in shorter ones, fixed together with customly designed internal sections. This logic favors the use of smaller FDM printers, making the process cheaper as a larger machine would result in much higher machine investment for the same benefits.

The process chain was verified in laboratory, where the *X-Winder* Desktop Filament Winding machine was mounted and used in pair with the *Dimension sst 1200es* FDM machine. A 2400K Glass Fiber roving - Epoxy resin combination was employed for the winding phase, whereas ABS was chosen for the AM printing phase. Two demonstrators representing the chosen NACA 0021 and optimized NACA 0015 blades were produced; for each one, production time and costs rough estimates were also presented. Experimental results may be summarized as:

- Convex components, ranging from simple cylinders and bars to NACA airfoils (e.g. the 0021 demonstrator), can be manufactured with satisfying quality from design to post-cure;
- Concave components are not limited by the FDM printing technology, but cannot be manufactured as designed during the Filament Winding phase: this represents an intrinsic limitation of the technology itself, thus to the AM-FW process chain. The optimized NACA 0015 blade was produced nonetheless, resulting in a sub-optimal component characterized by a straight pressure side. Though losing the aerodynamical performance gain over the baseline NACA 0015 blade, the structural enhancement was successfully reproduced: it is advisable to aim for the optimized blade design, as the baseline NACA 0015, its optimized and sub-optimal versions can be manufactured with approximately equal time/cost expenses;
- The *X-Winder* Desktop Filament Winder machine opens the FW technology up to a non-industrial level, allowing the manufacturing of good quality components for an economically favorable investment; paired with 2-to-4 axis configurations, the apparatus shows potential for a great number of applications. Nonetheless, the machine software and algorithms present several "hidden" bugs and limitations which often hinder the manufacturing process.

Bibliography

- [1] L. Battisti et al., “Analysis of Different Blade Architectures on small VAWT Performance,” *Journal of Physics*, 2016.
- [2] [Online]. Available: <https://www.3dhubs.com/knowledge-base/additive-manufacturing-technologies-overview>
- [3] G. J. M. Darrieus, “Turbine Having its Rotating Shaft Transverse to the Flow of the Current,” *US Patent 1,835,018*, 1931.
- [4] M. M. A. Bhutta et al., “Vertical Axis Wind Turbine - A review of various configurations and design techniques,” *Renewable and Sustainable Energy Reviews*, vol. 16, pp. 1926–1939, 2012.
- [5] S. Mertens et al., “Performnce of an H-Darrieus in the Skewed Flow on a Roof,” *Journal of Solar Energy*, vol. 125, pp. 433–440, 2003.
- [6] M. R. Castelli, E. Benini, “Comparison between Lift and Drag-Driven VAWT Concepts on Low-Wind Site AEO,” Jan. 2011.
- [7] J. Castillo, “Small-scale vertical axis wind turbine design,” Dec. 2011, bachelor’s Thesis.
- [8] International Energy Agency, 2017. [Online]. Available: <https://www.iea.org/publications/renewables2017/>
- [9] N. N. Sorte, S. M. Shiekh, “Design and Development of Micro Vertical Axis Wind Turbine for Rural Application,” *International Journal of Engineering And Computer Science*, vol. 3, pp. 7035–7040, 2014.
- [10] V. Adomavičius et al., “Comparison of Small Scale Wind Turbines’ Properties,” Kaunas, KTU, May 2009, pp. 374–379.
- [11] E. Hau, *Wind Turbines - Fundamentals, Technologies, Application, Economics*, 2013.
- [12] D. D. Fernández et al., “Design of a hydroformed metal blade for vertical-axis wind turbines,” *Journal of Renewable Sustainable Energy*, vol. 7, 2015.
- [13] C. Kong et al., “Aerodynamic and Structural Design of a High Efficiency Small Scale Composite Vertical Axis Wind Turbine Blade,” 2011, 18th International conference on Composite Materials.

- [14] S. A. Khan, K.V.S. Rao, “Design and manufacturing of low cost small vertical axis wind turbine,” *Journal of Chemical and Pharmaceutical Sciences*, 2014.
- [15] K. A. Brown, R. Brooks, “Design and analysis of vertical axis thermoplastic composite wind turbine blade,” *Plastics, Rubber and Composites*, vol. 39, pp. 111–121, 2010.
- [16] F. Guerrero-Villar et al., “Development of Vertical Wind Turbines via FDM Prototypes,” 2015, the Manufacturing Engineering Society International conference.
- [17] F. S. Fogliatto, G. J. C. da Silveira, *Mass Customization: Engineering and Managing Global Operations*. Springer, London, 2010.
- [18] I. Paoletti, “Mass customization with additive manufacturing: new perspectives for multi performative building components in architecture,” *Procedia Engineering*, vol. 180, pp. 1150–1159, 2017.
- [19] [Online]. Available: <http://www.xwinder.com/>
- [20] [Online]. Available: <https://www.mscsoftware.com/products>
- [21] [Online]. Available: <https://www.autodesk.com/products/netfabb/overview>
- [22] [Online]. Available: http://www.withinlab.com/benefits/new_index.php
- [23] [Online]. Available: <https://www.stratasys.com/solutions/additive-manufacturing>
- [24] [Online]. Available: http://www.withinlab.com/case-studies/new_index10.php
- [25] M. R. Castelli et al., “Numerical evaluation of aerodynamic and inertial contributions to Darrieus wind turbine blade deformation,” *Journal of Renewable Energy*, vol. 51, pp. 101–112, 2012.
- [26] [Online]. Available: <http://airfoiltools.com/airfoil/details?airfoil=naca0021-il>
- [27] B. Roscher et al., “Combined structural optimization and aeroelastic analysis of a Vertical Axis Wind Turbine,” 2015, 33rd Wind Energy Symposium.